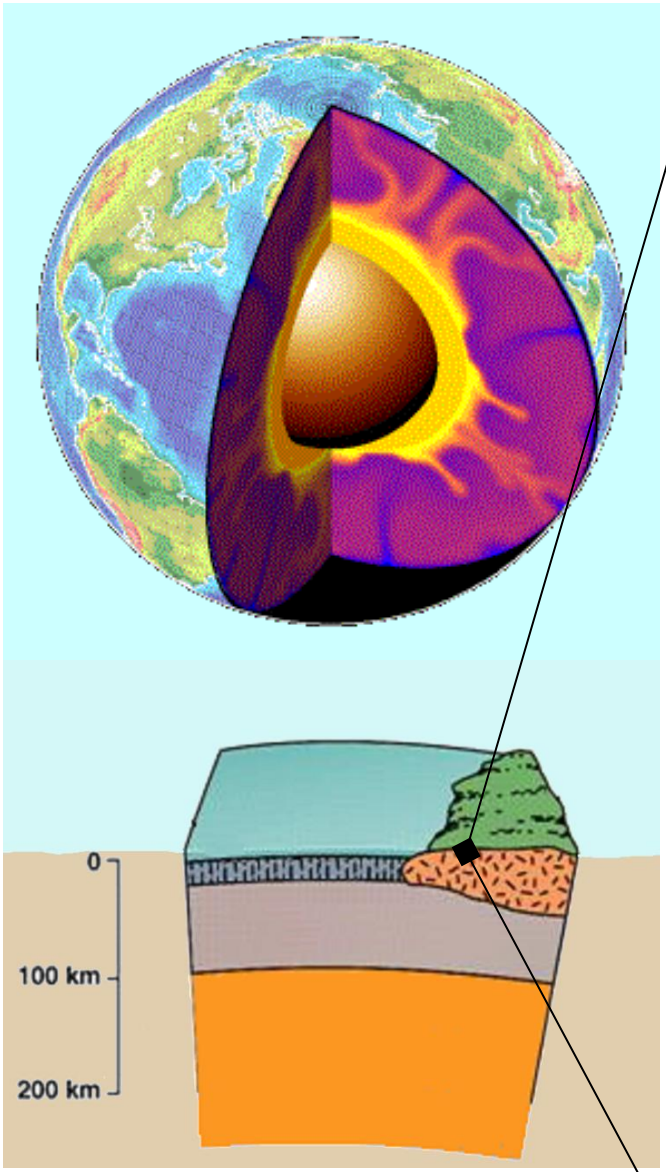

ΟΡΥΚΤΑ ΣΤΗ ΓΗ

ΑΤΜΟΣΦΑΙΡΑ

ΥΔΡΟΣΦΑΙΡΑ

ΒΙΟΣΦΑΙΡΑ

ΛΙΘΟΣΦΑΙΡΑ

ΓΕΩΣΦΑΙΡΑ

ΤΑ ΠΙΘΑΝΑ ΠΡΩΤΑΡΧΙΚΑ ΟΡΥΚΤΑ ΤΟΥ ΣΥΜΠΑΝΤΟΣ

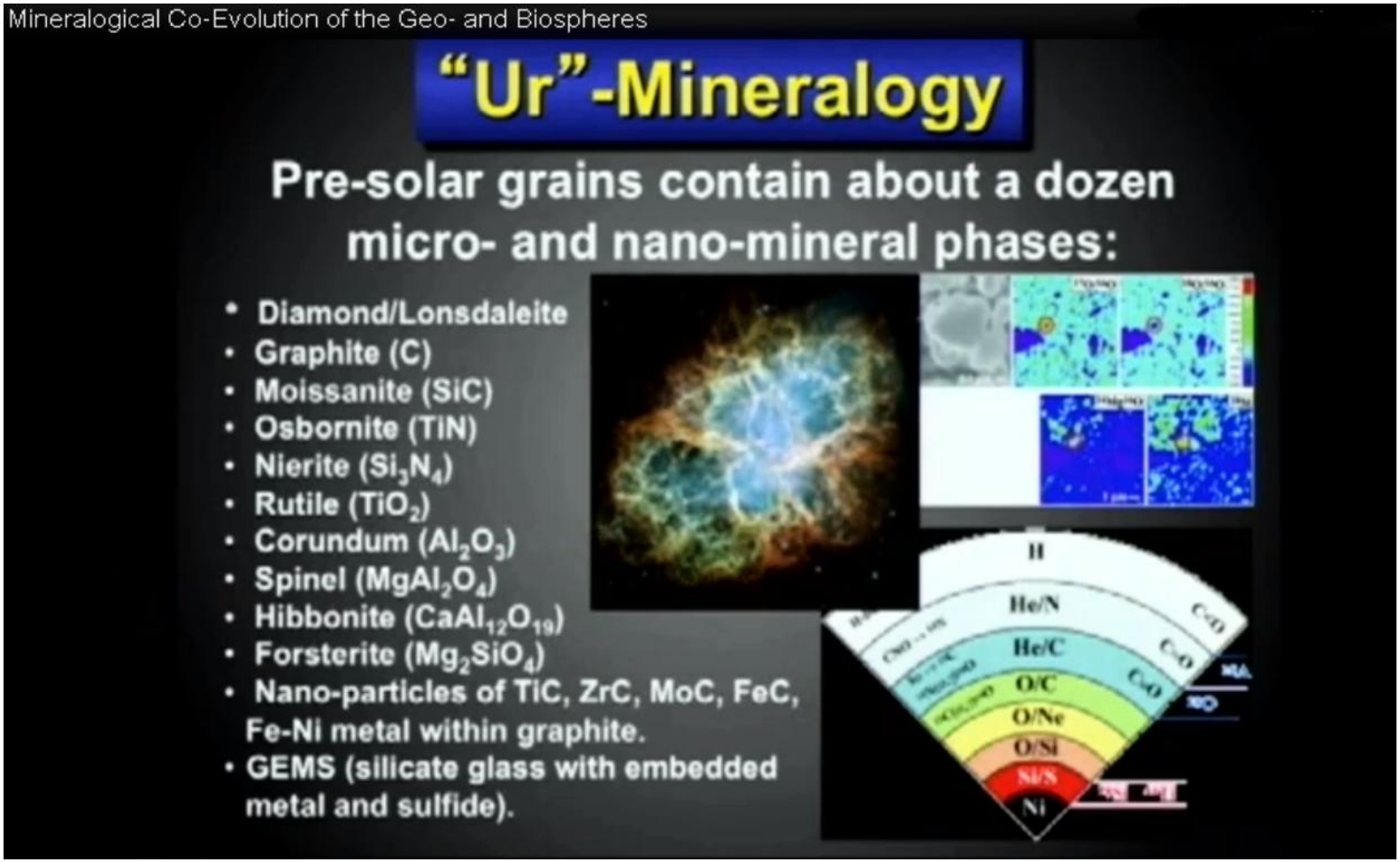

By Professor R. Hazen:
http://www.youtube.com/watch?v=PcktDStIfiQ

Η ΕΞΕΛΙΞΗ ΤΩΝ ΟΡΥΚΤΩΝ (ΣΤΗ ΓΗ) ΚΑΤΑ ΤΗΝ ΔΙΑΡΚΕΙΑ ΤΟΥ ΓΕΩΛΟΓΙΚΟΥ ΧΡΟΝΟΥ

American Mineralogist, Volume 93, pages 1693–1720, 2008

REVIEW PAPER

Mineral evolution

ROBERT M. HAZEN,[1,*] DOMINIC PAPINEAU,[1] WOUTER BLEEKER,[2] ROBERT T. DOWNS,[3]
JOHN M. FERRY,[4] TIMOTHY J. MCCOY,[5] DIMITRI A. SVERJENSKY,[4] AND HEXIONG YANG[3]

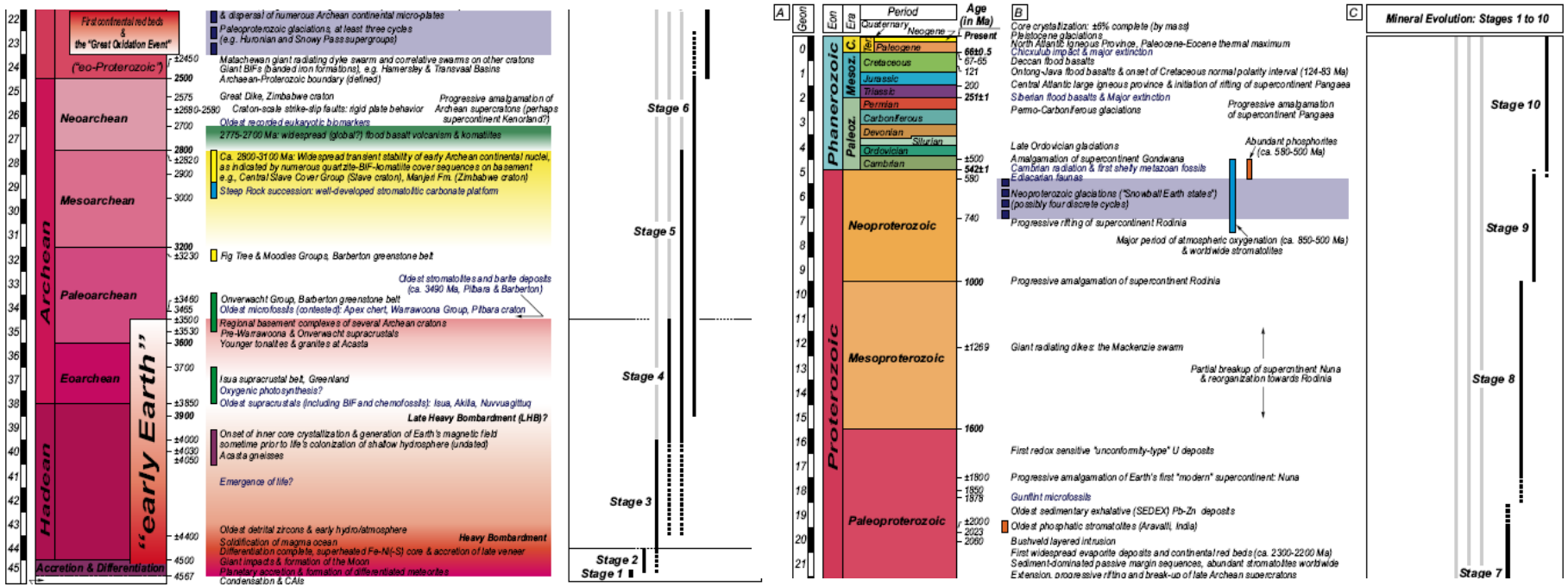

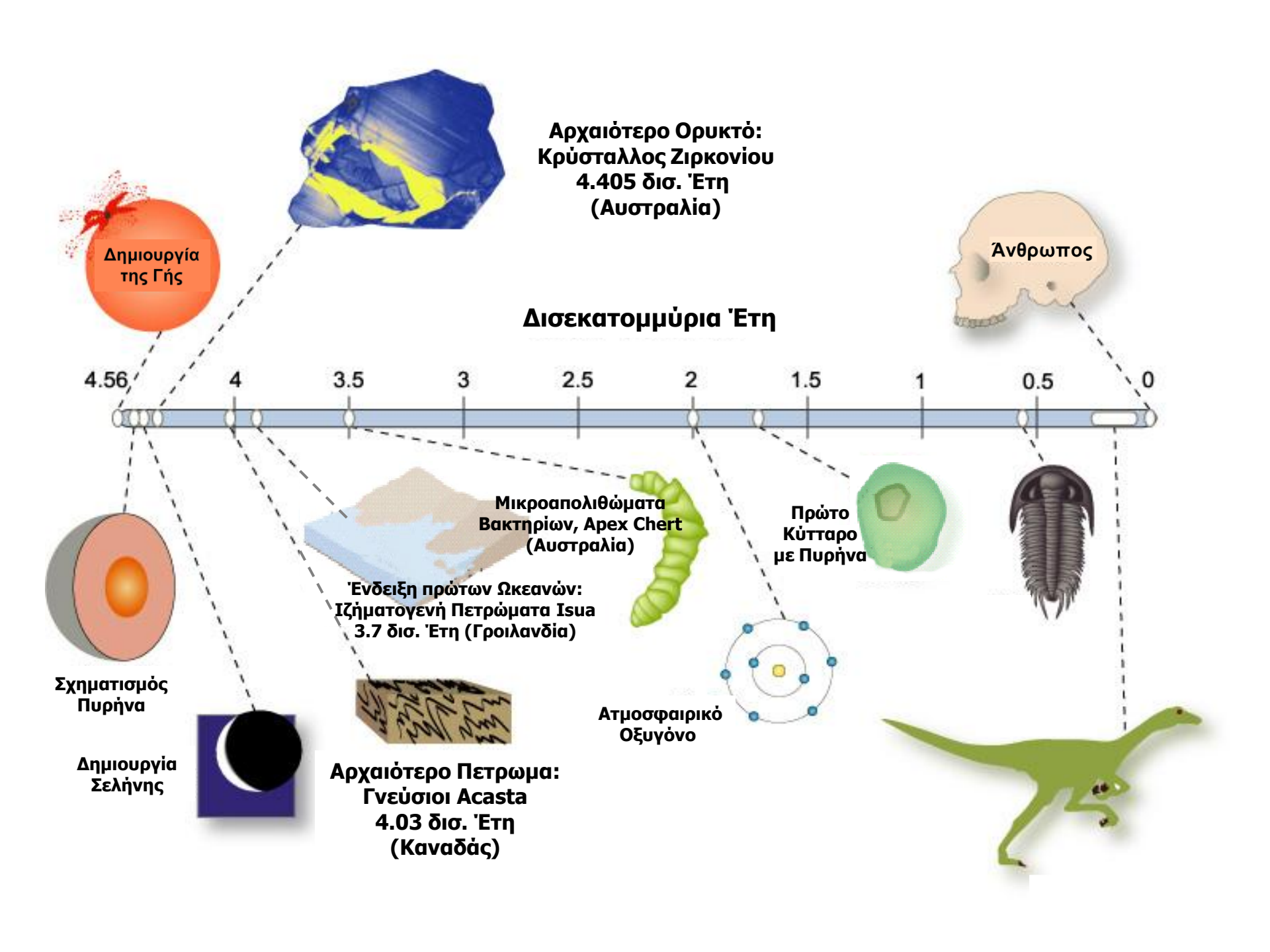
Αρχαιότερο Ορυκτό:
Κρύσταλλος Ζιρκονίου
4.405 δισ. Έτη
(Αυστραλία)
Δημιουργία της Γής
Άνθρωπος
Δισεκατομμύρια Έτη
4.56
4
3.5
3
2.5
2
1.5
1
0.5
0
Μικροαπολιθώματα Βακτηρίων, Apex Chert (Αυστραλία)
Πρώτο Κύτταρο με Πυρήνα
Ένδειξη πρώτων Ωκεανών:
Ιζήματογενή Πετρώματα Isua
3.7 δισ. Έτη (Γροιλανδία)
Σχηματισμός Πυρήνα
Ατμοσφαιρικό Οξυγόνο
Δημιουργία Σελήνης
Αρχαιότερο Πετρωμα:
Γνεύσιοι Acasta
4.03 δισ. Έτη
(Καναδάς)

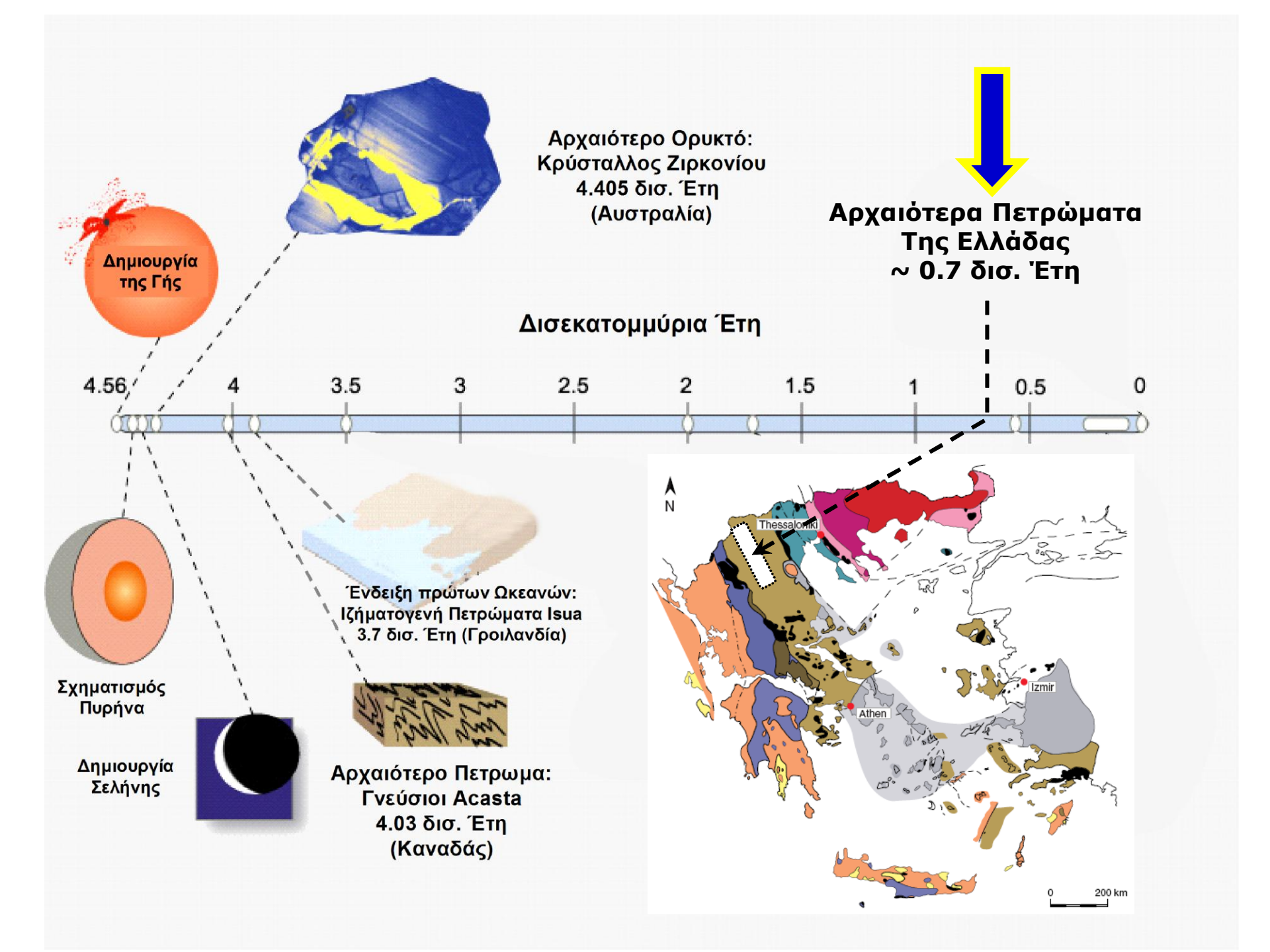
Αρχαιότερο Ορυκτό:
Κρύσταλλος Ζιρκονίου
4.405 δισ. Έτη
(Αυστραλία)
Αρχαιότερα Πετρώματα
Της Ελλάδας
~ 0.7 δισ. Έτη
Δημιουργία
της Γής
Δισεκατομμύρια Έτη
4.56
4
3.5
3
2.5
2
1.5
1
0.5
0
Ένδειξη πρώτων Ωκεανών:
Ιζήματογενή Πετρώματα Isua
3.7 δισ. Έτη (Γροιλανδία)
Σχηματισμός
Πυρήνα
Δημιουργία
Σελήνης
Αρχαιότερο Πετρωμα:
Γνεύσιοι Acasta
4.03 δισ. Έτη
(Καναδάς)
N
Thessaloniki
Izmir
Athen
0
200 km

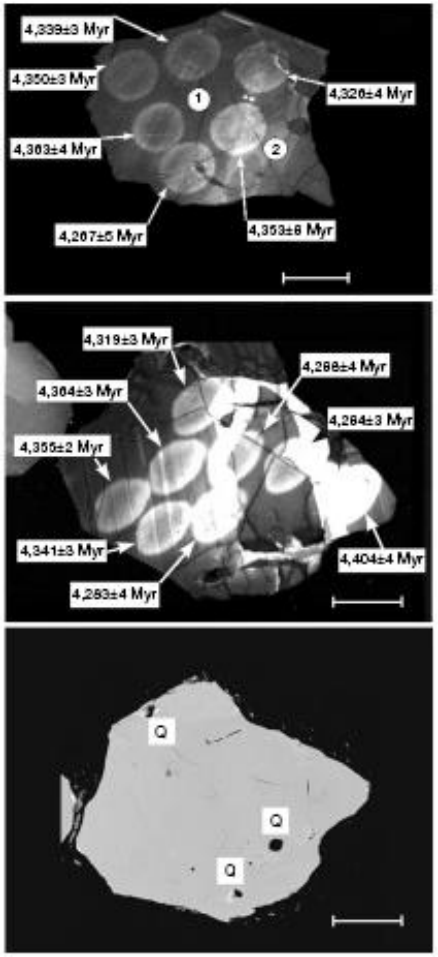

$^{207}Pb/^{206}Pb$

ΤΑ ΝΕΑ / Δευτέρα 11 Απριλίου 2005

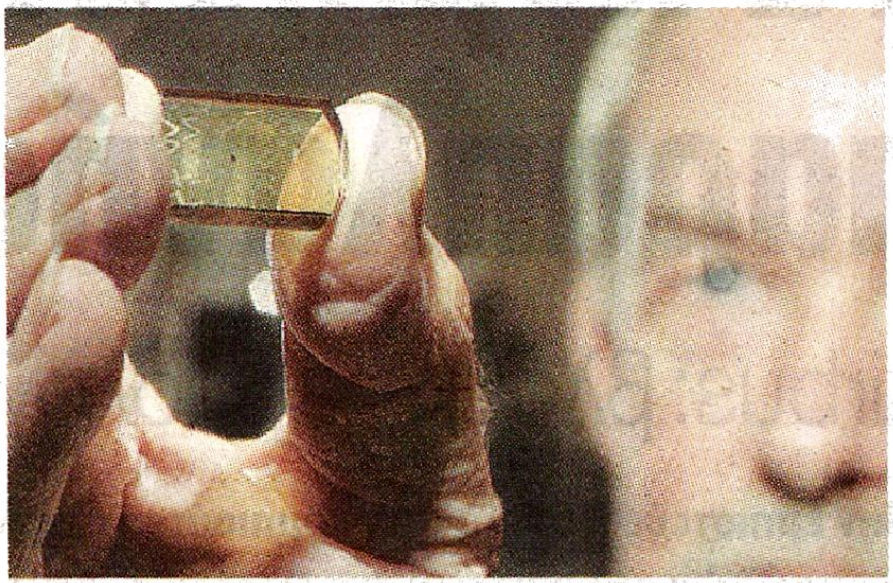

Κρύσταλλος ζιρκονίου. Έχει ηλικία 4,4 δισ. ετών

το συμπέρασμα ήταν ότι αρχικά η Γη δεν ήταν ένας συνεχώς κινούμενος ωκεανός μάγματος – όπως πιστεύαμε έως σήμερα – αλλά, αντίθετα, είχε αρκετά δροσερή ατμόσφαιρα, ώστε να δημιουργηθούν ωκεανοί και ήπειροι, προϋποθέσεις απαραίτητες για τη δημιουργία και την εμφάνιση της ζωής

ZIPKONIO ($ZrSiO_4$)

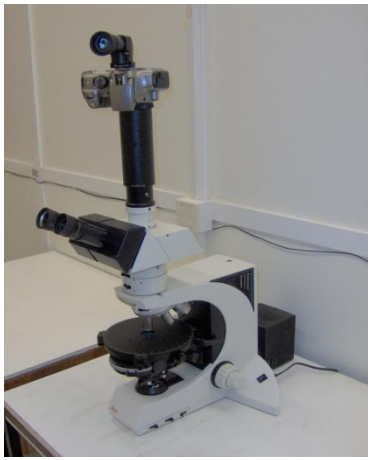

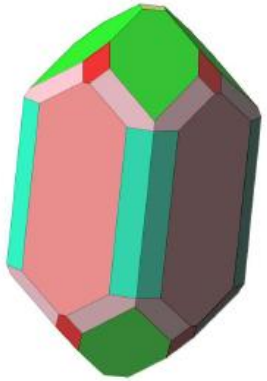

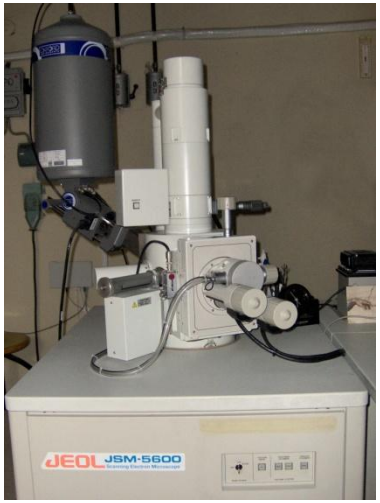

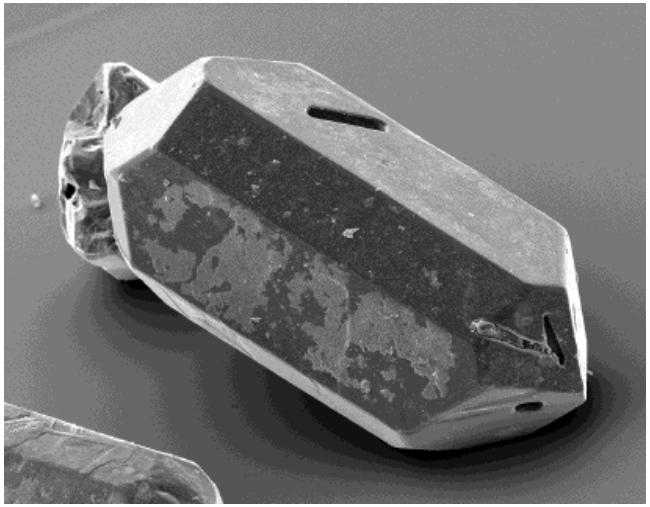

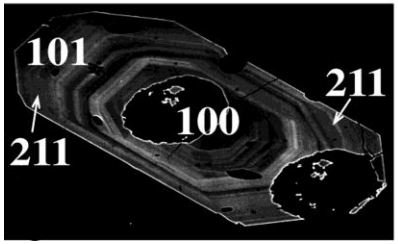

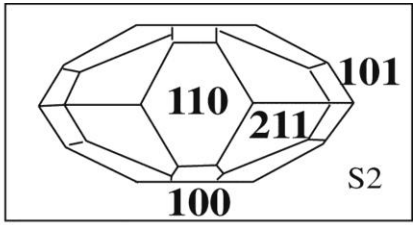

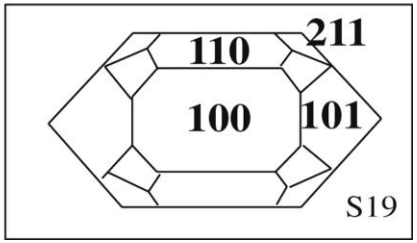

International Journal of Earth Sciences
https://doi.org/10.1007/s00531-019-01773-z

ORIGINAL PAPER

Triassic evolution of the western Neotethys: constraints from microfabrics and U–Pb detrital zircon ages of the Plattenkalk Unit (External Hellenides, Greece)

G. Zulauf[1] · W. Dörr[1] · P. Xypolias[2] · A. Gerdes[1] · G. Kowalczyk[1] · J. Linckens[1]

Received: 26 April 2019 / Accepted: 9 September 2019

Abstract

The Plattenkalk Unit forms the structurally deepest nappe of the External Hellenides and plays a key role for the reconstruction of Triassic paleogeography in the western Tethyan realm. To shed light on the provenance of the Plattenkalk Unit, we present microfabrics and U–Pb detrital zircon data obtained from quartzite and metaconglomerate of its basal part (Kastania and Transitional Beds exposed on the southern Peloponnesus). A Minoan-type age spectrum of detrital zircons, together with inherited deformation microfabrics of detrital components, points to a very low- to low-grade metamorphic basement as source rock that was situated along the northern passive margin of Apulia facing the Neotethys in the north. The siliciclastic rocks of the Kastania Beds reflect the late Permian/early Triassic opening of the Neotethys, whereas the Transitional Beds indicate the late Triassic facies change toward the Pantokrator-type dolomite, which is a characteristic rock of late Triassic Tethyan carbonate platforms. Dolomite and evaporites of the Trypali Unit, on the other hand, were deposited vis-à-vis along the southern passive margin of Cimmeria. This Triassic configuration of Tethyan basins fits well with the S/SW-directed transport and the recent vertical succession of the Hellenic nappes. The proposed Triassic position of the Plattenkalk basin implies that the Apulian microplate was not part of the Cimmerian block since Permian times. The separation of the Apulian microplate from Gondwana is attributed to the Jurassic breakup of Pangea resulting in the opening of the Mesogean ocean, the relics of which are undergoing subduction beneath the Aegean microplate still today.

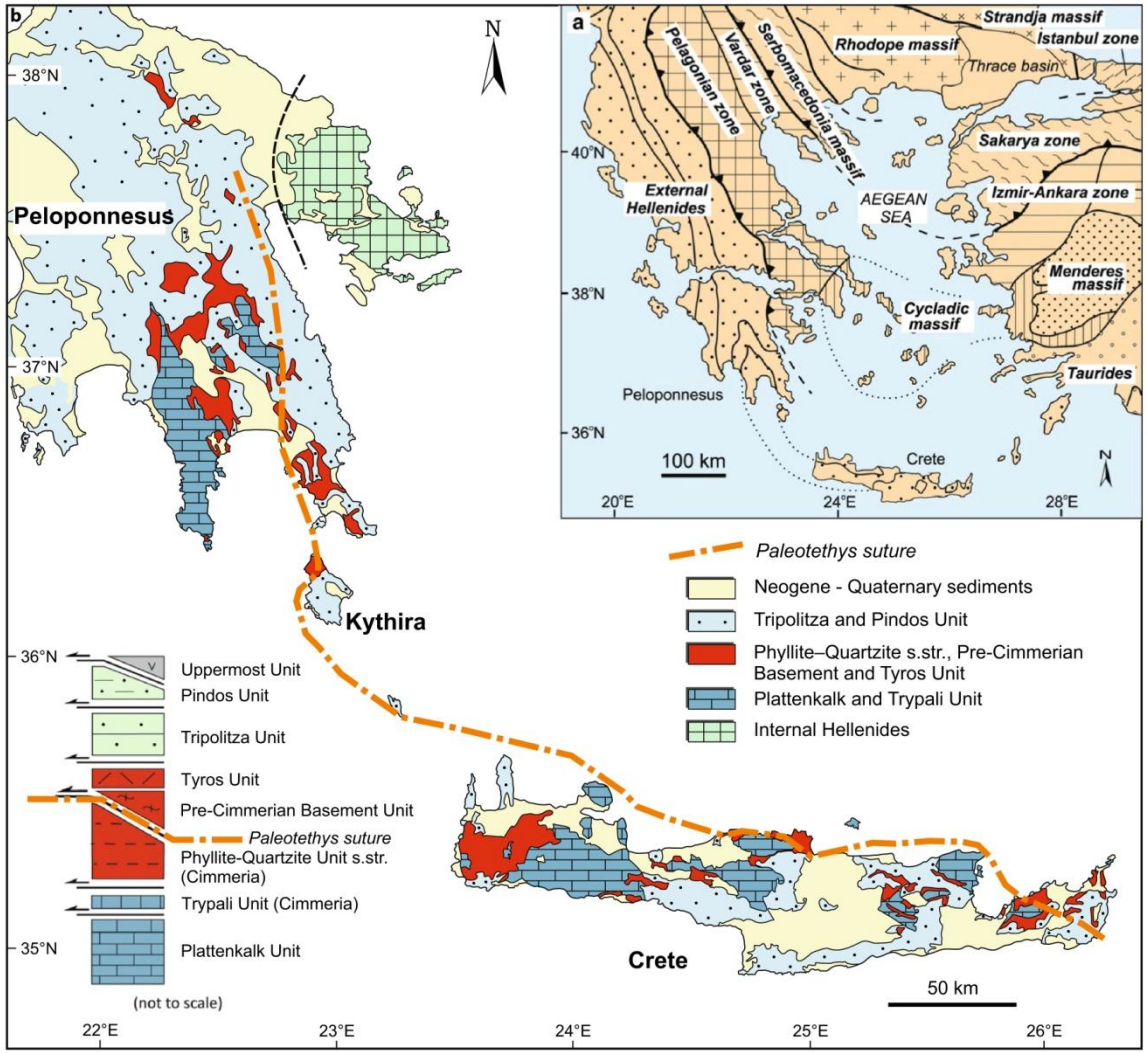

Fig. 1 **a** Map showing the distribution of main tectonic units in Greece and western Turkey in the eastern Mediterranean region (modified after Xypolias et al. 2006). **b** Simplified geological map of the External Hellenides in Peloponnesus and Crete (modified after Xypolias et al. 2007; Chatzaras et al. 2016). The trace of the Paleotethys suture (orange dashed line) is based on Dörr et al. (2015), Zulauf et al. (2015, 2016, 2018) and Chatzaras et al. (2016)

ΕΡΓΑΣΙΑ
ΥΠΑΙΘΡΟΥ

Hardness of minerals I: the Mohs scale

Mineralogists conventionally characterize the hardness of minerals by the Mohs Scale, which was devised by the German mineralogist Friedrich Mohs in 1812. This scale runs from 1 at the softest to 10 at the hardest, and any mineral assigned a greater value can scratch any mineral with a lesser value. Common minerals define the integer values on this scale, as is shown here. Common substances like glass and the human fingernail provide additional benchmarks convenient to measuring hardness according to the Mohs scale.

The Mohs scale is not linear, the integers assigned to key minerals do not allow determination of non-integer intermediate values, and the procedure for "scratching" was not well defined. More quantitative schemes to measure hardness include the Knoop scale, devised by Frederick Knoop of the U.S. National Bureau of Standards in 1939. Knoop hardness of a substance is determined by measuring the area of a "diamond-shaped" indentation made by a particular set of facets of a diamond pressed into the substance at a set pressure for a set time. Another scheme is the Vickers hardness test, devised by R.L. Smith and G.E. Sandland, engineers at Vickers, Ltd. of the United Kingdom in the 1920s. Vickers hardness is similarly determined by measuring the area of a square indentation made by a diamond at a given pressure. Other measures of hardness include Brinell Hardness, which measures the area of the indentation made by a steel sphere, and Rockwell Hardness, which measures the depth of the indentation made by a steel sphere or a diamond-tipped cone.

This plot shows the non-linearity of the Mohs scale by comparing the hardness of its index minerals to their hardness as measured by the Knoop and Vickers methods. Further pages in this series seek to explain some of the controls on hardness of minerals.

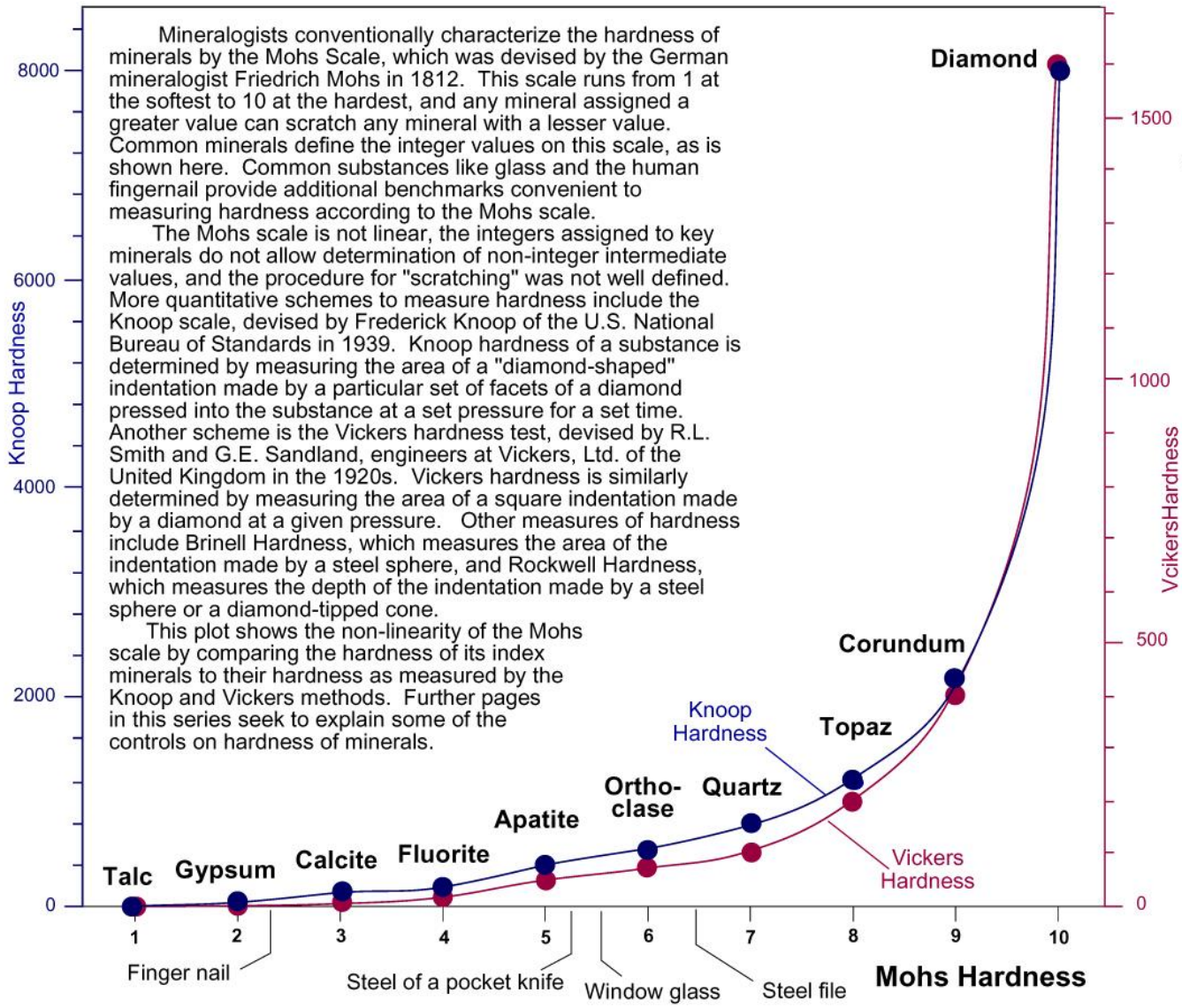

A Knoop indenter:

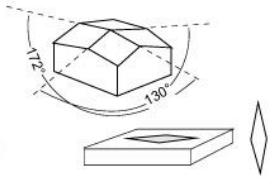

A Vickers indenter:

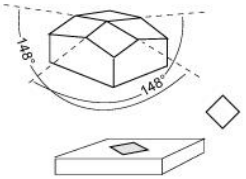

Original literature:
Mohs Hardness: Mohs, F., 1822, *Grundriß der Mineralogie* (two volumes, 1822 and 1824): Dresden, Arnoldschen Buchhandlung (translated to English by Wilhelm Ritter von Haidinger as *Treatise on Mineralogy* in 1825 and published by Constable & Co. Ltd. of Edinburgh).
Vickers Hardness: Smith, R.L., and Sandland, G.E., 1925, Some notes on the use of a diamond pyramid for hardness testing: *J. Iron St. Inst.*, v. 111, p. 285-294.
Knoop Hardness: Knoop, F., Peters, C.G., and Emerson, W.B., 1939, A sensitive pyramidal-diamond tool for indentation measurements: *Journal of Research of the National Bureau of Standards*, v. 23, p. 39-61 (see esp. Table 8).

Other sources:
University of Maryland Center for Advanced Life Cycle Engineering, ~2005, *Material Hardness:* www.calce.umd.edu/general/Facilities/Hardness_ad_.htm#3.6.2.
Archae Solenhofen, 2003, *Rock properties and their importance to stoneworking,carving, and lapidary working of rocks and minerals by the ancient Egyptians:* www.geocities.com/unforbidden_geology/rock_properties.htm

Hardness of minerals VI: effect of crystal face and direction

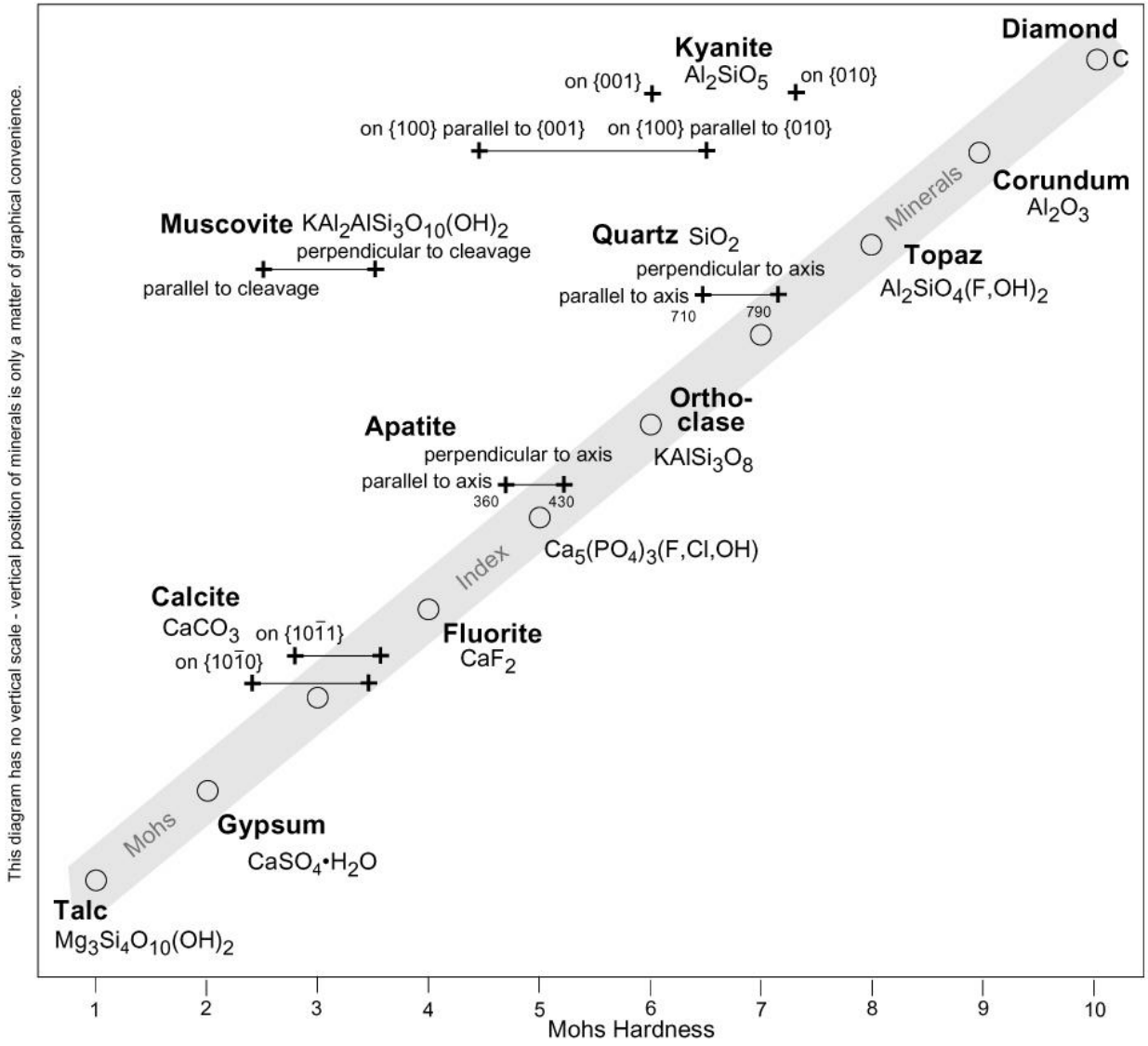

Simple discussions of hardness of minerals assume that any mineral has one value of hardness. In fact, in many minerals hardness varies from crystal face to crystal face, and it also commonly varies with direction on any one crystal face. Hardness in therefore said to be "anisotropic", or to vary with direction relative to the crystal structure. This dependence of hardness on orientation is to be expected if one appreciates that hardness is measured by defornation (scratching or indentation) of the crystal structure via the breakage of bonds, and that different surfaces intersect the crystal structure at different orientations, subjecting different bonds, and different frequencies of bonds, to breakage.

One of the most strking examples of this effect is kyanite, where hardness varies across several units of the Mohs scale. Significant variation also exists within quartz, apatite, and calcite, three index minerals of the Mohs scale. Thus defining integer values of Mohs hardness by the hardness of a particular mineral is problematic, because at least some of those minerals, and probably all of them, have hardnesses that vary.

Sources:

Knoop, F., Peters, C.G., and Emerson, W.B., 1939, A sensitive pyramidal-diamond tool for indentation measurements: *Journal of Research of the National Bureau of Standards*, v. 23, p. 39-61 (see esp. Table 8).

Gaines, R.V., et al., 1997, *Dana's New Mineralogy:* New York, John Wiley & Sons, 1819 p.

von Tertsch, H., 1950, Beobachtungen über Vickers-microhärte am kalkspat: *Mikroskopie: Zentralblatt für Mikroskopische Forschung und Methodik*, v. 5, p. 172-183. Depiction of von Tertsch's data here is best considered qualitative, because the quantitative data reported defy simple transfer to this diagram.

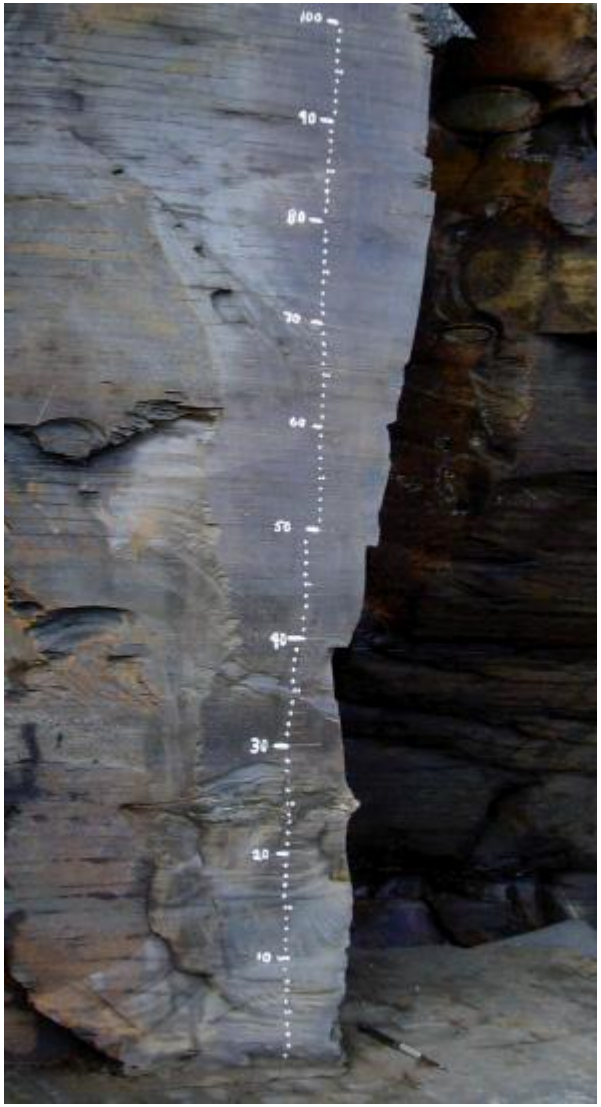

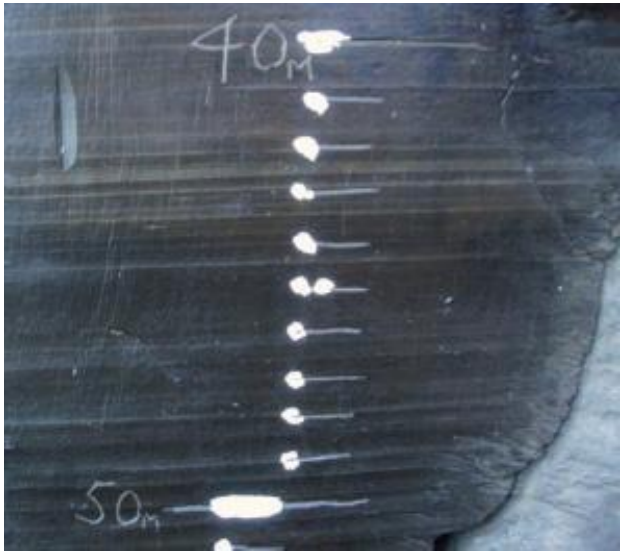

ΦΟΡΗΤΟ ΦΑΣΜΑΤΟΜΕΤΡΟ ΦΘΟΡΙΣΜΟΥ ΑΚΤΙΝΩΝ-Χ (XRF)

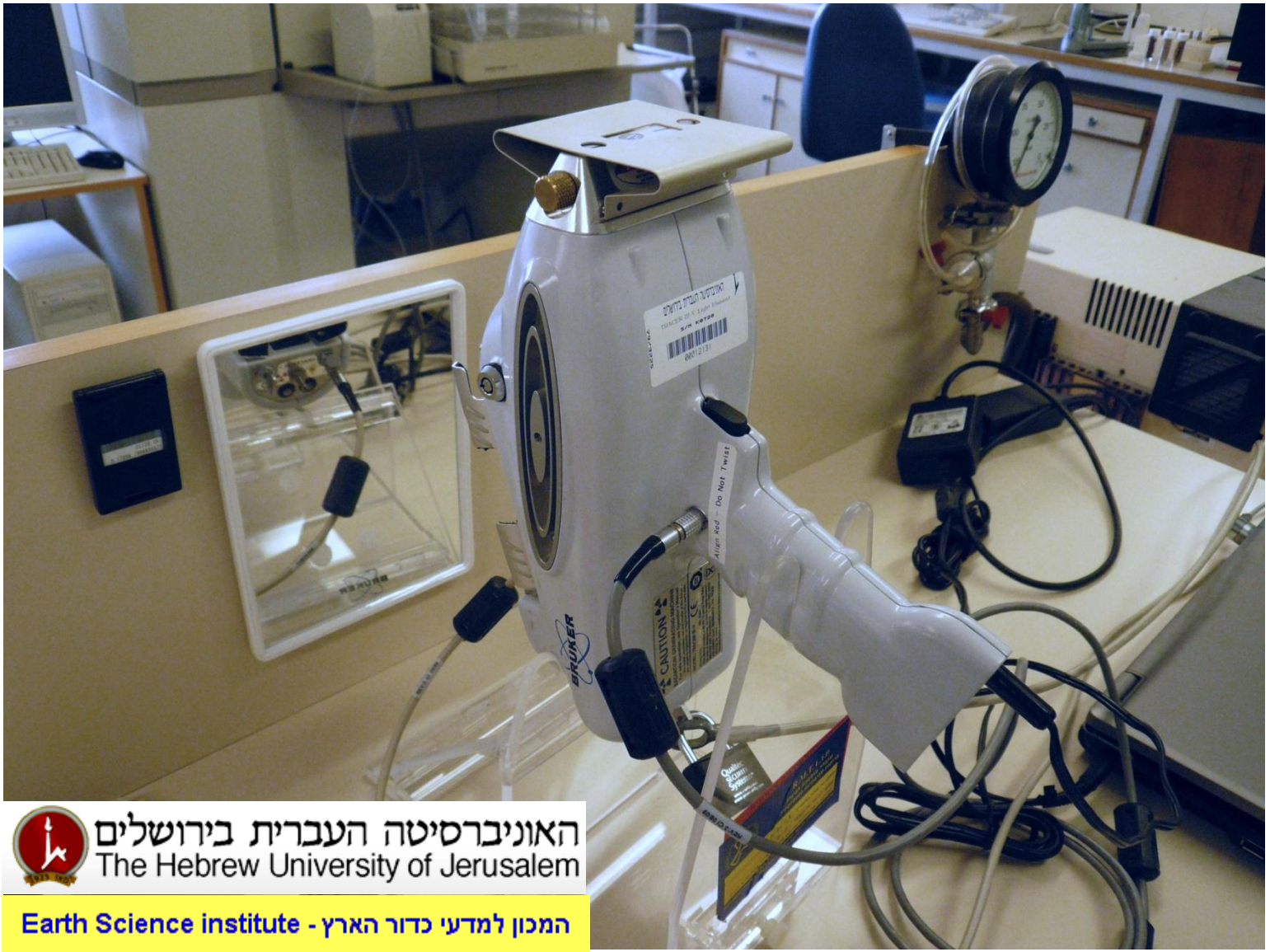

האוניברסיטה העברית בירושלים
The Hebrew University of Jerusalem

Earth Science institute - המכון למדעי כדור הארץ

ΦΟΡΗΤΟ ΠΕΡΙΘΛΑΣΙΜΕΤΡΟ ΑΚΤΙΝΩΝ-Χ (XRD)

inXitu

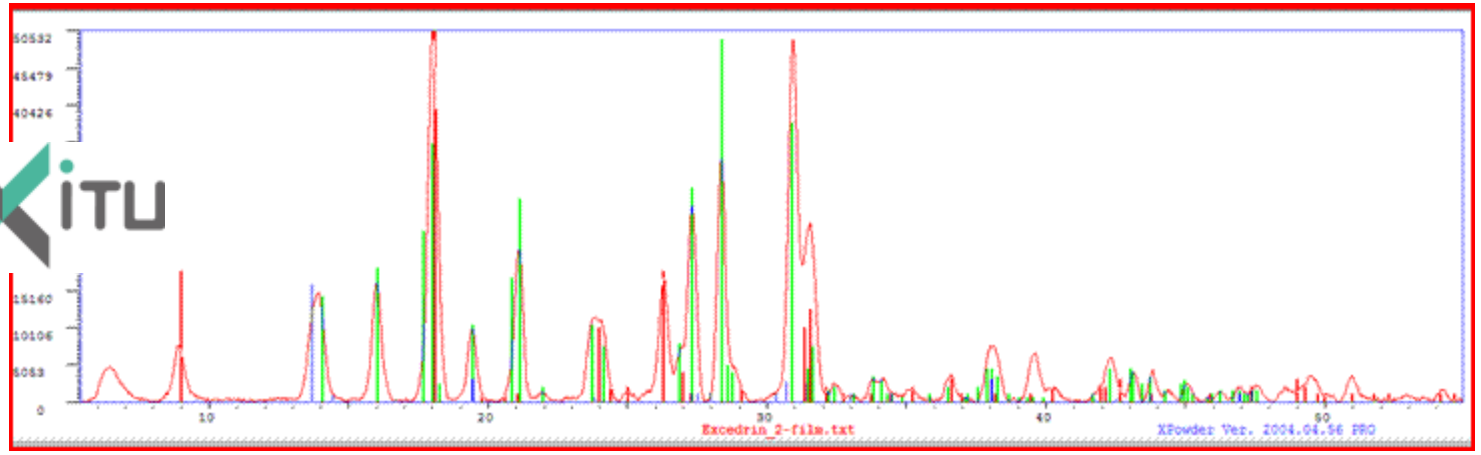

Lunar and Planetary Science XXXVIII (2007)

MINERALOGICAL IN-SITU INVESTIGATION OF ACID-SULFATE SAMPLES FROM THE RIO TINTO RIVER, SPAIN, WITH A PORTABLE XRD/XRF INSTRUMENT. P. Sarrazin[1], D.W. Ming[2], R.V. Morris[2], D. Fernández-Remolar[3], R. Amils[3], R.E. Arvidson[4], D. Blake[5], D. L. Bish[6], [1]inXitu Inc., 2551 Casey Ave Ste A, Mountain View, CA 94043 psarrazin@inxitu.com; [2] NASA Johnson Space Center, Mail Code KX3, Houston, TX 77058; [3] Centro de Astrobiología (CSIC/INTA) 28850 Torrejón de Ardoz, Madrid, Spain; [4] Earth and Planetary Sciences, Washington University, St. Louis, MO 63130; [5] NASA Ames Research Center, Moffett Field, CA 94035; [6] Dept. of Geological Sciences, Indiana Univ., Bloomington, IN 47405-1405.

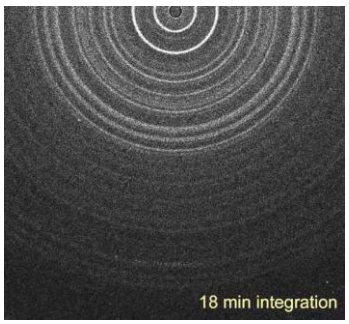

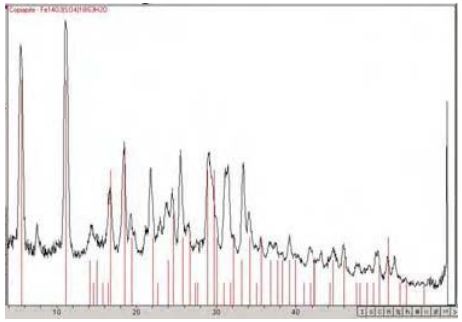

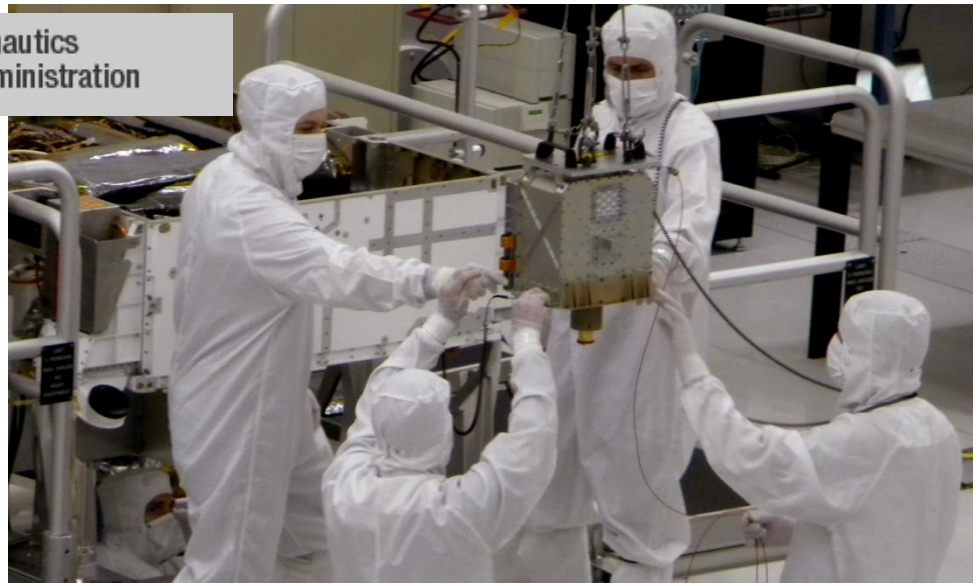

PHILIPPE SARRAZIN

inXitu

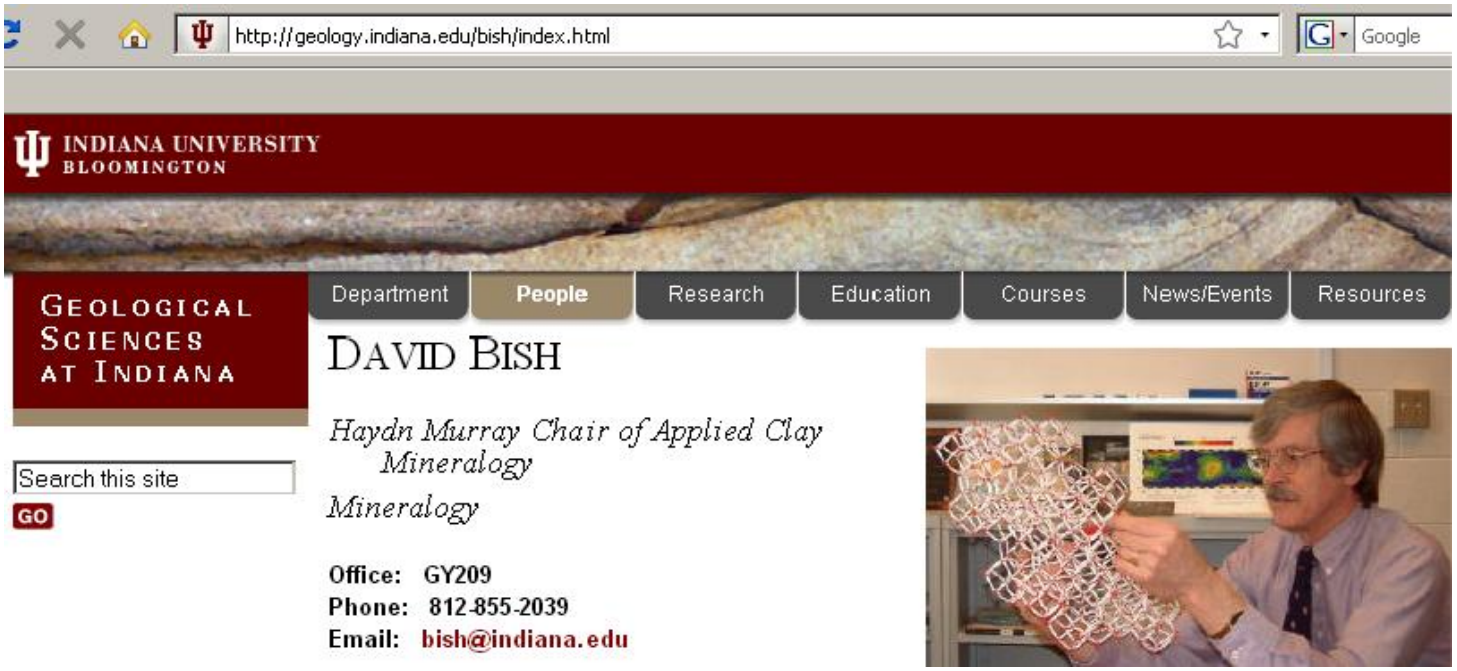

ΠΙΣΩ ΣΤΟ ΕΡΓΑΣΤΗΡΙΟ

ΠΕΡΙΘΛΑΣΗ ΑΚΤΙΝΩΝ-Χ

Περιθλασίμετρο Ακτίνων-Χ Σκόνης

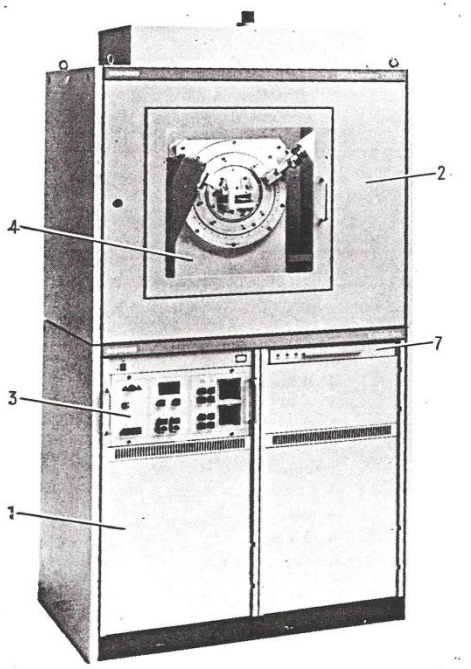

1 Standgehäuse
Console
Console

2 Strahlenschutzgehäuse
Radiation protection
Boîtier de protection des radiations

3 Röntgengenerator KRISTALLOFLEX®
KRISTALLOFLEX® X-ray generator
Générateur de rayons X KRISTALLOFLEX®

4 Goniometer
Goniometer
Goniomètre

7 Bedienfeld
Control panel
Panneau de commande

ΟΠΤΙΚΟ ΜΙΚΡΟΣΚΟΠΙΟ ΔΙΕΡΧΟΜΕΝΟΥ ΦΩΤΟΣ (ΠΟΛΩΤΙΚΟ-ΠΕΤΡΟΓΡΑΦΙΚΟ) & ΑΝΑΚΛΩΜΕΝΟΥ ΦΩΤΟΣ (ΜΕΤΑΛΛΟΓΡΑΦΙΚΟ)

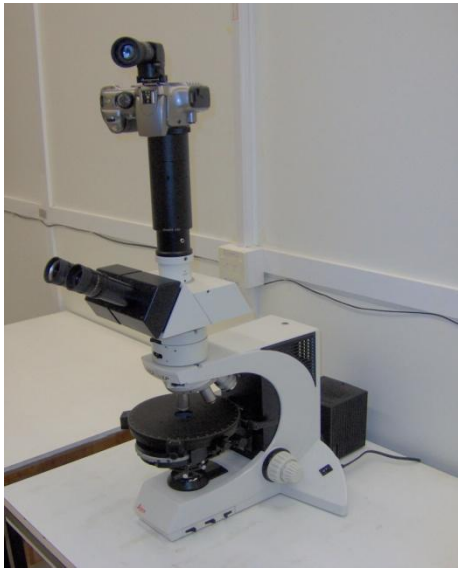

ΣΑΡΩΤΙΚΟ ΗΛΕΚΤΡΟΝΙΚΟ ΜΙΚΡΟΣΚΟΠΙΟ (SEM)

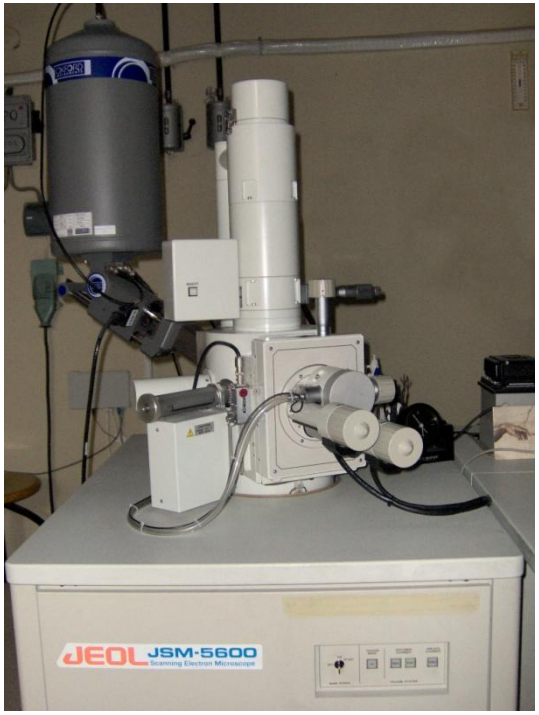

ΗΛΕΚΤΡΟΝΙΚΟ ΜΙΚΡΟΣΚΟΠΙΟ ΔΙΕΡΧΟΜΕΝΩΝ ΗΛΕΚΤΡΟΝΙΩΝ (TEM)

ΜΙΚΡΟΣΚΟΠΙΟ ΑΤΟΜΙΚΗΣ ΔΥΝΑΜΗΣ (AFM)

ΣΑΡΩΤΙΚΟ ΗΛΕΚΤΡΟΝΙΚΟ ΜΙΚΡΟΣΚΟΠΙΟ (SEM) – **ΗΛΕΚΤΡΟΝΙΚΗ ΜΙΚΡΟΑΝΑΛΥΣΗ (EPMA)**

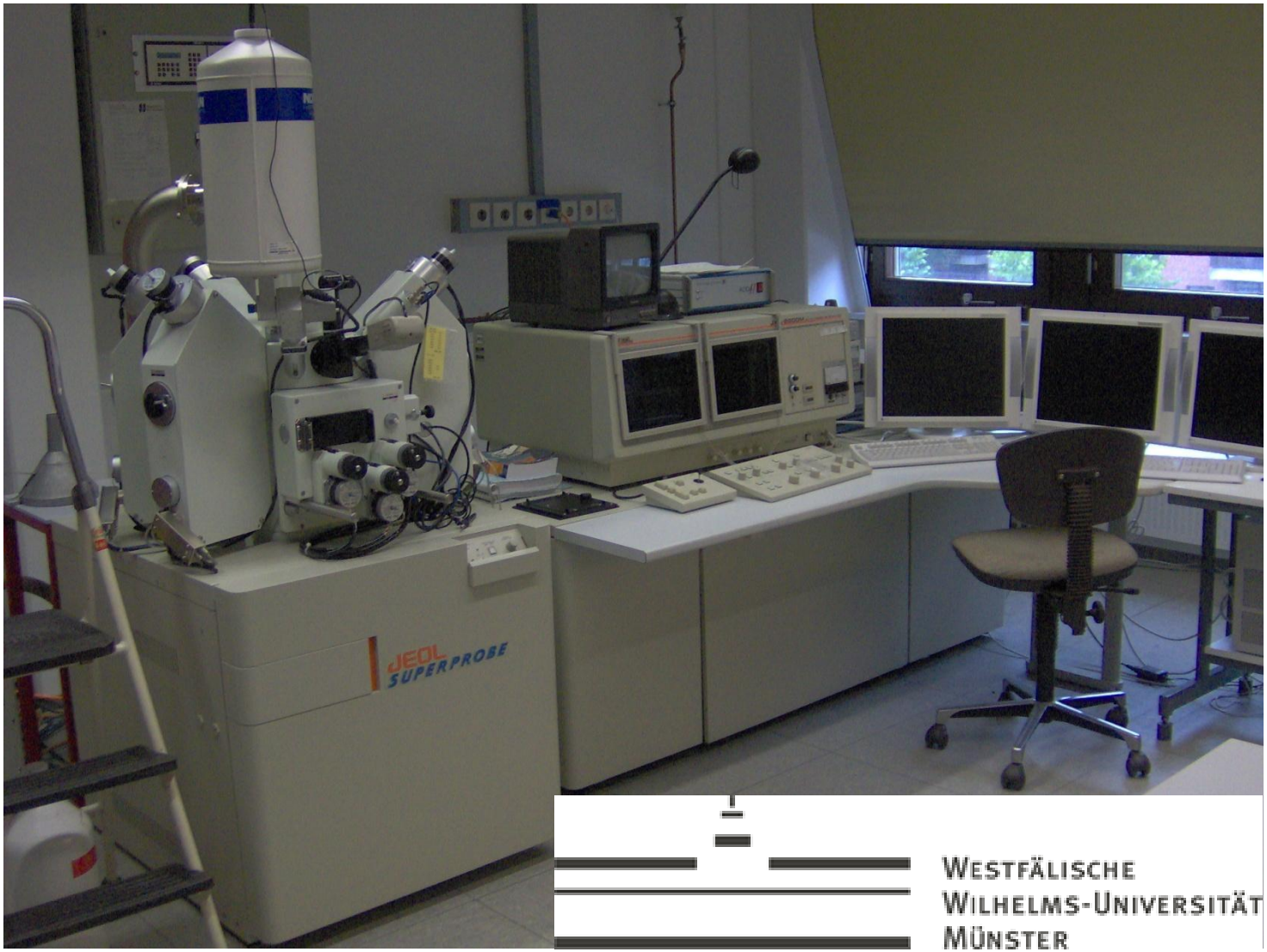

WESTFÄLISCHE
WILHELMS-UNIVERSITÄT
MÜNSTER

ΟΛΙΚΗ ΑΝΑΛΥΣΗ ΙΧΝΟΣΤΟΙΧΕΙΩΝ

ICP-MS

האוניברסיטה העברית בירושלים
The Hebrew University of Jerusalem

Earth Science institute - המכון למדעי כדור הארץ

ΣΗΜΕΙΑΚΗ ΑΝΑΛΥΣΗ ΙΧΝΟΣΤΟΙΧΕΙΩΝ

LA-ICP-MS

ΟΛΙΚΗ & ΣΗΜΕΙΑΚΗ ΑΝΑΛΥΣΗ ΙΣΟΤΟΠΩΝ

LA-MC-ICP-MS

האוניברסיטה העברית בירושלים
The Hebrew University of Jerusalem

Earth Science institute - המכון למדעי כדור הארץ

ΨΥΞΗ ΜΑΓΜΑΤΟΣ
(σειρά κρυστάλλωσης ορυκτών κατά Bowen)

VOLUME XXX NUMBER 3

THE

JOURNAL OF GEOLOGY

April-May 1922

THE REACTION PRINCIPLE IN PETROGENESIS

N. L. BOWEN
Geophysical Laboratory, Carnegie Institution of Washington

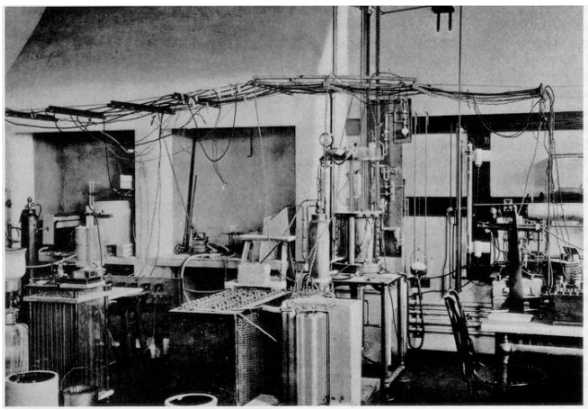

TABLE II

REACTION SERIES IN SUB-ALKALINE ROCKS

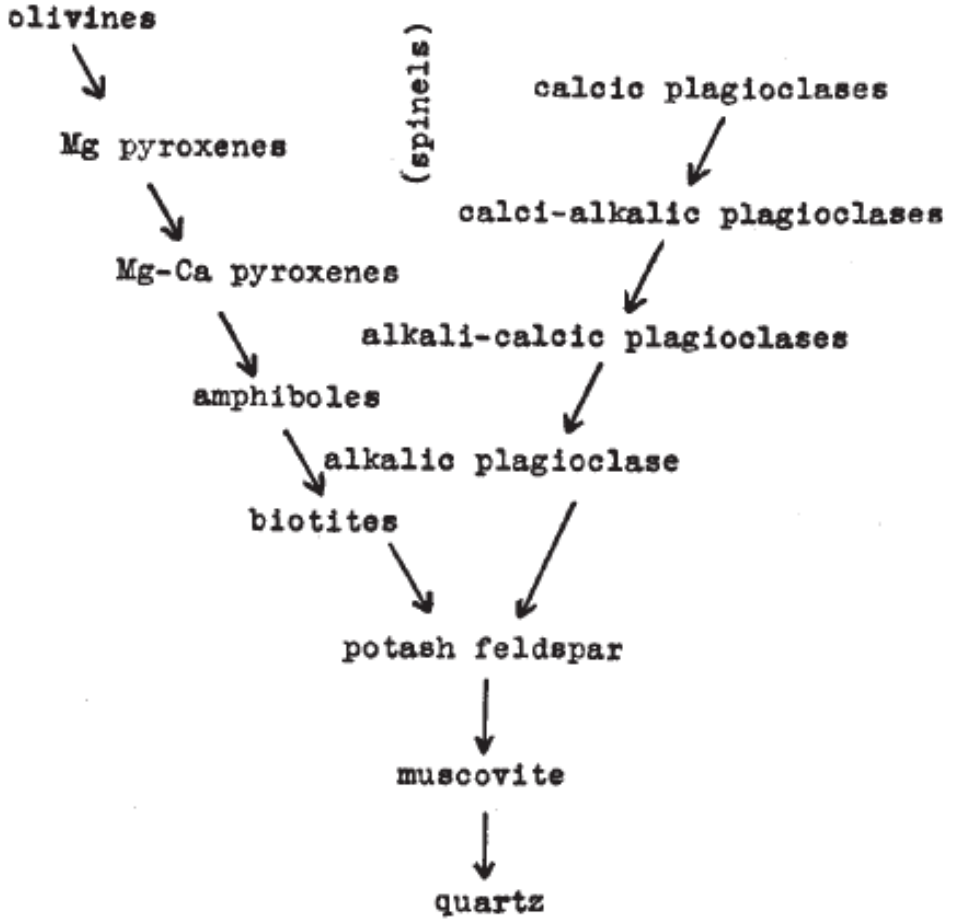


ΧΑΛΑΖΙΑΣ :
SiO_2

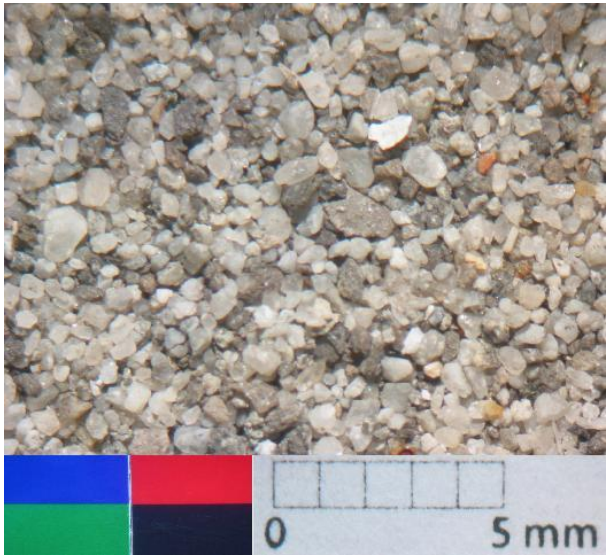
0
5 mm

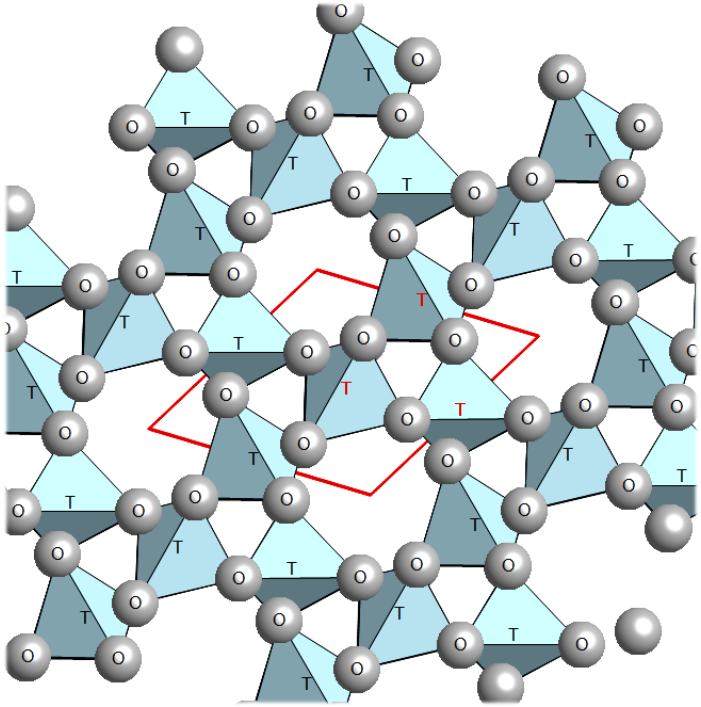
O
T

ΣΚΛΗΡΟΤΗΤΑ (Mohs) = 7

ΔΕΝ ΑΝΑΒΡΑΖΕΙ

X

Χαλαζίας χαμηλής Τ
(low quartz)
α-Χαλαζίας
Κρυσταλλώνεται σε
T<573 °C

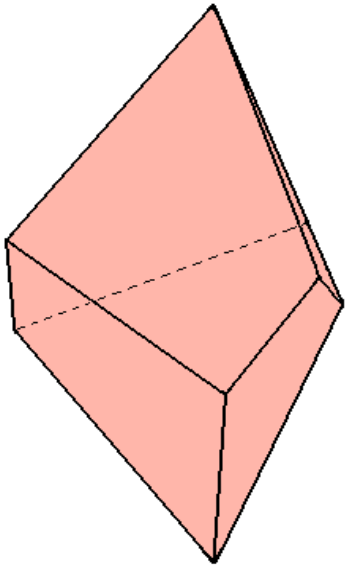

Τριγωνικό Τραπεζόεδρο

$L^3\ 3L^2_{πολ.}$

Χαλαζίας υψηλής Τ
(high quartz)
β-Χαλαζίας
Κρυσταλλώνεται σε
T>573 °C

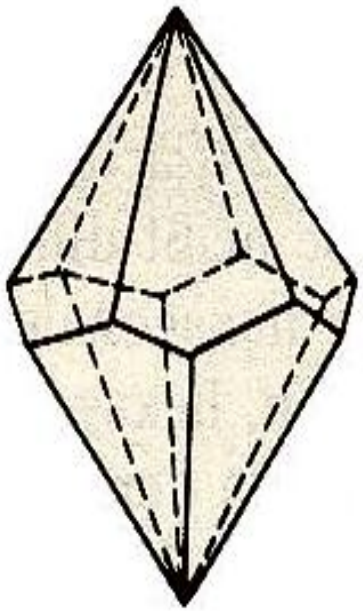

Εξαγωνικό Τραπεζόεδρο

$L^6\ 3L^2\ 3L'^2$

ΠΟΛΥΜΟΡΦΙΣΜΟΣ ΦΥΣΙΚΟΥ SiO_2

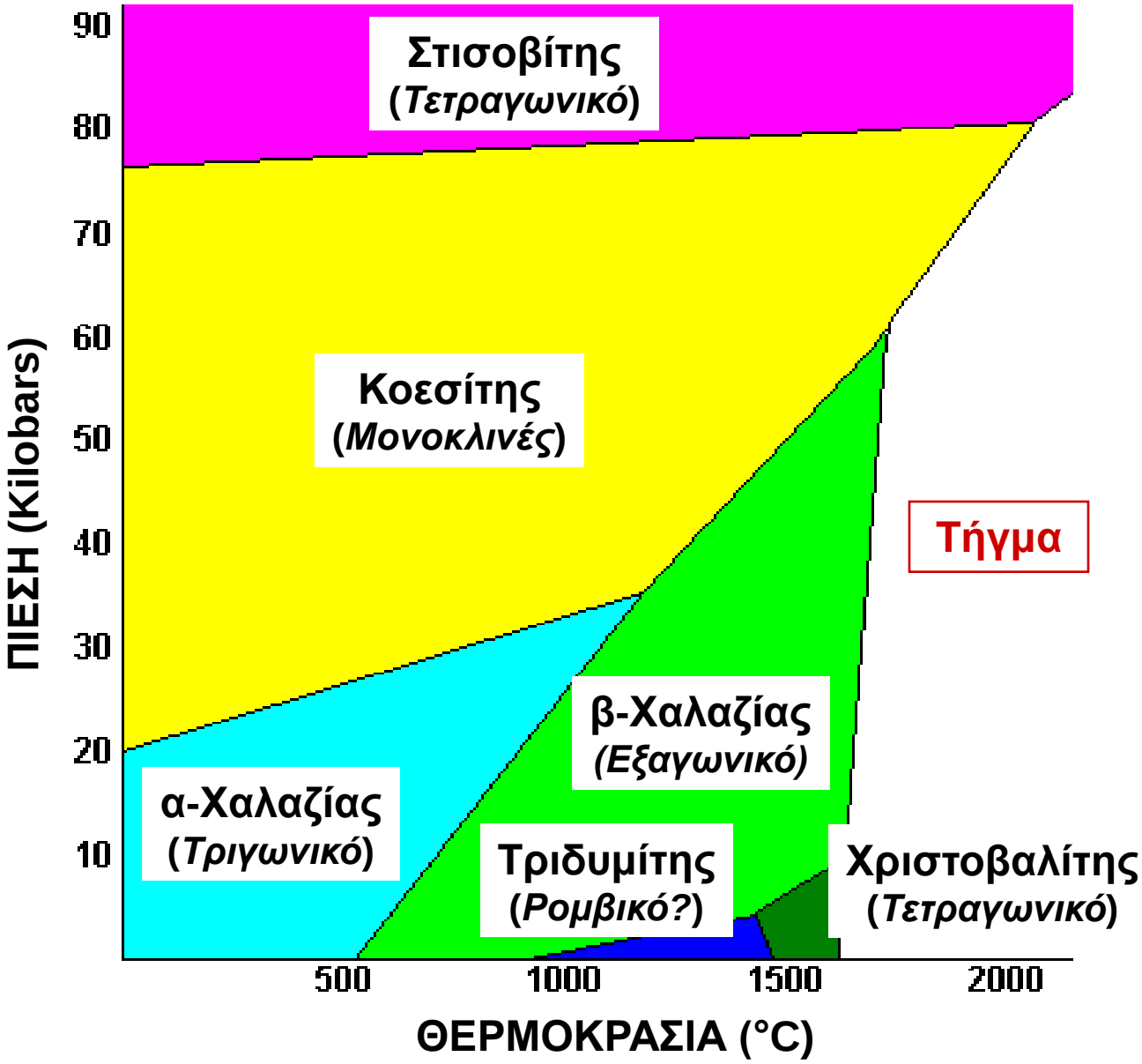

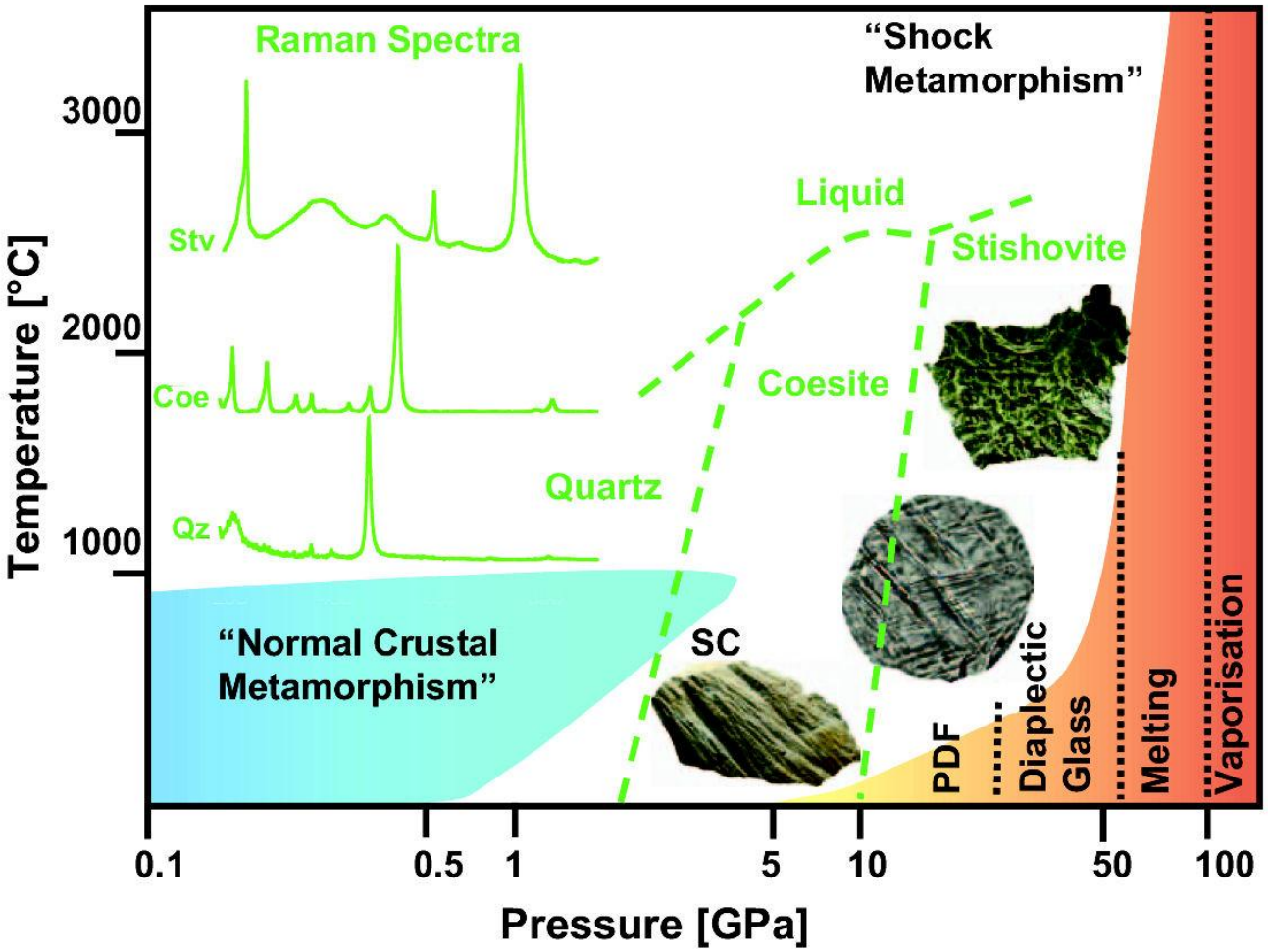

FIGURE 3 Pressure (P)–temperature (T) diagram, showing the different regimes for "normal" crustal metamorphism and shock metamorphism. Various P–T regions characterized by the development of specific shock-metamorphic effects are indicated. Also shown are the stability fields for quartz (Qz), coesite (Coe), and stishovite (Stv), typical Raman spectra for these minerals, and liquidi for the various SiO_2 polymorphs. SC = shatter cone; PDF = planar deformation feature. DIAGRAM BY JORG FRITZ, MUSEUM FÜR NATURKUNDE BERLIN

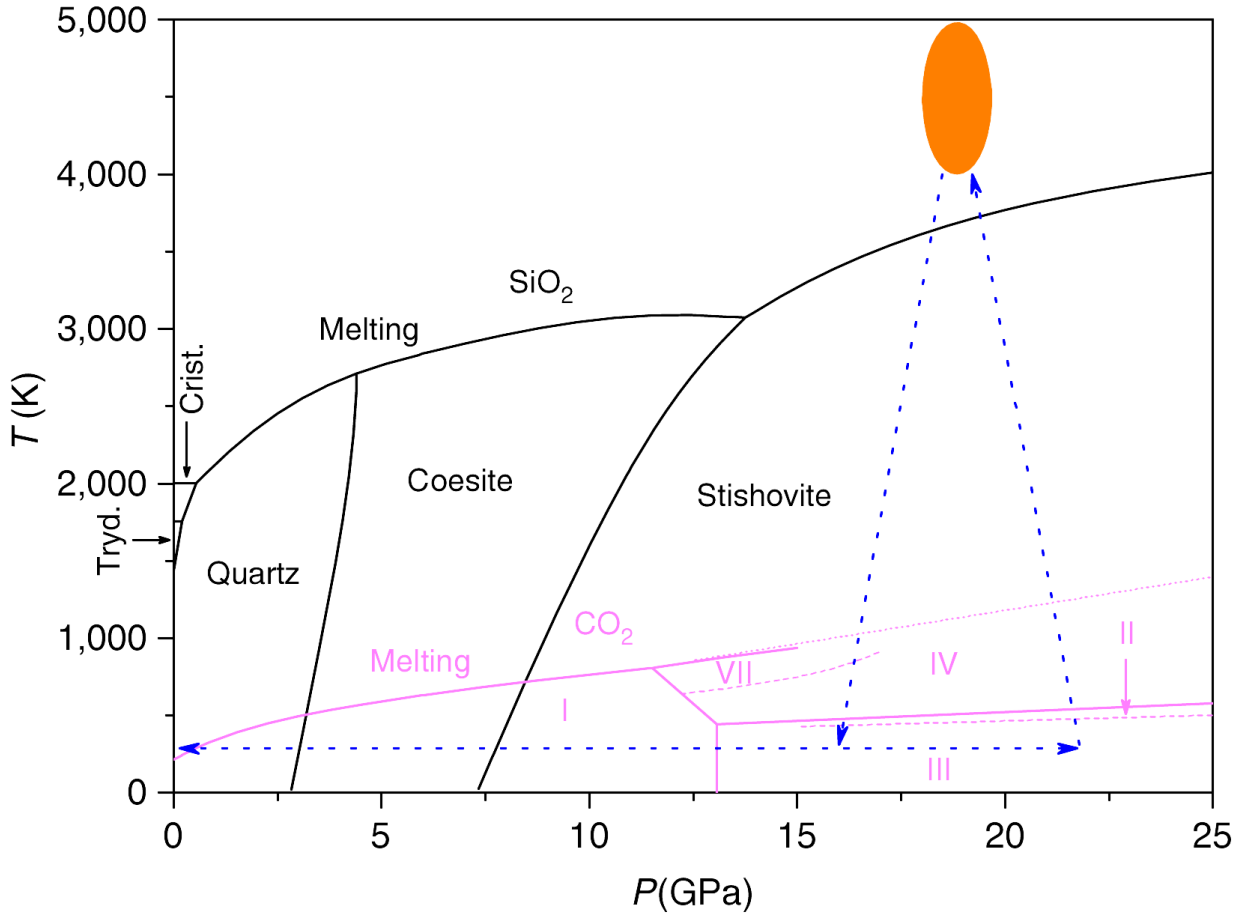

Figure 1 | Pure SiO_2 and CO_2 phase diagrams and P-T path. Black lines: SiO_2 phase boundaries[17]. Light magenta, continuous and dotted lines: CO_2 phase boundaries; light magenta, dashed lines: kinetic boundaries for CO_2[11,18–20]. Blue dashed arrows and orange ellipse: P-T path followed in this study. All five solid phases of CO_2 shown are molecular crystals. Non-molecular CO_2 phases are formed above 25–30 GPa. Crist, cristobalite; Tryd, trydimite.

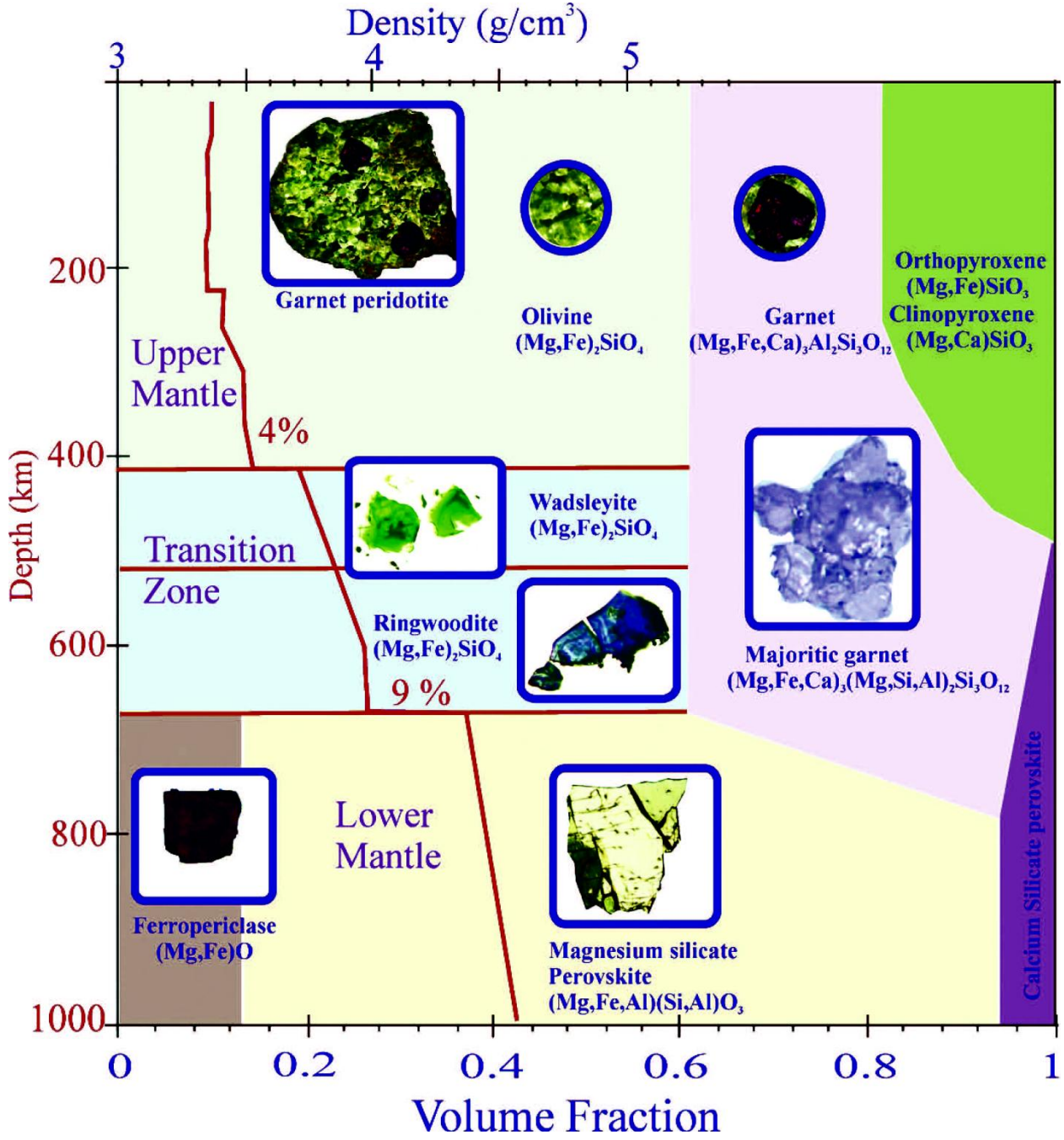
Density (g/cm3)
3
4
5
Depth (km)
200
400
600
800
1000
0
0.2
0.4
0.6
0.8
1
Volume Fraction
Upper Mantle
4%
Transition Zone
9 %
Lower Mantle
Garnet peridotite
Olivine
(Mg,Fe)2SiO4
Garnet
(Mg,Fe,Ca)3Al2Si3O12
Orthopyroxene
(Mg,Fe)SiO3
Clinopyroxene
(Mg,Ca)SiO3
Wadsleyite
(Mg,Fe)2SiO4
Ringwoodite
(Mg,Fe)2SiO4
Majoritic garnet
(Mg,Fe,Ca)3(Mg,Si,Al)2Si3O12
Ferropericlase
(Mg,Fe)O
Magnesium silicate
Perovskite
(Mg,Fe,Al)(Si,Al)O3
Calcium Silicate perovskite

Μπριντγκμανίτης (bridgmanite-$MgSiO_3$)

AGU Blogosphere
American Geophysical Union
A community
HOME BLOGS ABOUT

GeoSpace
Earth and space science
HOME ABOUT CONTACT US

6 JUNE 2014

Earth's most abundant mineral finally gets a name

Posted by nbompey

By JoAnna Wendel

The mineral said to be the most abundant of our planet, but found so deep within Earth's interior that scientists usually cannot observe it directly, now has a name.

On June 2, bridgmanite was approved as the formal name for one of the Earth's most plentiful yet elusive minerals known to exist in the Earth's lower mantle. Bridgmanite, which was formerly known simply as silicate-perovskite, is named after the 1946 Nobel Prize winning physicist Percy Bridgman.

Scientists have known for decades that bridgmanite existed in the Earth's interior, but had been unable to successfully characterize a naturally occurring sample until this year.

"This [find] fills a vexing gap in the taxonomy of minerals," Oliver Tschauner, an associate research professor at the University of Nevada-Las Vegas who characterized the mineral, said in an email.

Tschauner, along with Chi Ma, a senior scientist and mineralogist at the California Institute of Technology in Pasadena, Calif., have been working to chemically and structurally characterize natural silicate-perovskite ($MgSiO_3$) since 2009.

Ο άνθρακας (C) στο εσωτερικό της Γής

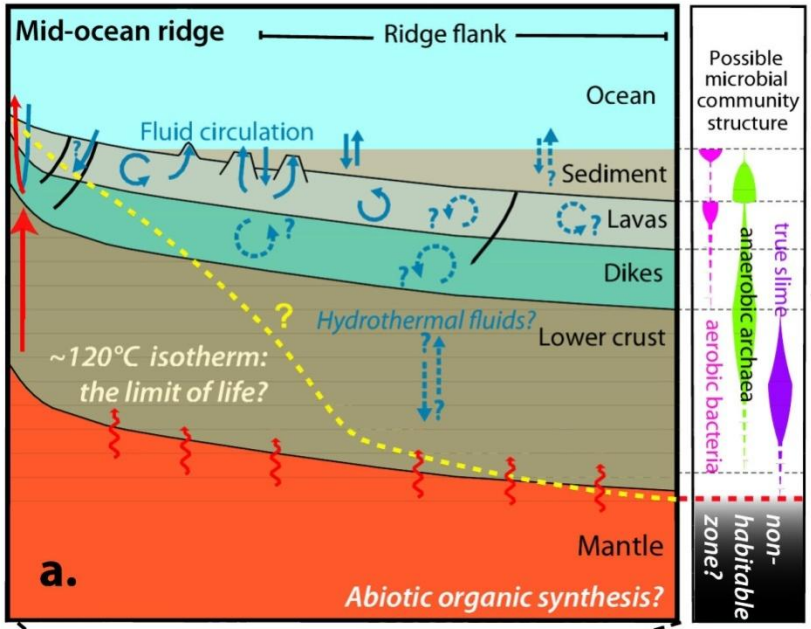

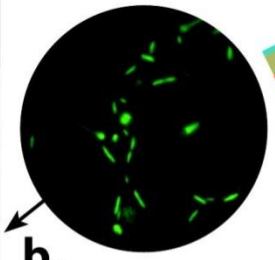

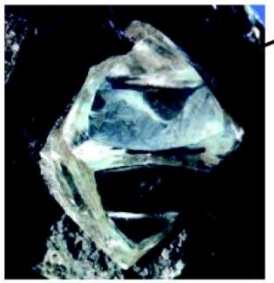

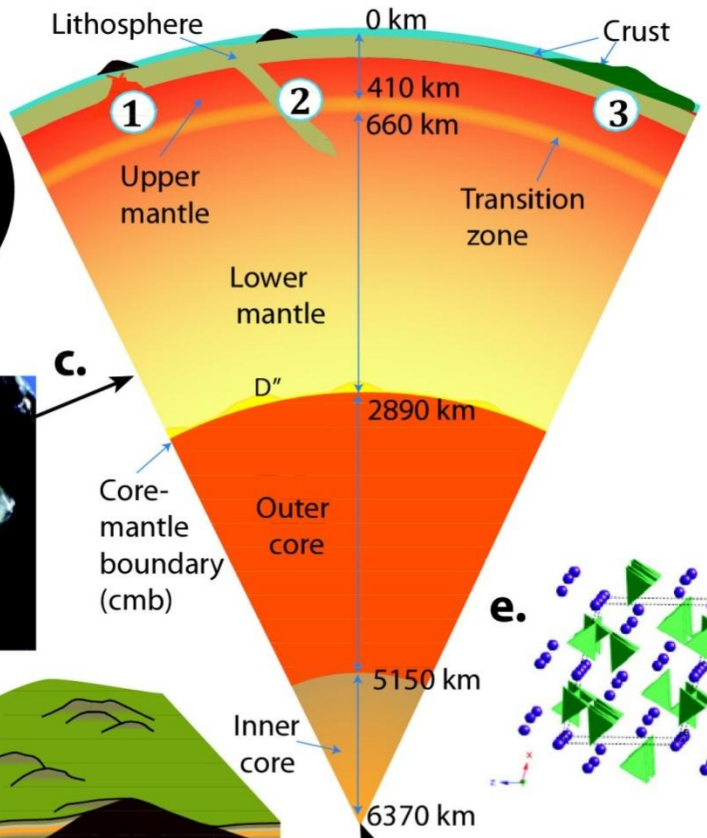

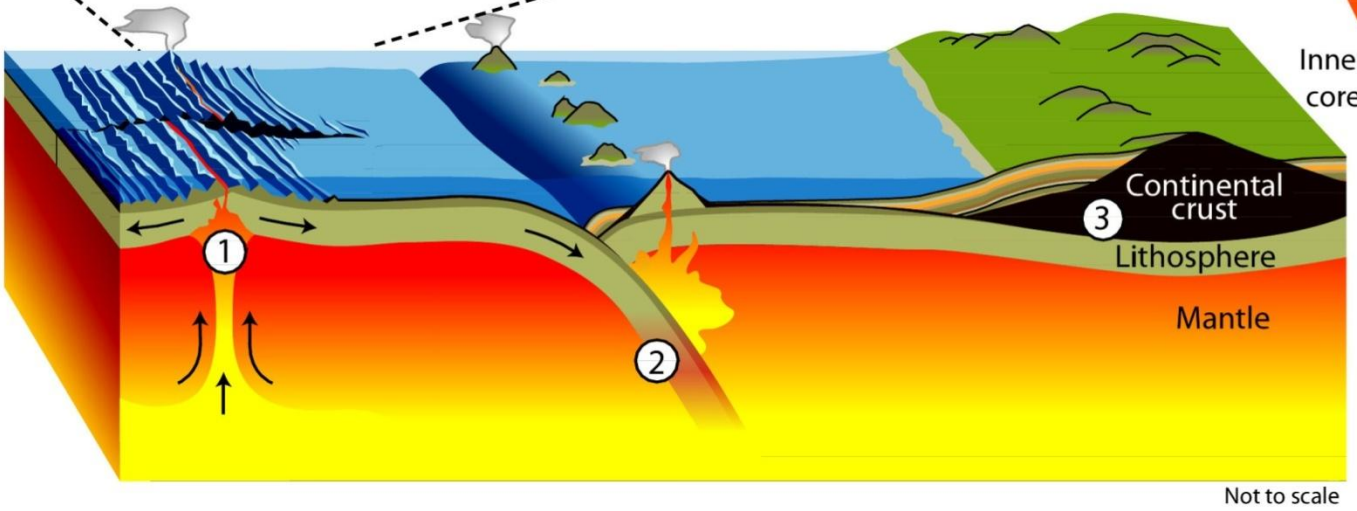

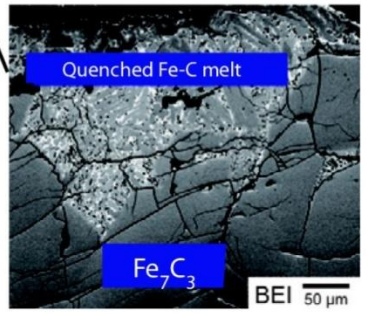

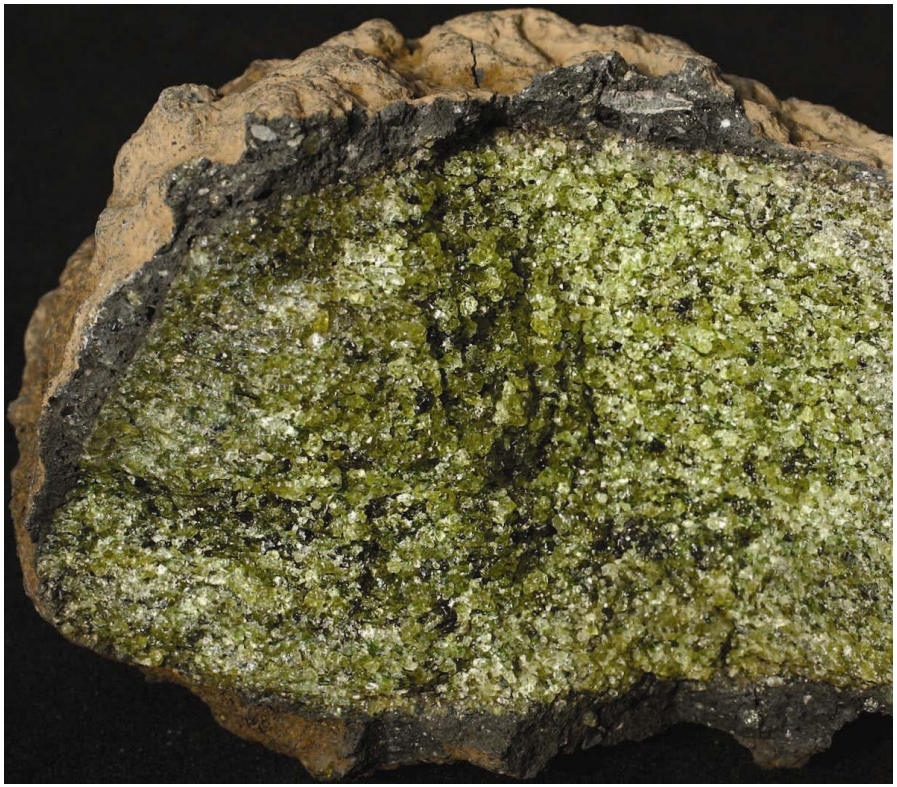

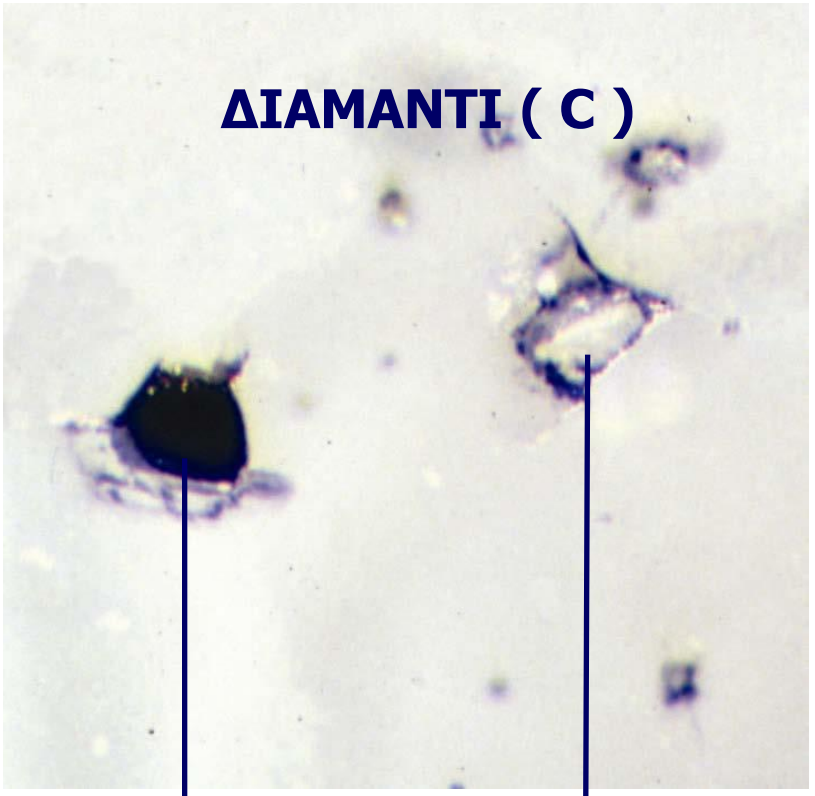

Fe-ΠΕΡΙΚΛΑΣΤΟ
(Mg,Fe)O

Πυρόξενος
από μετασχηματισμό
ΠΕΡΟΒΣΚΙΤΗ
($MgSiO_3$)

DEEP CARBON OBSERVATORY

Mantle Carbon Content Influences Plate Tectonics

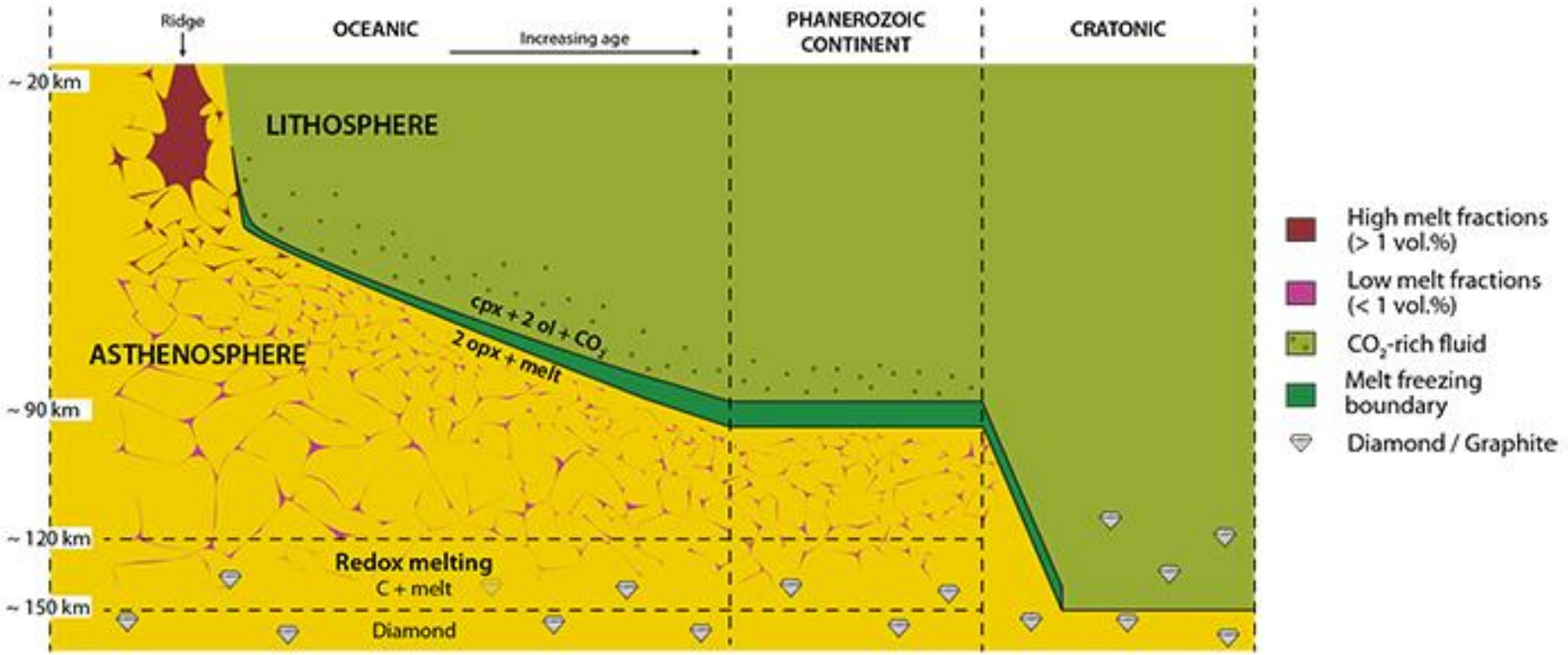

Image credit: Sifré D. (CNRS Orléans, France)

nature geoscience

NATURE GEOSCIENCE | LETTER

Carbon dioxide released from subduction zones by fluid-mediated reactions

Jay J. Ague & Stefan Nicolescu

Affiliations | Contributions | Corresponding author

Nature Geoscience **7**, 355–360 (2014) | doi:10.1038/ngeo2143

Received 19 September 2013 | Accepted 17 March 2014 | Published online 20 April 2014

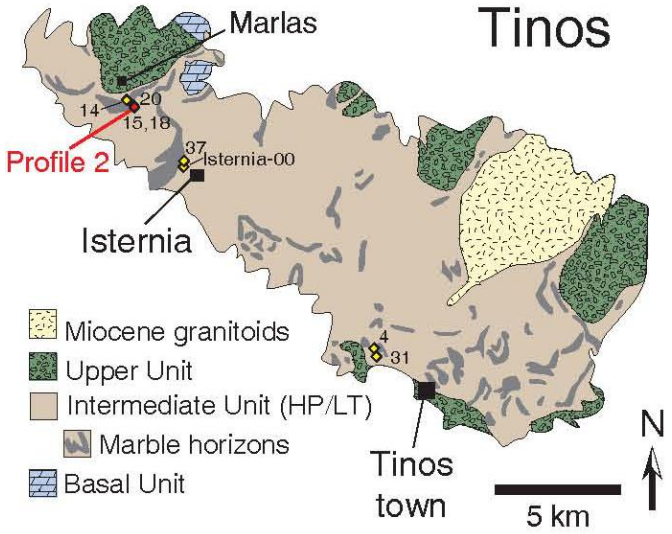

Κρύσταλλοι επιδότου στα πετρώματα της Τήνου

Crystals of epidote from a quartz vein on Tinos island, Greece

Μονοκλινές

Επίδοτο

epidote

$Ca_2Fe^{3+}Al_2O(Si_2O_7)(SiO_4)(OH)$

$\angle \beta = 115{,}4°$

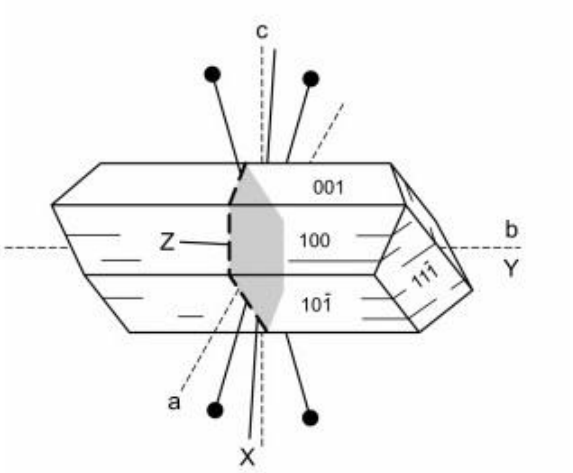

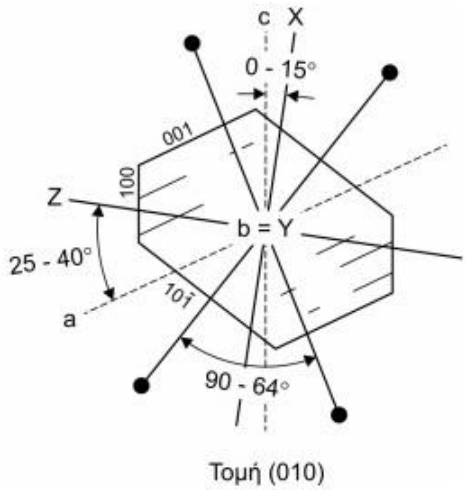

Τομή (010)

n_α	= 1,715 - 1,751	Διάξονας (–)
n_β	= 1,725 - 1,784	$2V_\alpha$ = 90-64°
n_γ	= 1,734 - 1,797	a:Z = 25-40°, b = Y, c:X = 0-15°
δ	= 0,012 - 0,049	EOA // (010)
		r>v ισχυρός

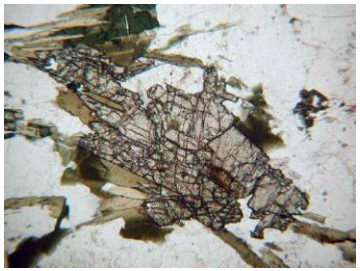

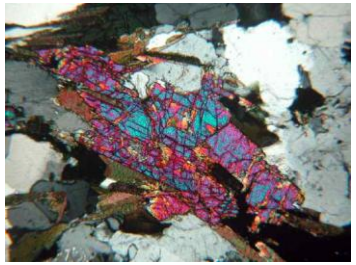

http://www.geo.auth.gr/courses/gmo/gmo212y/

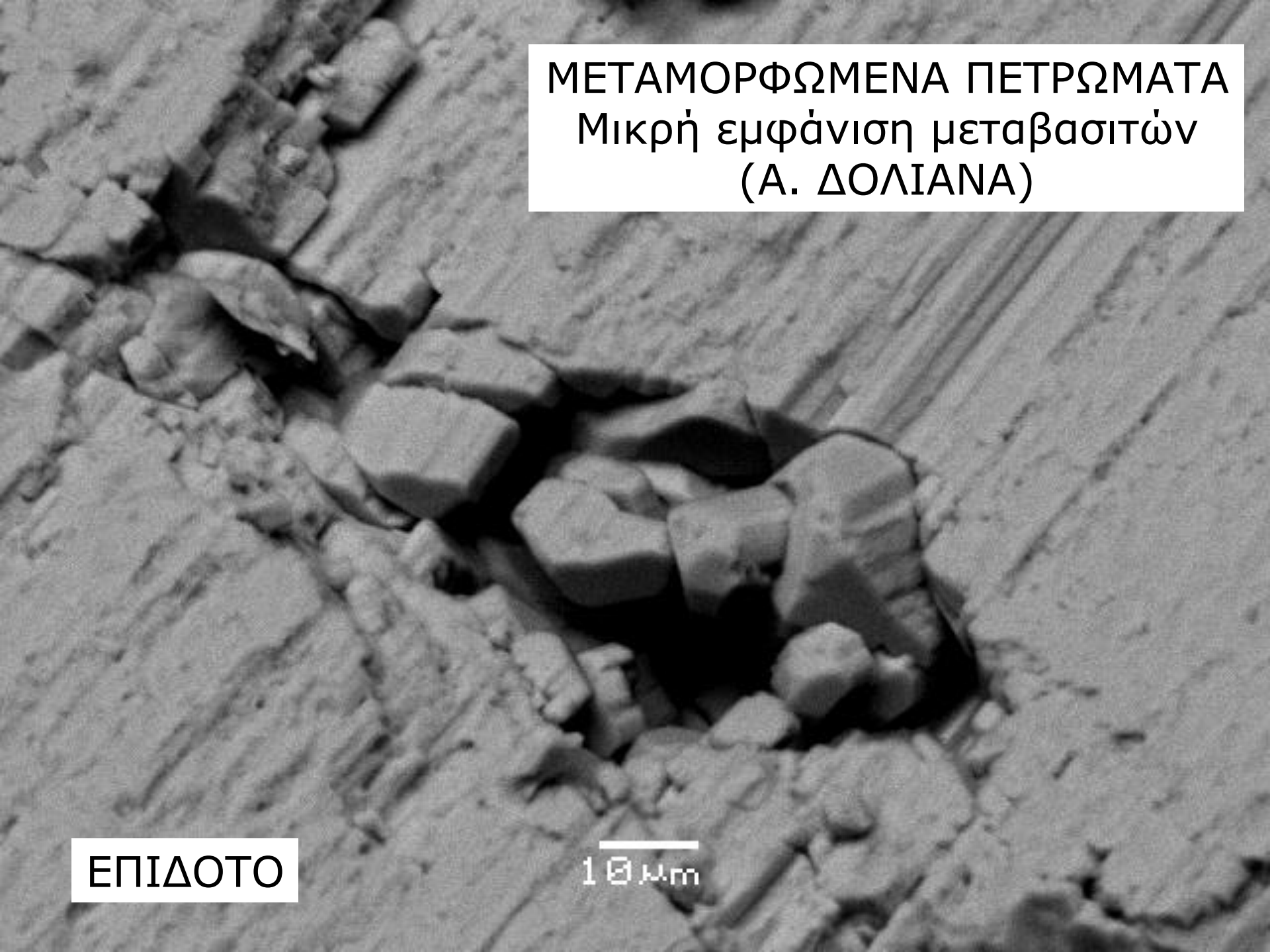
ΜΕΤΑΜΟΡΦΩΜΕΝΑ ΠΕΤΡΩΜΑΤΑ
Μικρή εμφάνιση μεταβασιτών
(Α. ΔΟΛΙΑΝΑ)
ΕΠΙΔΟΤΟ
10 μm

Α. ΔΟΛΙΑΝΑ

ΕΠΙΔΟΤΟ

ΑΣΤΡΙΟΙ

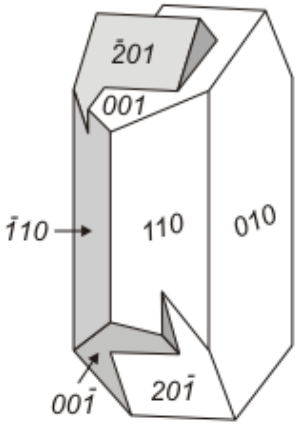

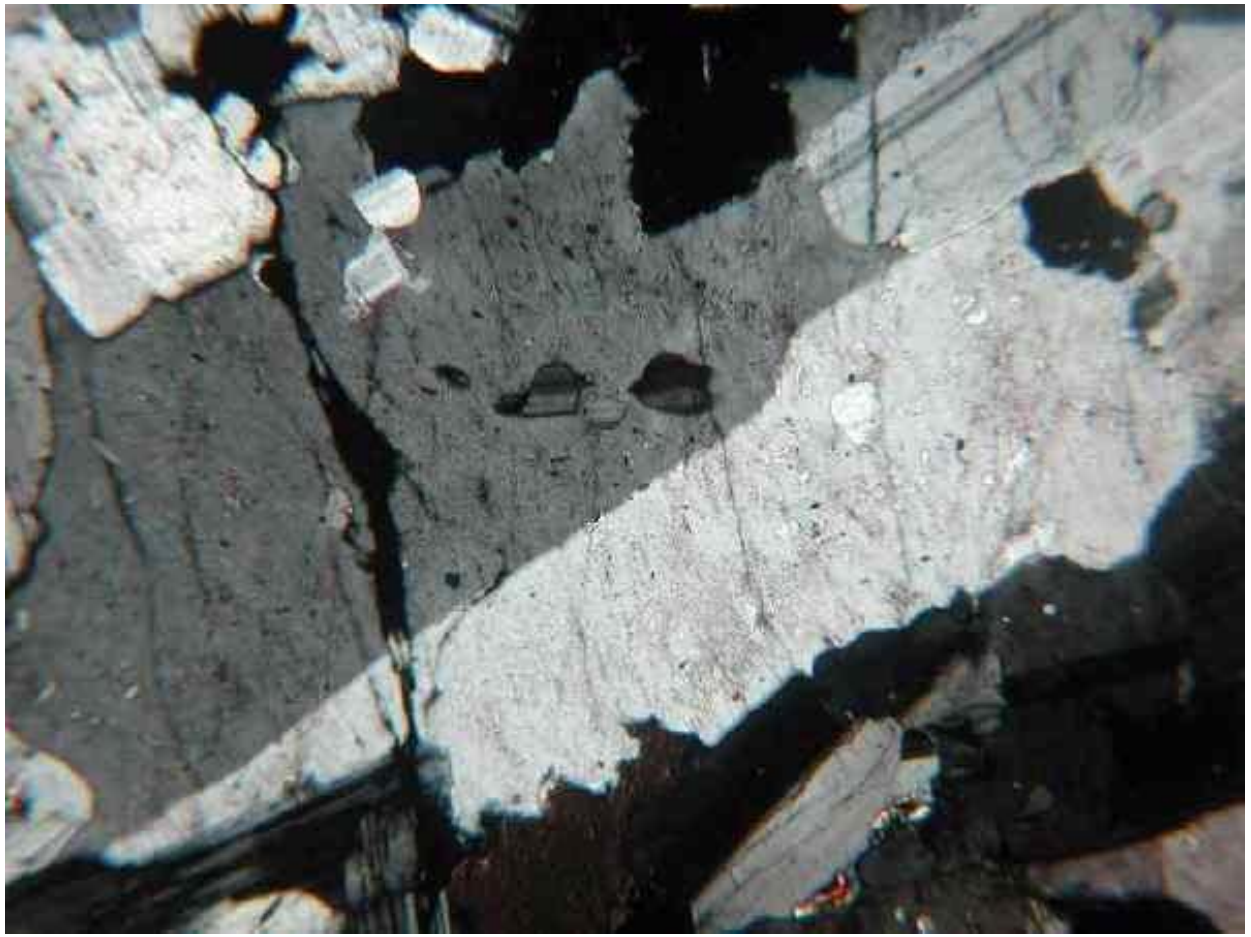

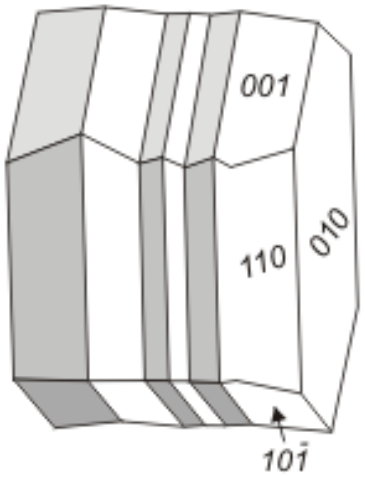

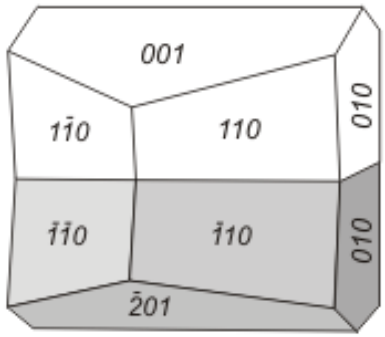

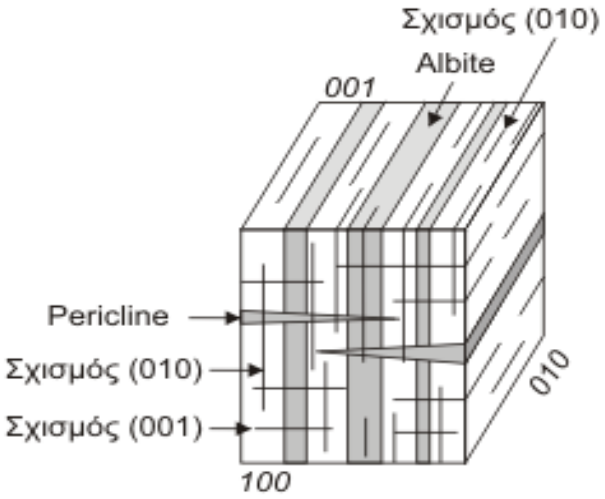

Albite
Επίπεδο διδυμίας (010)
Άξονας διδυμίας _|_ (010)

Pericline
Επίπεδο διδυμίας (h0l)
Άξονας διδυμίας [010]

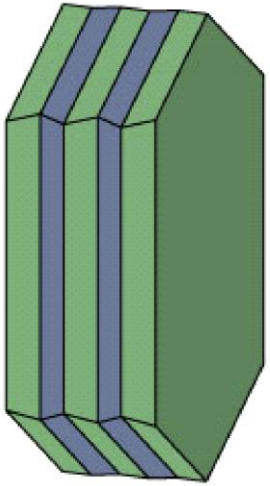

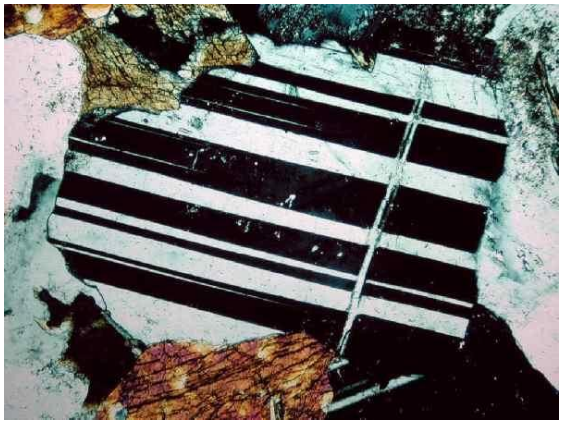

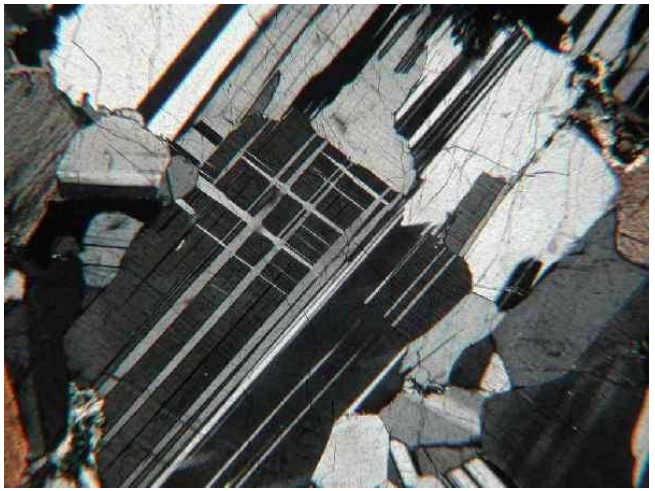

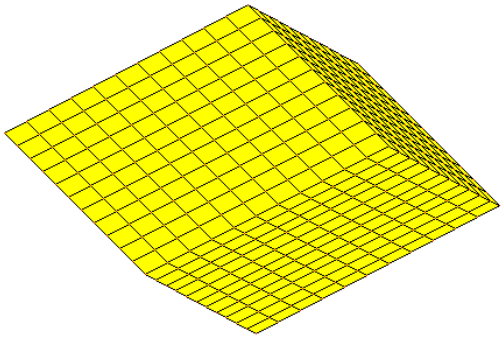

ΑΣΒΕΣΤΙΤΗΣ : $CaCO_3$

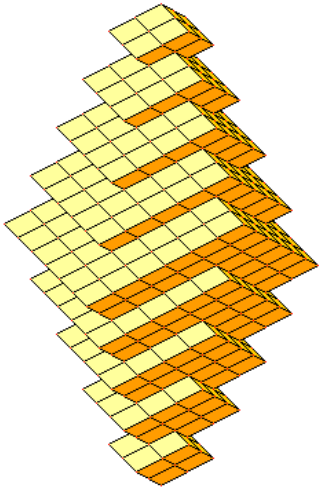

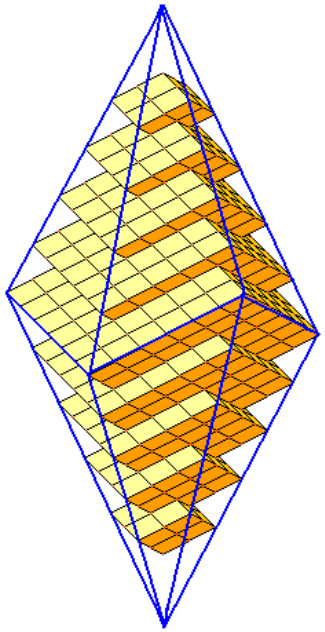

Σκαληνόεδρο (scalenohedron) ασβεστίτη

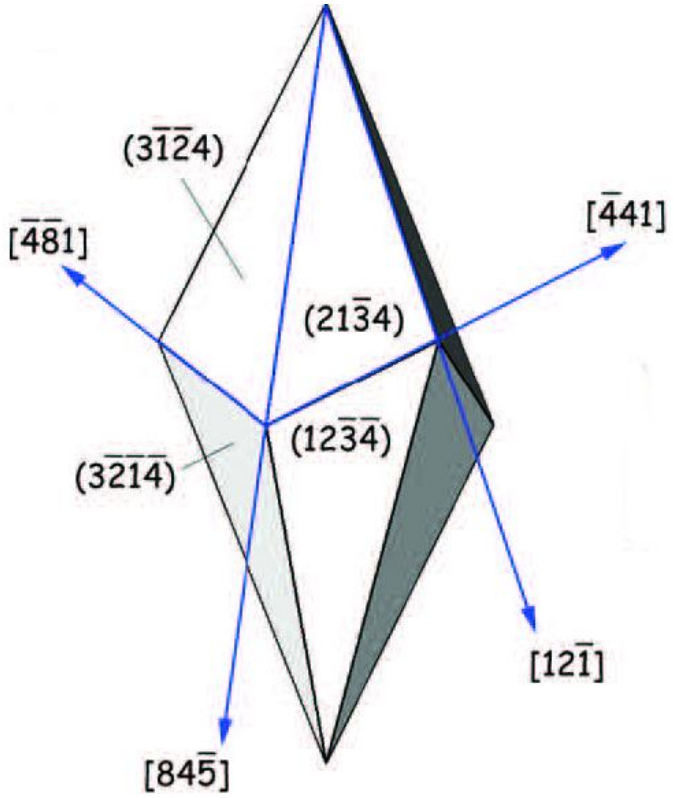

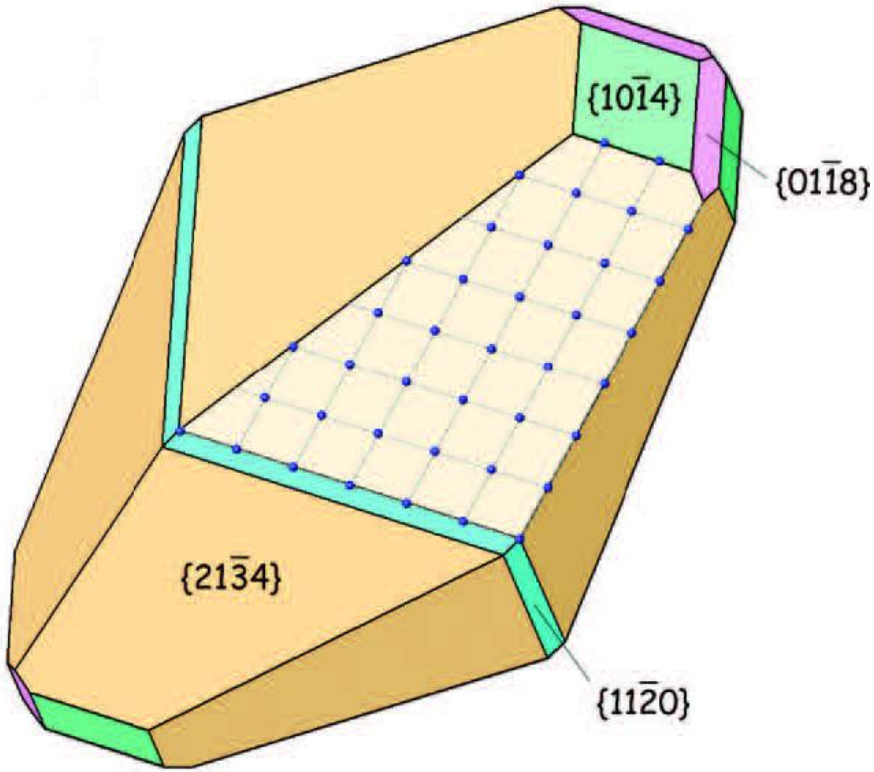

Ασβεστόλιθοι - Μάρμαρα

Α. ΔΟΛΙΑΝΑ

Α. ΔΟΛΙΑΝΑ

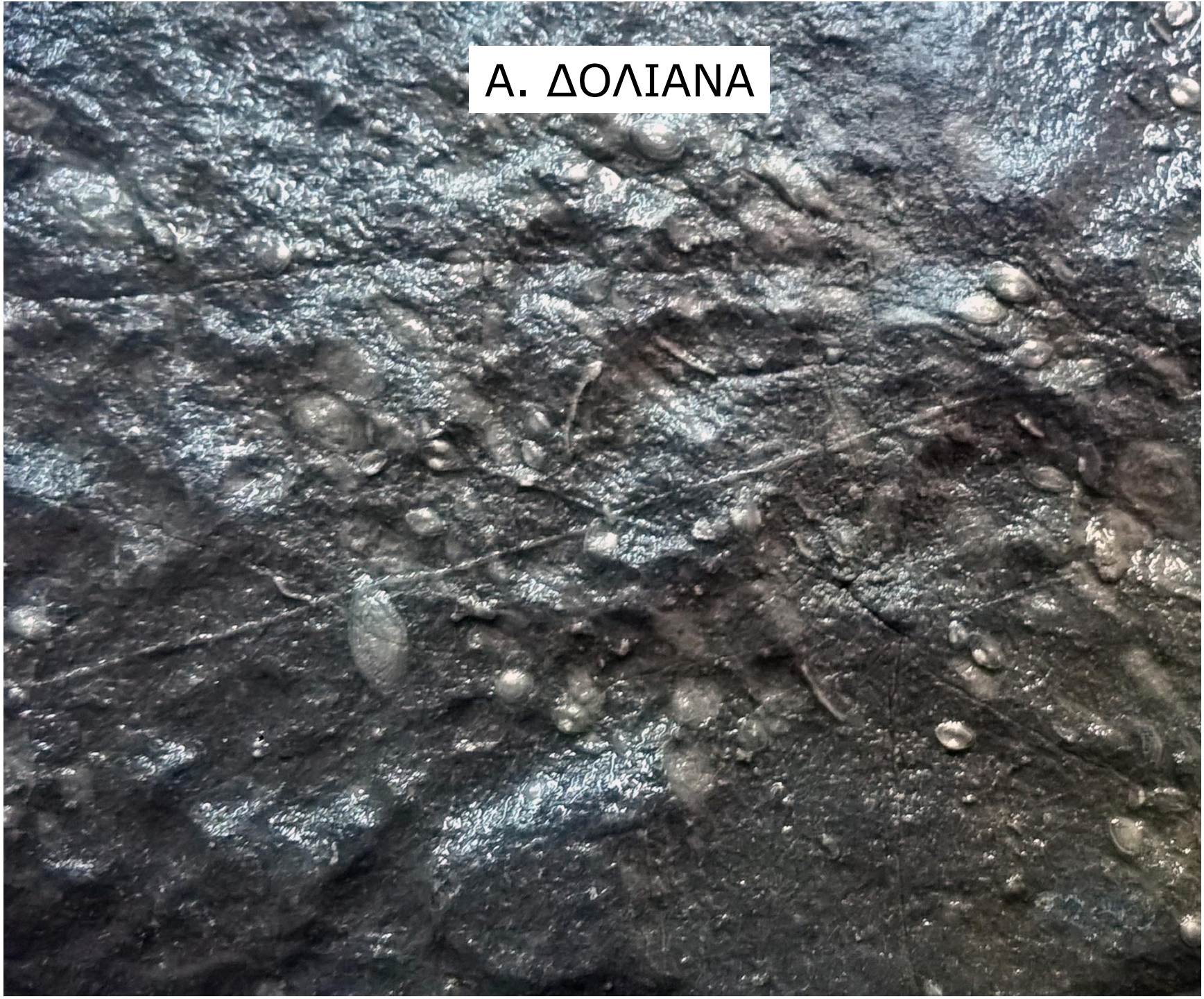
Α. ΔΟΛΙΑΝΑ

Α. ΔΟΛΙΑΝΑ

ΣΚΛΗΡΟΤΗΤΑ (Mohs) = 3

ΑΝΑΒΡΑΖΕΙ

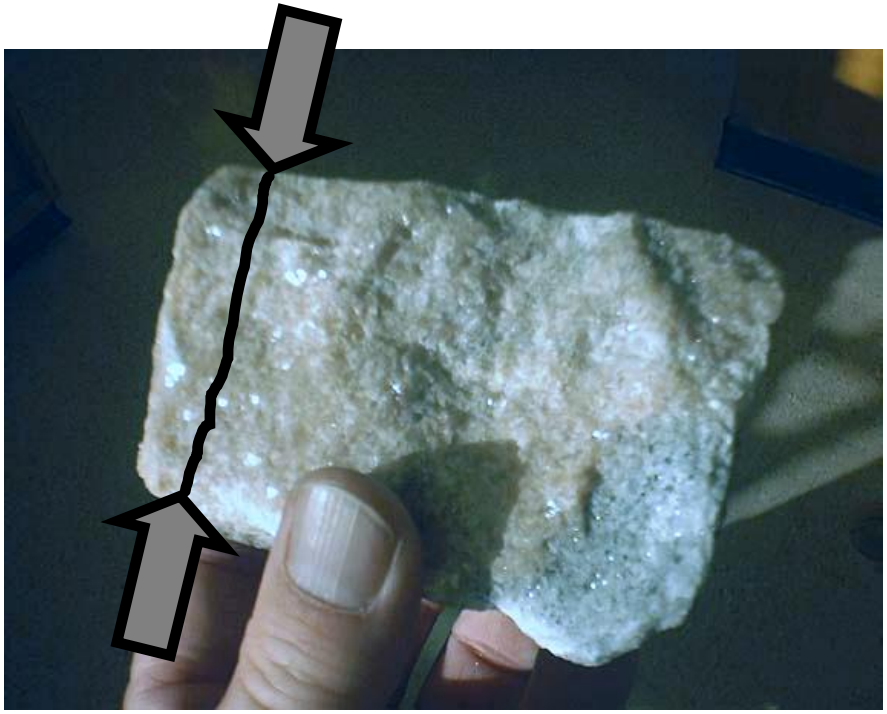

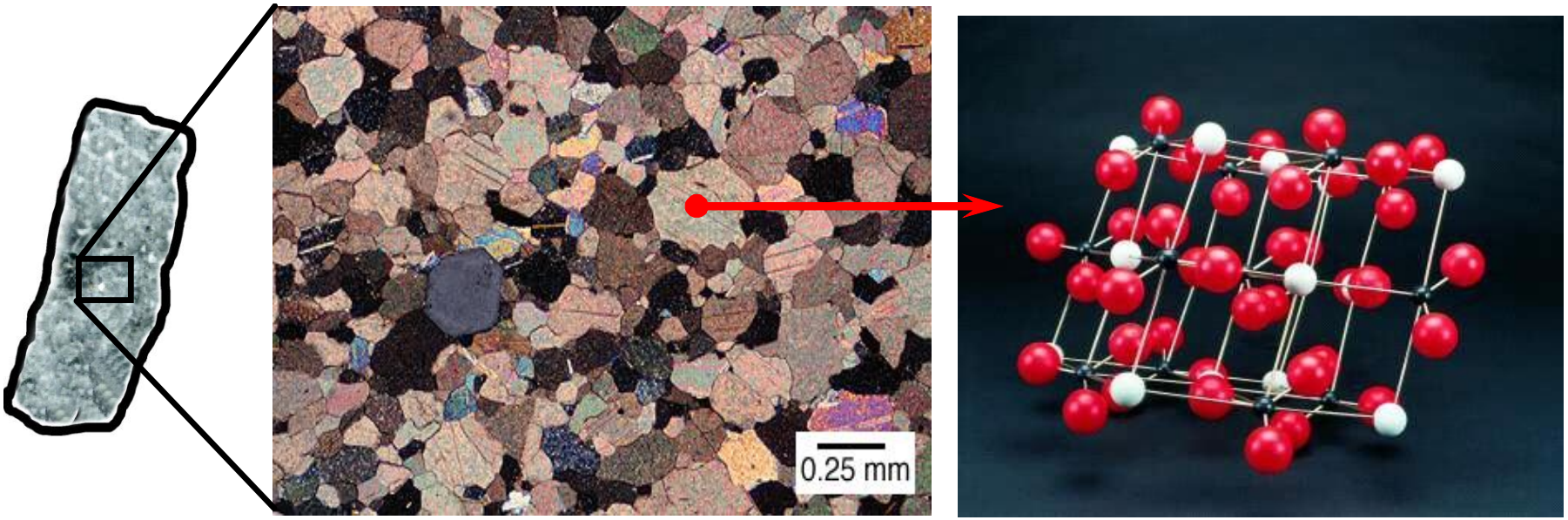
0.25 mm

ΠΟΛΥΜΟΡΦΙΣΜΟΣ (Polymorphism)

ΚΥΡΙΑ ΠΟΛΥΜΟΡΦΑ ΤΟΥ $CaCO_3$

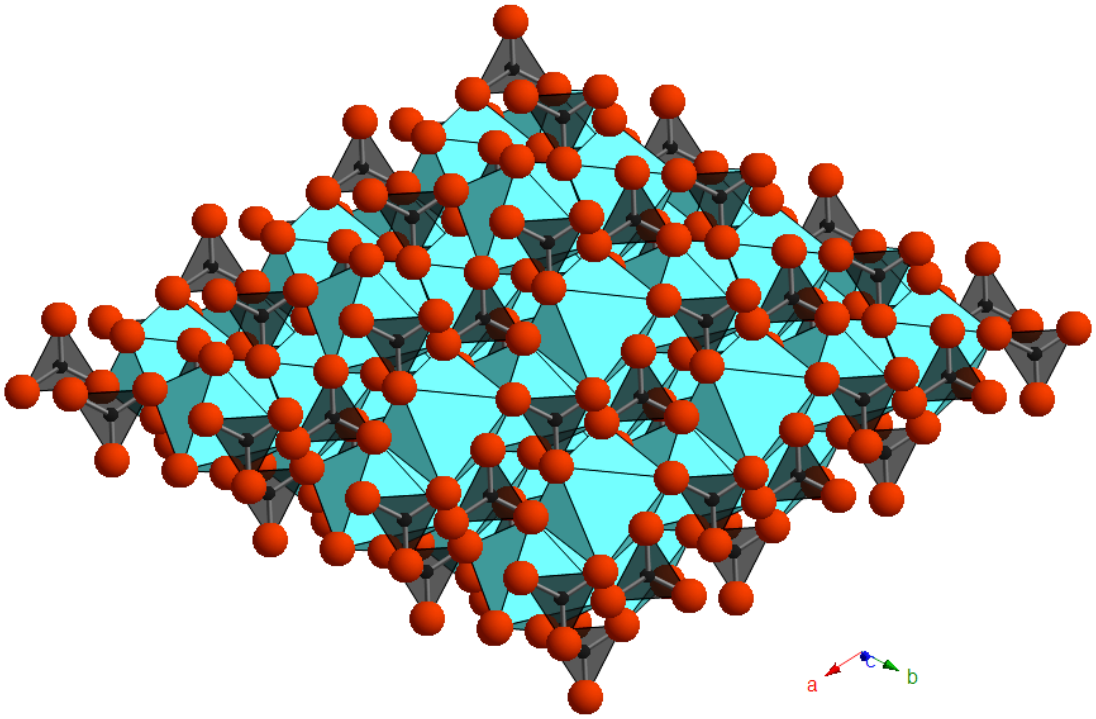

ΑΣΒΕΣΤΙΤΗΣ ($CaCO_3$)

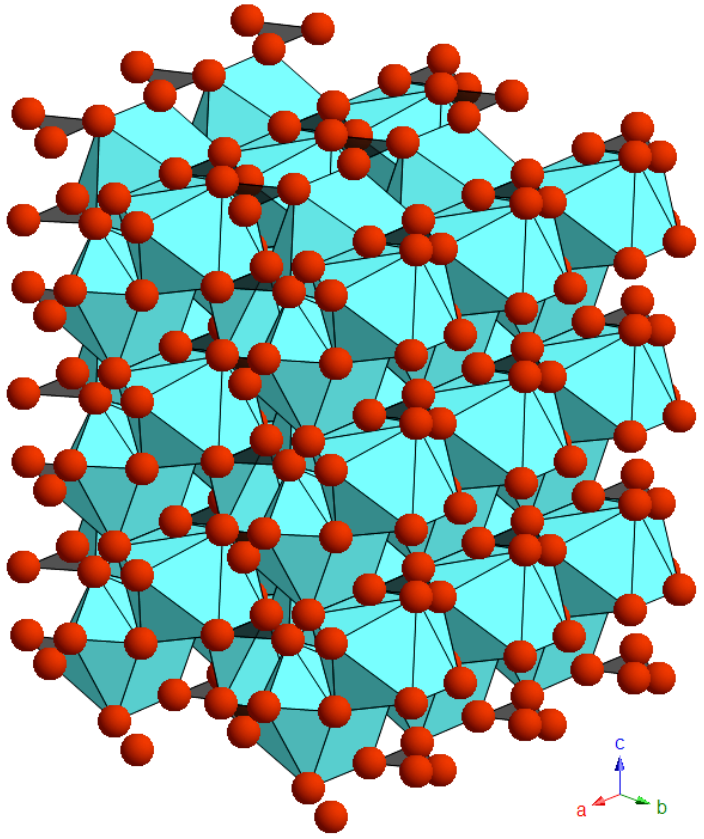

ΑΡΑΓΟΝΙΤΗΣ ($CaCO_3$)

ΠΟΛΥΜΟΡΦΑ ΤΟΥ $CaCO_3$ ΣΤΗ ΦΥΣΗ

→ **ΑΣΒΕΣΤΙΤΗΣ ($CaCO_3$) – *Τριγωνικό***

→ **ΑΡΑΓΟΝΙΤΗΣ ($CaCO_3$) – *Ρομβικό***

→ **ΒΑΤΕΡΙΤΗΣ ($CaCO_3$) – *Εξαγωνικό***

→ **Μονοϋδροασβεστίτης ($CaCO_3 \cdot H_2O$) – *Τριγωνικό***

→ **Ικαϊτης ($CaCO_3 \cdot 6H_2O$) – *Μονοκλινές***

→ **Αμορφο $CaCO_3$**

ΔΟΜΗ ΑΣΒΕΣΤΙΤΗ

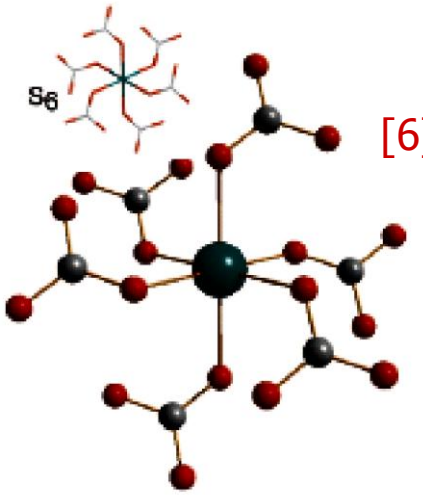

$^{[6]}r_{Ca2+}$=1 Å

[CN]=6

ΔΟΜΗ ΑΡΑΓΟΝΙΤΗ

$^{[9]}r_{Ca2+}$=1.18 Å

[CN]=9

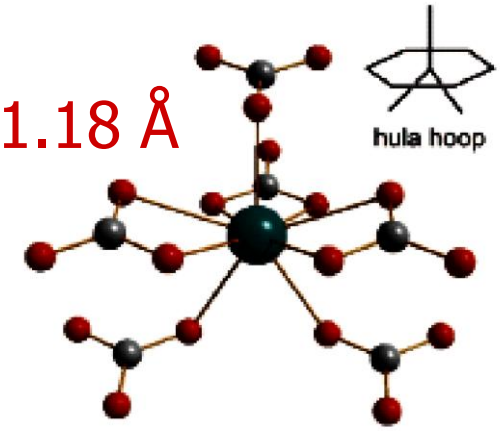

ION	Σθένος (V)	Η λ. Διαμόρφωση	[CN]	"Κρυσταλλική" Ακτίνα	Ιοντική Ακτίνα (*r*)	V/*r*
Ca^{2+}	**2**	**$3p^6$**	**6**	**1.14**	**1.00**	**2.00**
Ca^{2+}	2	3p6	7	1.20	1.06	1.89
Ca^{2+}	2	3p6	8	1.26	1.12	1.79
Ca^{2+}	**2**	**3p6**	**9**	**1.32**	**1.18**	**1.69**
Ca^{2+}	2	3p6	10	1.37	1.23	1.63
Ca^{2+}	2	3p6	12	1.40	1.34	1.49

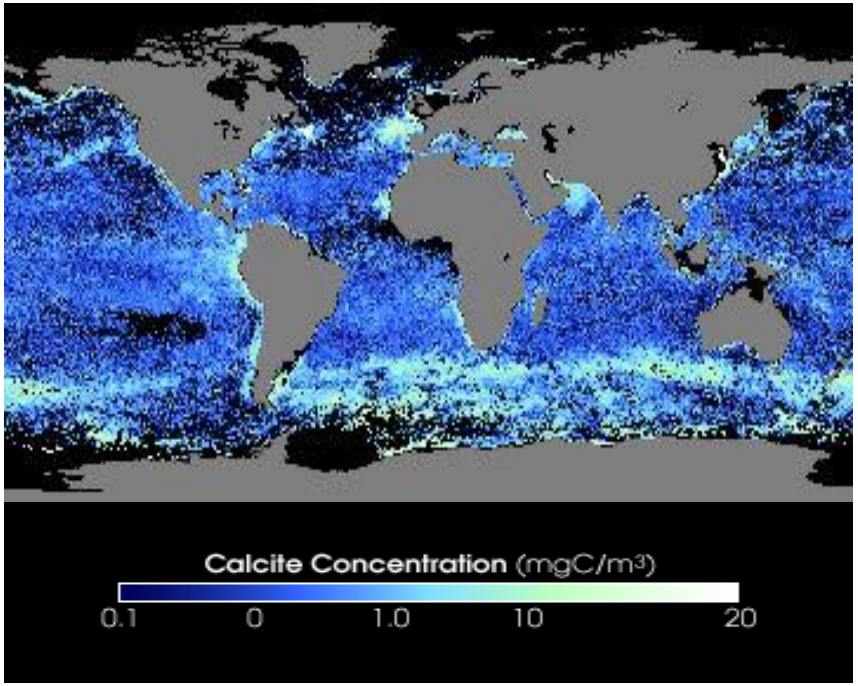

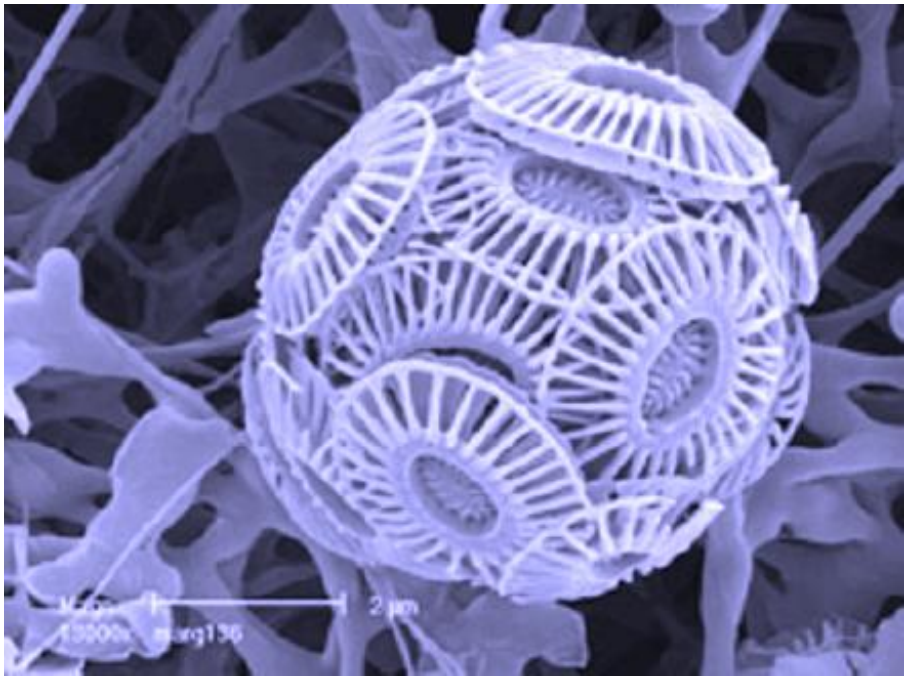

ΒΙΟ-ΑΣΒΕΣΤΙΤΗΣ

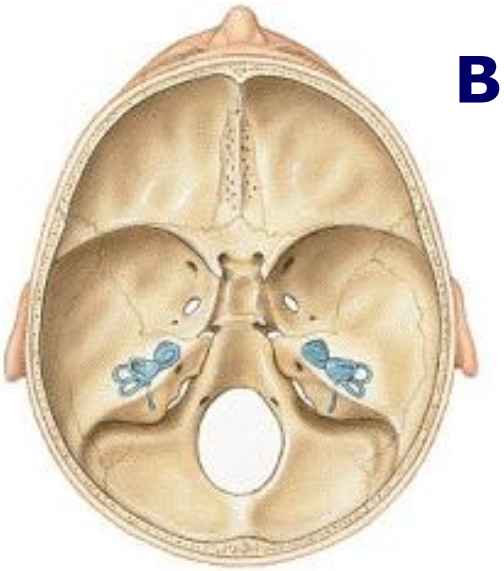

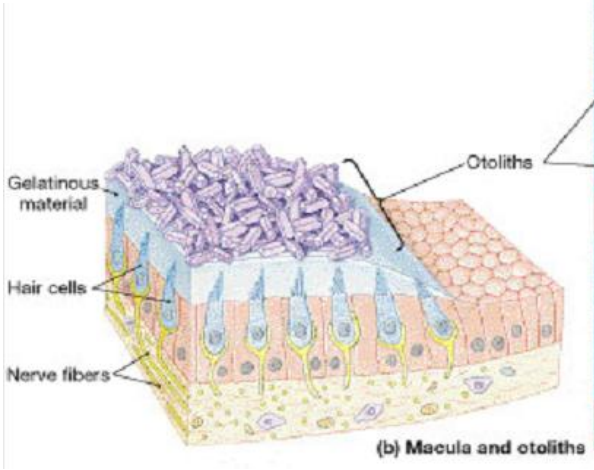

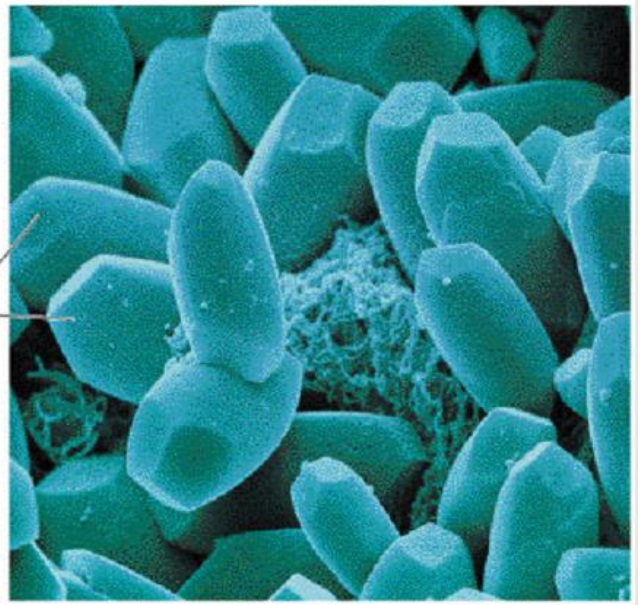

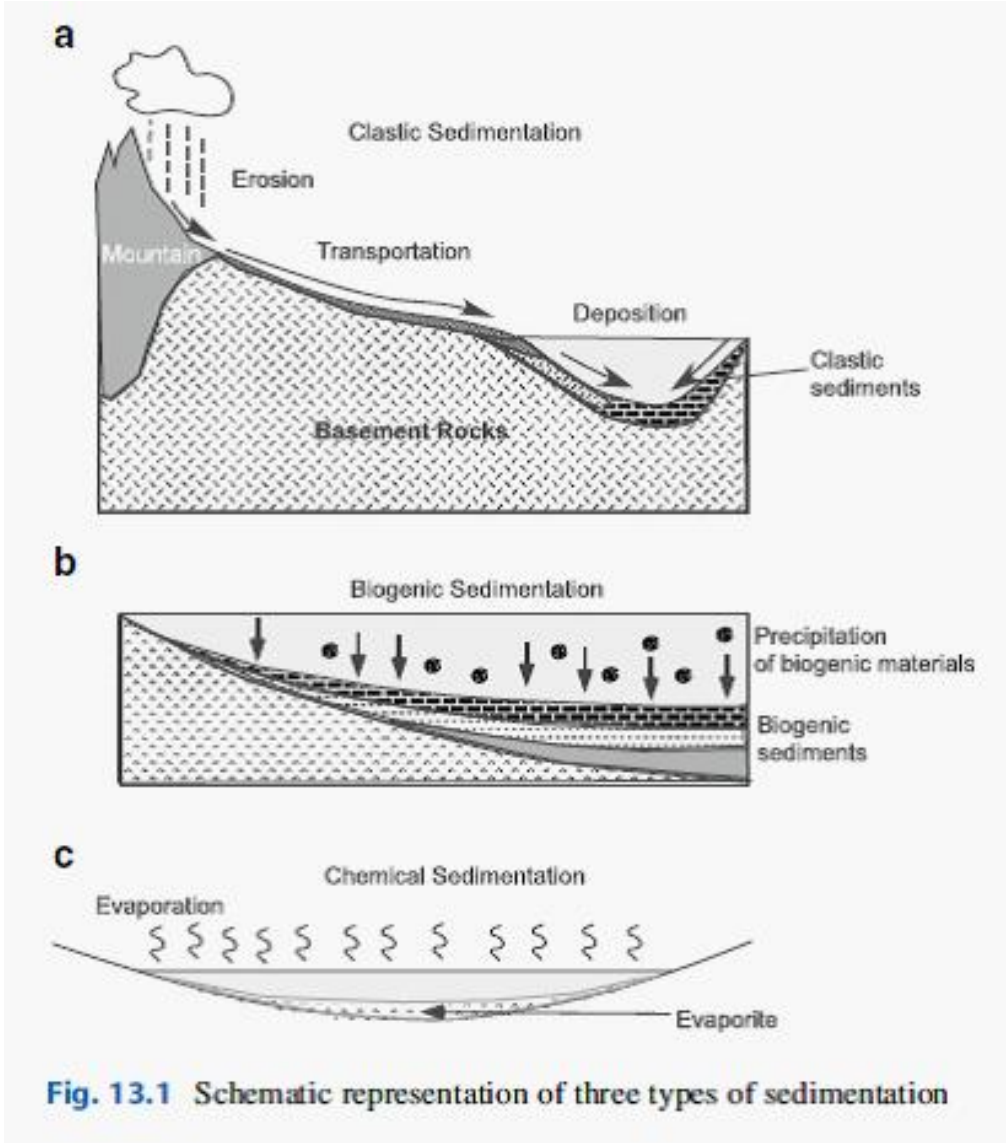

Fig. 13.1 Schematic representation of three types of sedimentation

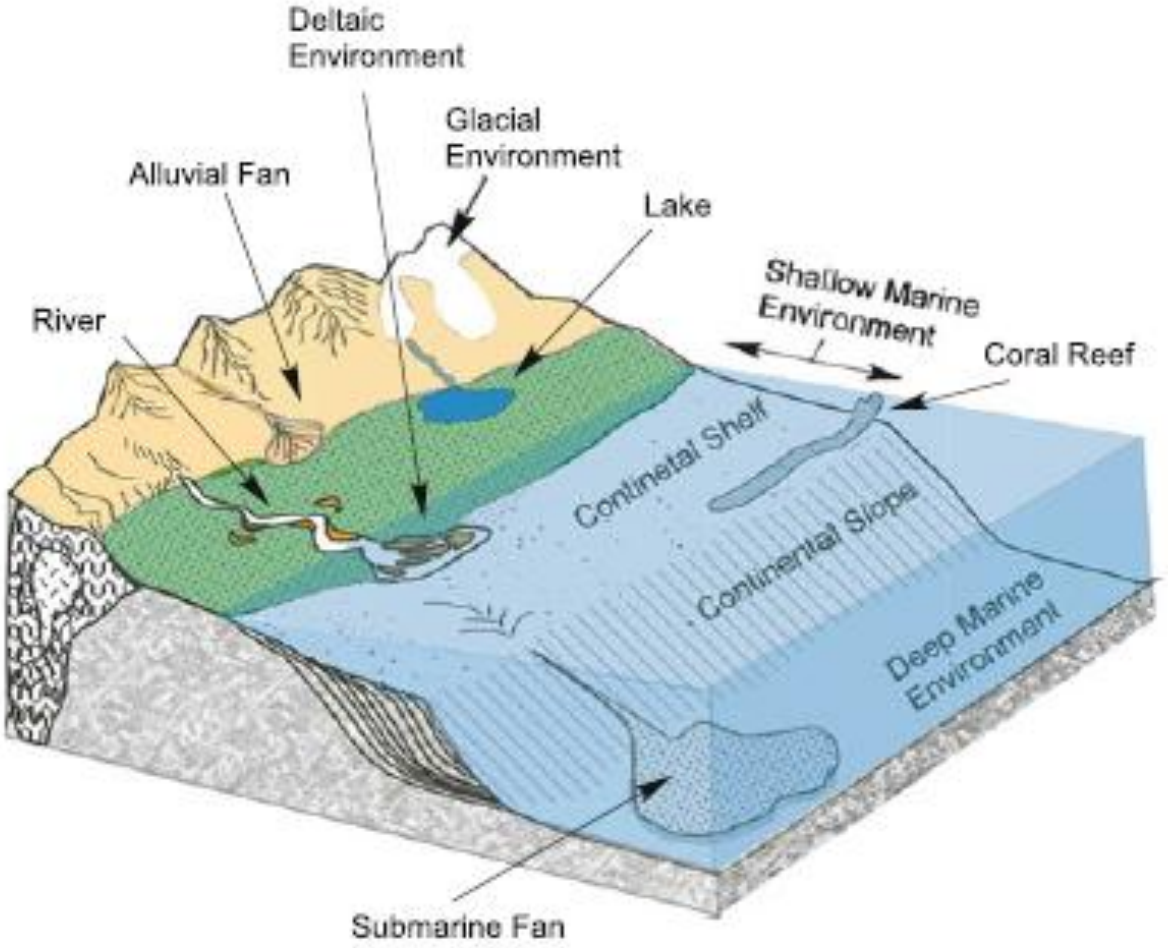

Fig. 13.18 A schematic diagram showing various continental, transitional, and marine environments of deposition

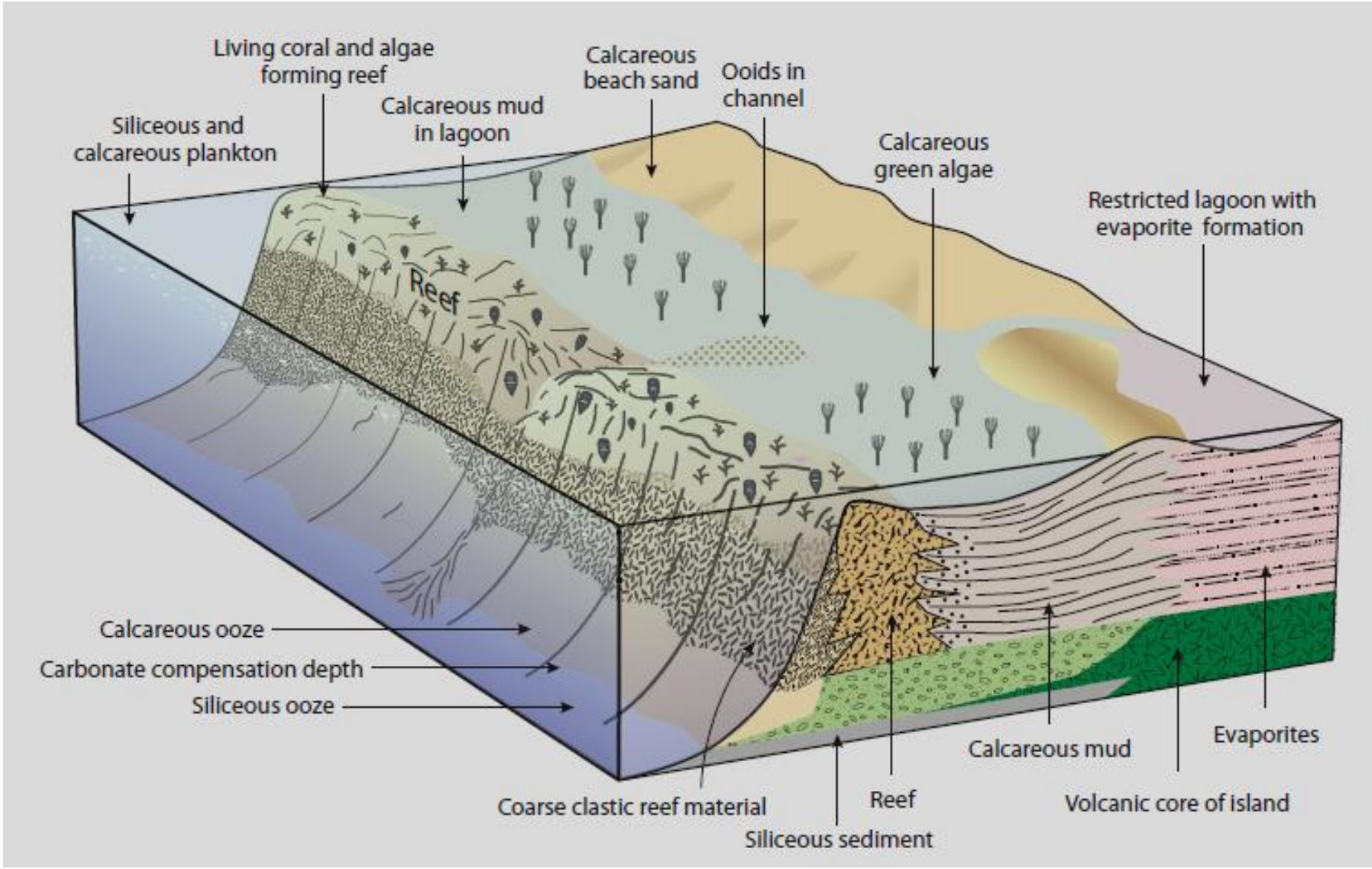

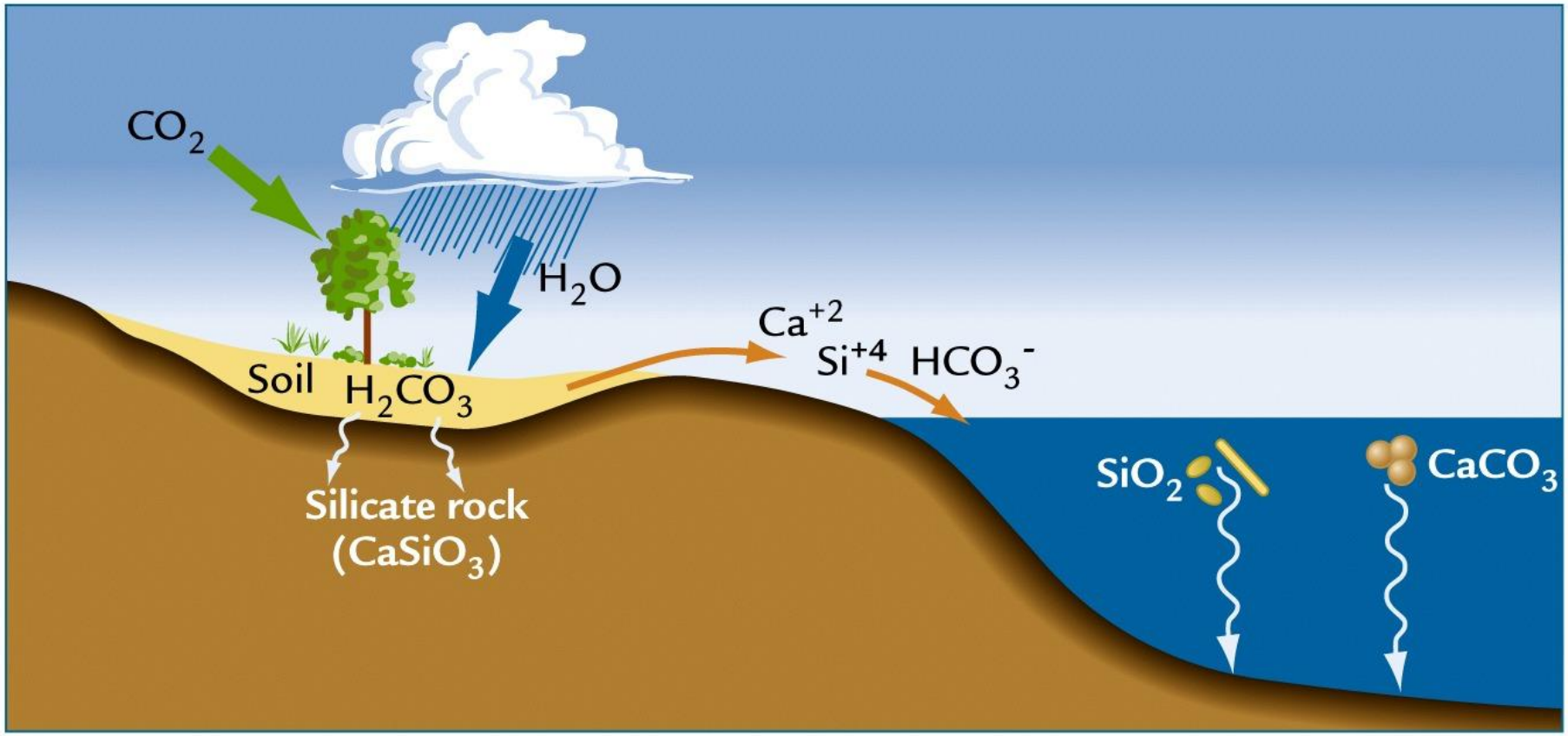

$CaSiO_3$ + **H_2CO_3**

Silicate bedrock + Carbonic acid in soils

Weathering on land

Ca^{+2} Si^{+4} HCO_3^-

Ions dissolved in river water

Transport in rivers

SiO_2 + $CaCO_3$

Shells of ocean plankton

Deposition in ocean

Reactions for the precipitation of $CaCO_3$

The ultimate fundamental chemical expression of the precipitation of $CaCO_3$ is this reaction:

$$Ca^{2+} + CO_3^{2-} \rightarrow CaCO_{3(s)}$$

However, the most abundant form of inorganic carbon in most natural waters is HCO_3^- rather than CO_3^{2-}. Thus, to understand natural processes, the better chemical expression for the precipitation of $CaCO_3$ is this reaction:

$$\mathbf{Ca^{2+} + 2HCO_3^- \rightarrow CaCO_{3(s)} + H_2O + CO_2}$$

One should realize the two bicarbonate ions have very different fates. One goes into the $CaCO_3$ and the other is liberated as CO_2:

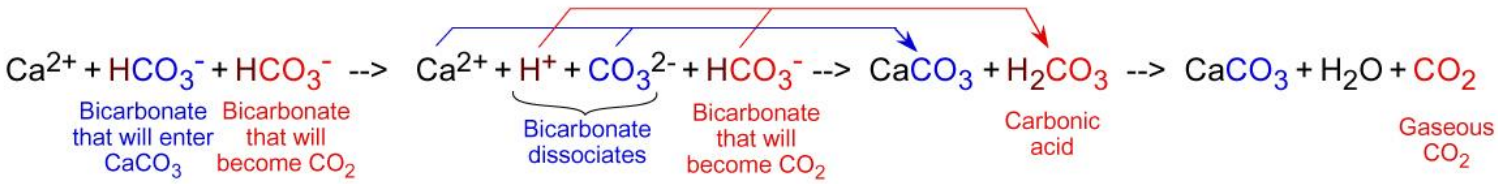

The reaction in bold letters shows that any natural process removing CO_2 from a solution favors precipitation of $CaCO_3$. That helps explain why $CaCO_3$ precipitates when

1. CO_2 degasses from dripwaters in caves,
2. CO_2 degasses from springs at which travertine forms,
3. CO_2 degasses at travertine dams,
4. CO_2 degasses with warming of seawater,
5. CO_2 degasses with agitation of seawater by waves,
6. CO_2 degasses with upwelling of seawater,
7. CO_2 is removed from water by photosynthesis.

In marine precipitation of $CaCO_3$, Processes 4 to 7 can all occur at shelf breaks (changes in slope from shallower landward to deeper seaward). These are common sites of reefs or ooid shoals.

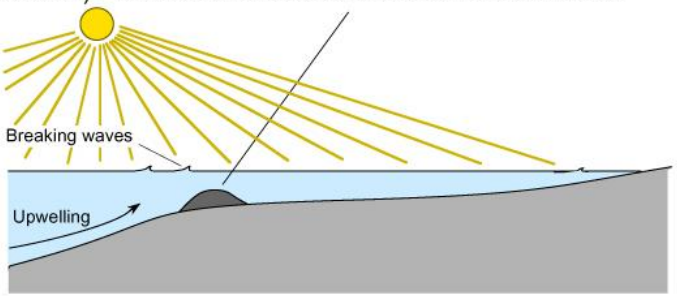

There is a corresponding page titled "Reactions for the dissolution of $CaCO_3$".

Variation in concentration of solutes in the oceans IIIa: carbon dioxide and the carbonate compensation depth (CCD)

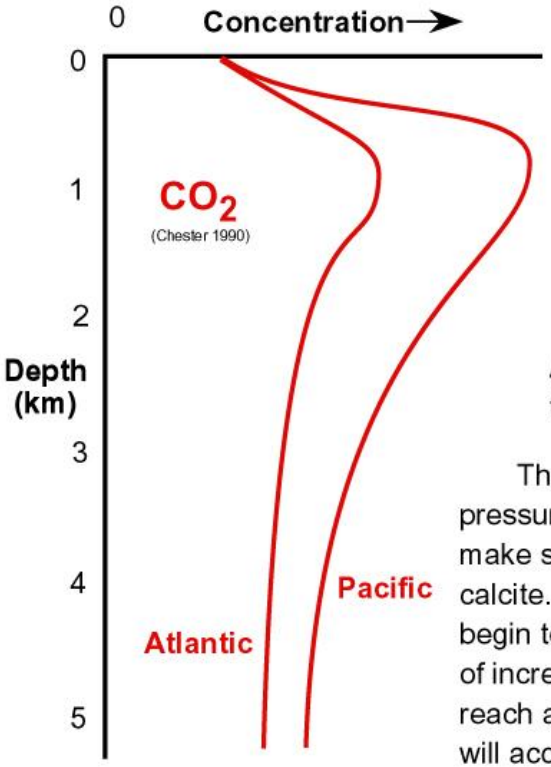

In the deeper reaches of the ocean, $CaCO_3$ is more prone to dissolve for three reasons:[1]

a) lower temperature (K_{sp} for both calcite and aragonite increases with decreasing T)

b) greater pressure (K_{sp} for both calcite and aragonite increases with increasing P) [2]

c) acidity resulting from the presence of CO_2, as suggested by these reactions:

$$CO_2 + H_2O \rightarrow H_2CO_3$$

Carbon dioxide — Carbonic acid

$$H_2CO_3 + CaCO_3 \rightarrow Ca^{2+} + 2HCO_3^-$$

Carbonic acid — Calcite — Bicarbonate

As discussed in Part III of this series, concentrations of CO_2 in abyssal waters are greater than those in surface waters because oxidation of sinking organic particles produces CO_2.

Thus at depth in the ocean, temperature, pressure and acidity commonly combine to make seawater undersaturated with respect to calcite. Calcite particles sinking past this depth begin to dissolve in a lysocline (the depth zone of increasing dissolution rate) and eventually reach a depth at which no carbonate sediment will accumulate on the seafloor. This depth is the carbonate compensation depth (CCD),[3] which is thus named because it is the depth at which the rate of dissolution of $CaCO_3$ equals ("compensates for") the rate of $CaCO_3$ sedimentation. Thus seafloor deeper than the CCD will be devoid of carbonate sediments. The CCD is higher (less deep) in the Pacific because deep water in the Pacific has more CO_2 and so is more acidic.

Notes:

[1] Morse & Mackenzie (1990) p. 23 etc.

[2] Morse & Mackenzie (1990) p. 24.

[3] More technically, one speaks of a "calcite compensation depth" and higher (lesser) "aragonite compensation depth" (ACD).

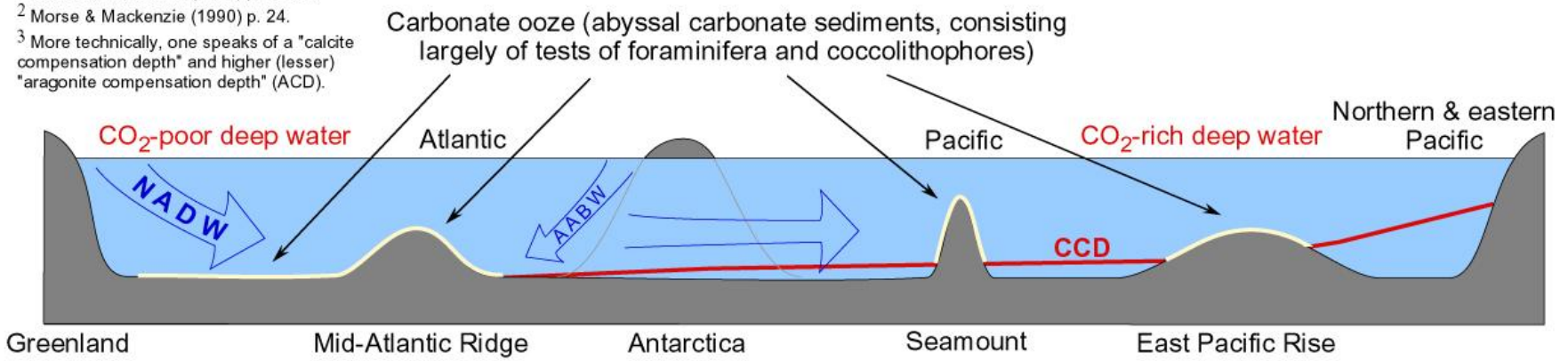

Seamounts: "the snow-capped peaks of the abyssal Pacific"

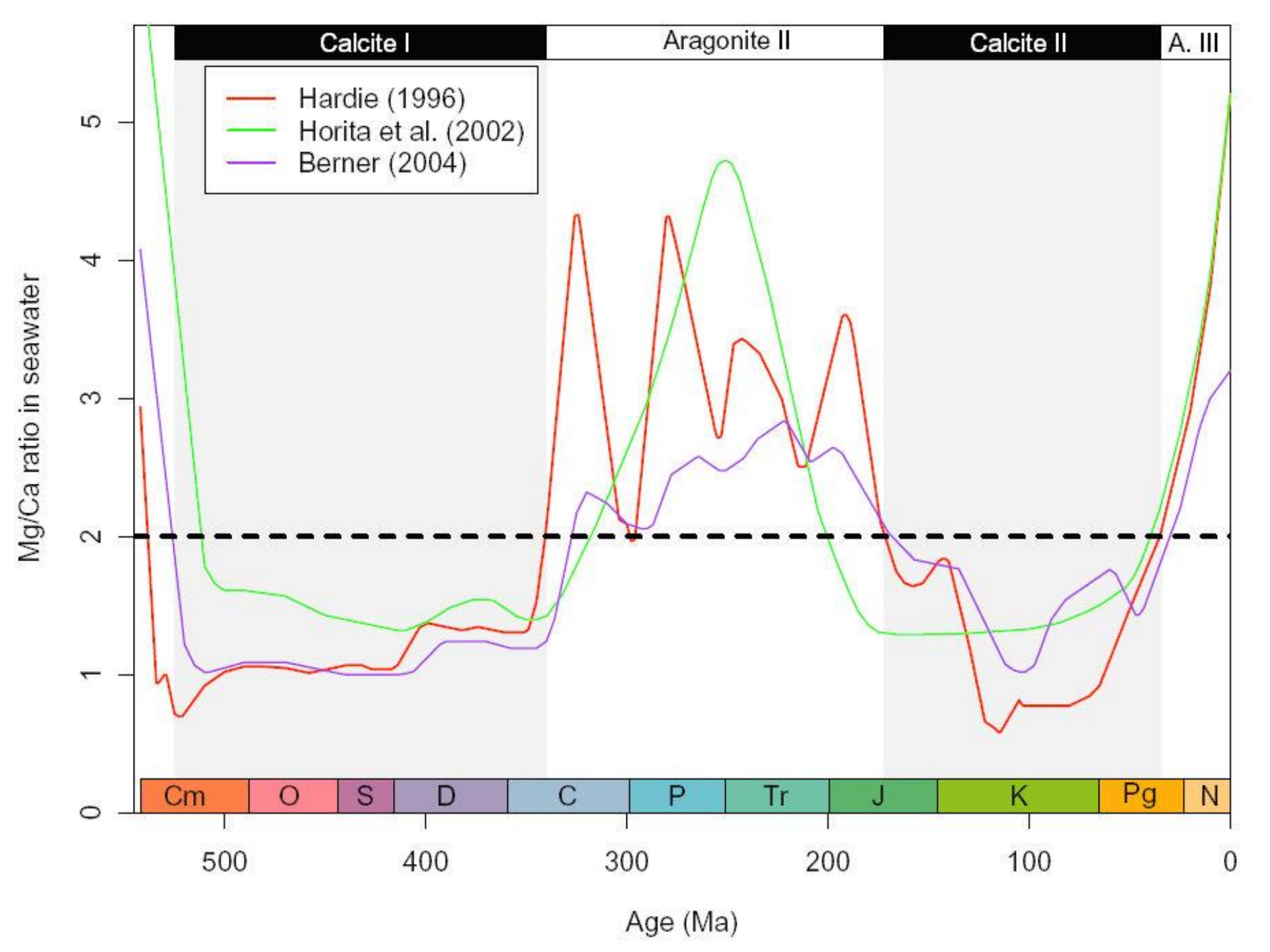
Calcite I
Aragonite II
Calcite II
A. III
Hardie (1996)
Horita et al. (2002)
Berner (2004)
Mg/Ca ratio in seawater
0
1
2
3
4
5
Cm
O
S
D
C
P
Tr
J
K
Pg
N
500
400
300
200
100
0
Age (Ma)

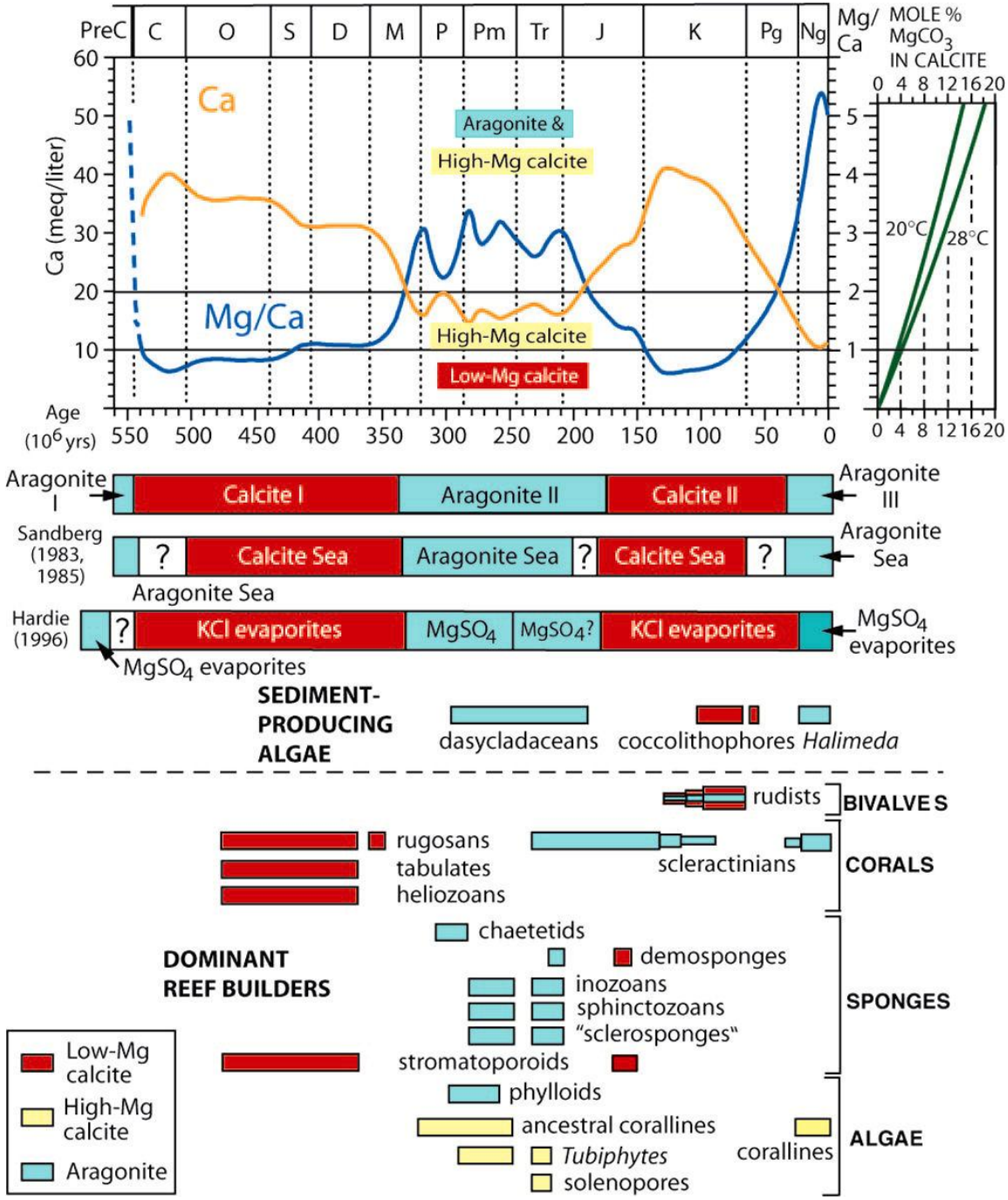
PreC
C
O
S
D
M
P
Pm
Tr
J
K
Pg
Ng
Mg/Ca
MOLE % MgCO3 IN CALCITE
Ca (meq/liter)
Ca
Mg/Ca
Aragonite &
High-Mg calcite
High-Mg calcite
Low-Mg calcite
20°C
28°C
Age (10^6 yrs)
Aragonite I
Calcite I
Aragonite II
Calcite II
Aragonite III
Sandberg (1983, 1985)
Calcite Sea
Aragonite Sea
Calcite Sea
Aragonite Sea
Aragonite Sea
Hardie (1996)
KCl evaporites
MgSO4
MgSO4?
KCl evaporites
MgSO4 evaporites
MgSO4 evaporites
SEDIMENT-PRODUCING ALGAE
dasycladaceans
coccolithophores
Halimeda
rudists
BIVALVES
rugosans
tabulates
heliozoans
scleractinians
CORALS
DOMINANT REEF BUILDERS
chaetetids
demosponges
inozoans
sphinctozoans
"sclerosponges"
SPONGES
stromatoporoids
phylloids
ancestral corallines
Tubiphytes
solenopores
corallines
ALGAE
Low-Mg calcite
High-Mg calcite
Aragonite

Α. ΔΟΛΙΑΝΑ

ΒΙΤΟΥΜΕΝΟΥΧΟΣ ΔΟΛΟΜΙΤΙΚΟΣ ΑΣΒΕΣΤΟΛΙΘΟΣ

Doliana_carbonate

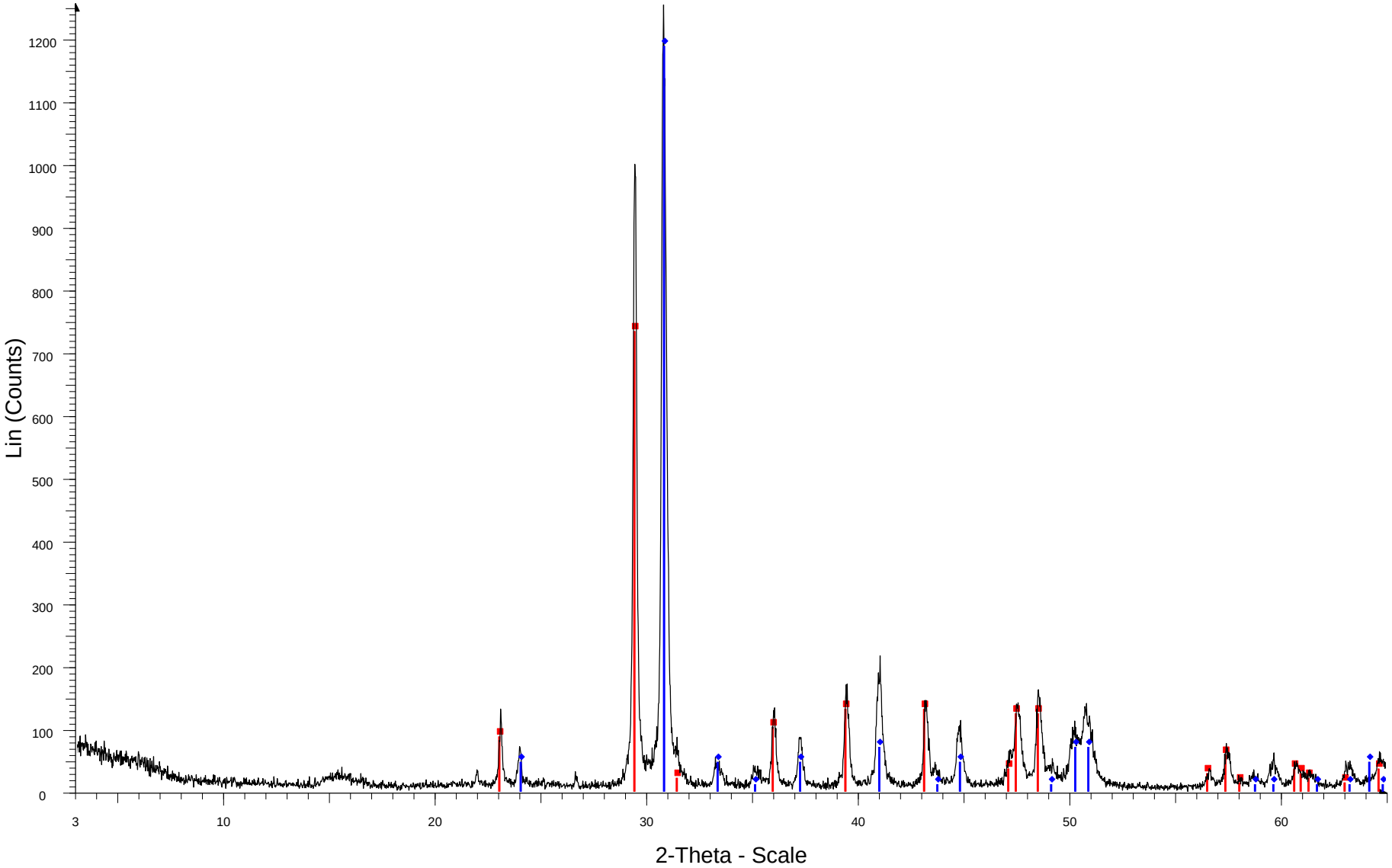

Doliana_carbonate - File: Doliana_carbonate.raw - Type: 2Th/Th locked - Start: 3.000 ° - End: 65.000 ° - Step: 0.020 ° - Step time: 1. s - Temp.: 25 °C (Room) - Time Started: 15 s - 2-Theta: 3.000 ° - Theta: 1.500 ° - Operations: Import

00-034-0517 (D) - Dolomite, ferroan - Ca(Mg,Fe)(CO3)2 - Y: 94.78 % - d x by: 1. - WL: 1.5406 - 0 -

00-005-0586 (*) - Calcite, syn - CaCO3 - Y: 58.54 % - d x by: 1. - WL: 1.5406 - 0 - I/Ic PDF 2. -

ΦΥΛΛΟΠΥΡΙΤΙΚΑ ΟΡΥΚΤΑ

- **ΜΑΡΜΑΡΥΓΙΕΣ**

ΦΥΛΛΟΠΥΡΙΤΙΚΑ ΟΡΥΚΤΑ

- **ΜΑΡΜΑΡΥΓΙΕΣ**


ΠΕΝΤΕΛΗ

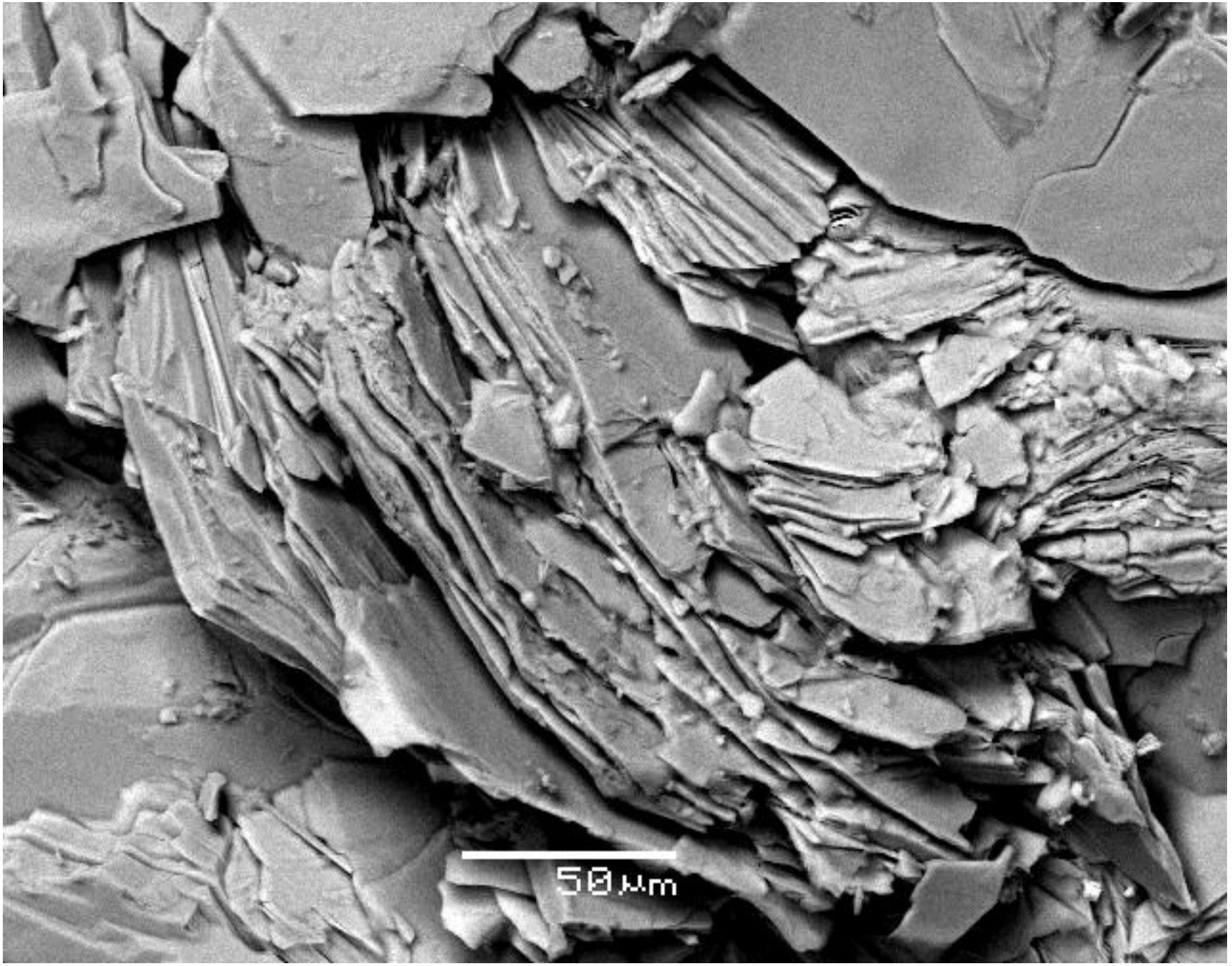
50µm

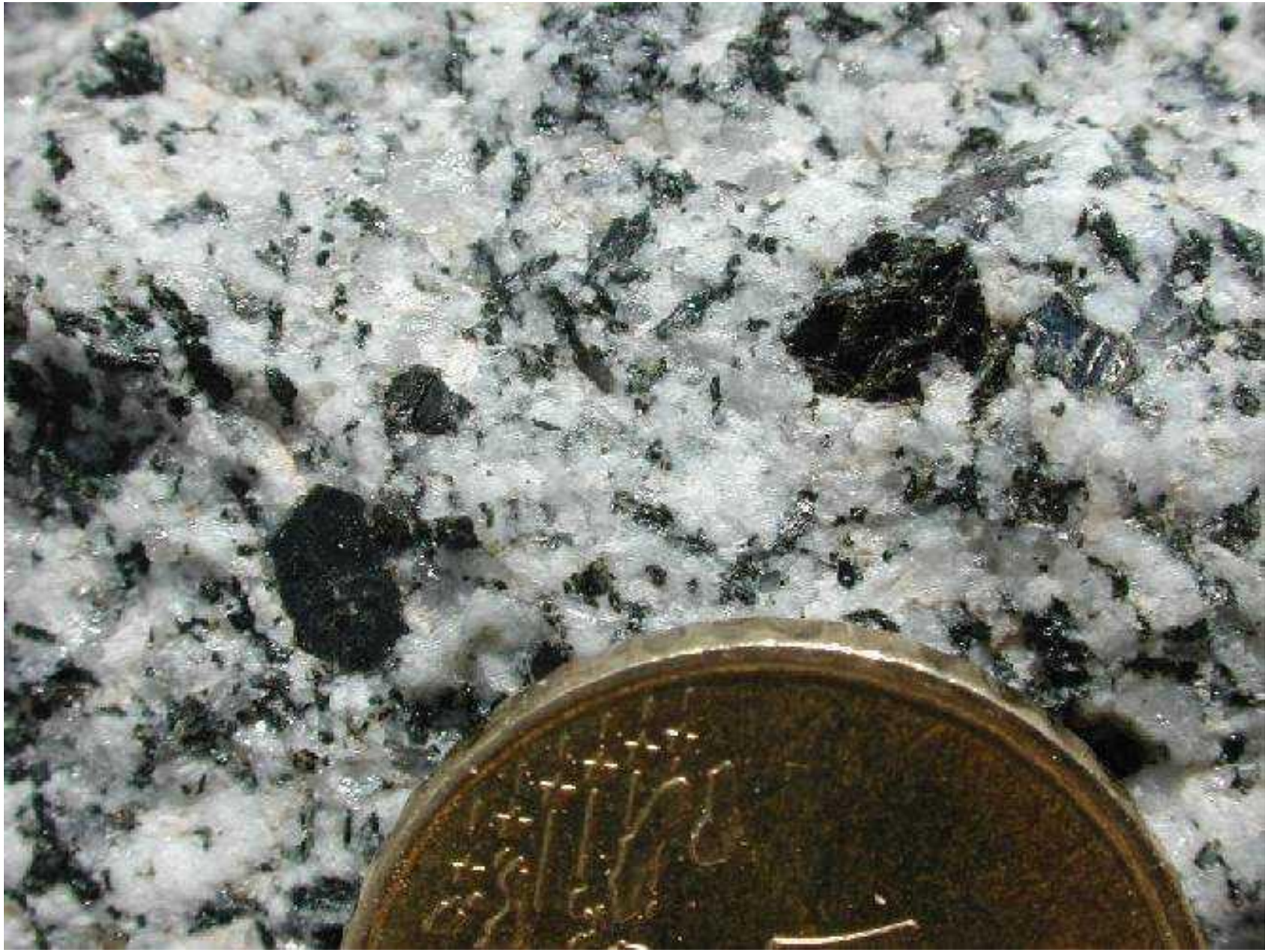

Η ΚΡΥΣΤΑΛΛΙΚΗ ΔΟΜΗ ΤΟΥ ΜΑΡΜΑΡΥΓΙΑ **BIOTITH**

$(K[Mg,Fe^{2+}]_3[Al,Fe^{3+}]Si_3O_{10}[OH,F]_2) \perp \boldsymbol{a}$

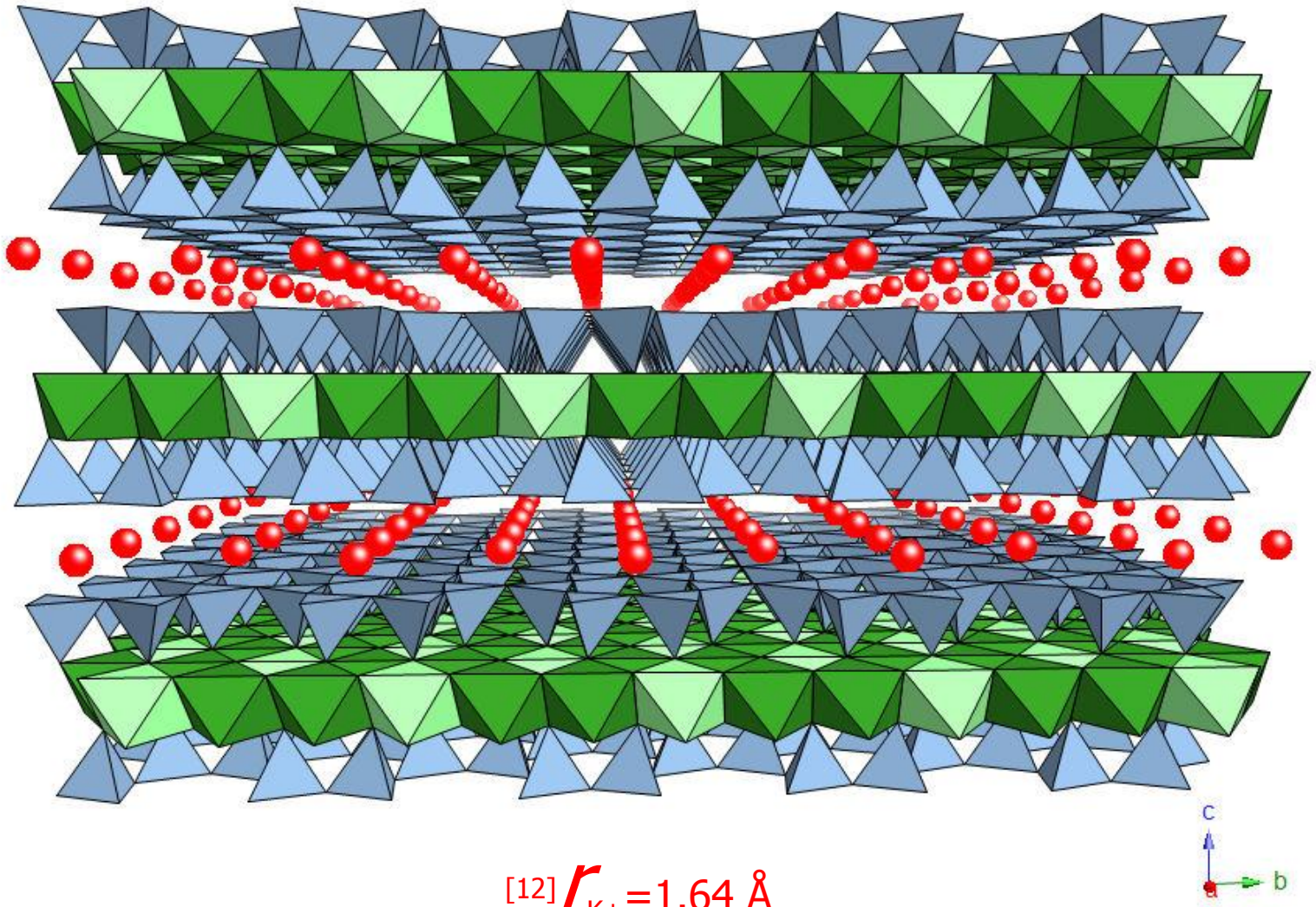

$^{[12]}r_{K+}=1.64$ Å

Η ΚΡΥΣΤΑΛΛΙΚΗ ΔΟΜΗ ΤΟΥ ΜΑΡΜΑΡΥΓΙΑ **BIOTITH** ΣΤΟ TEM

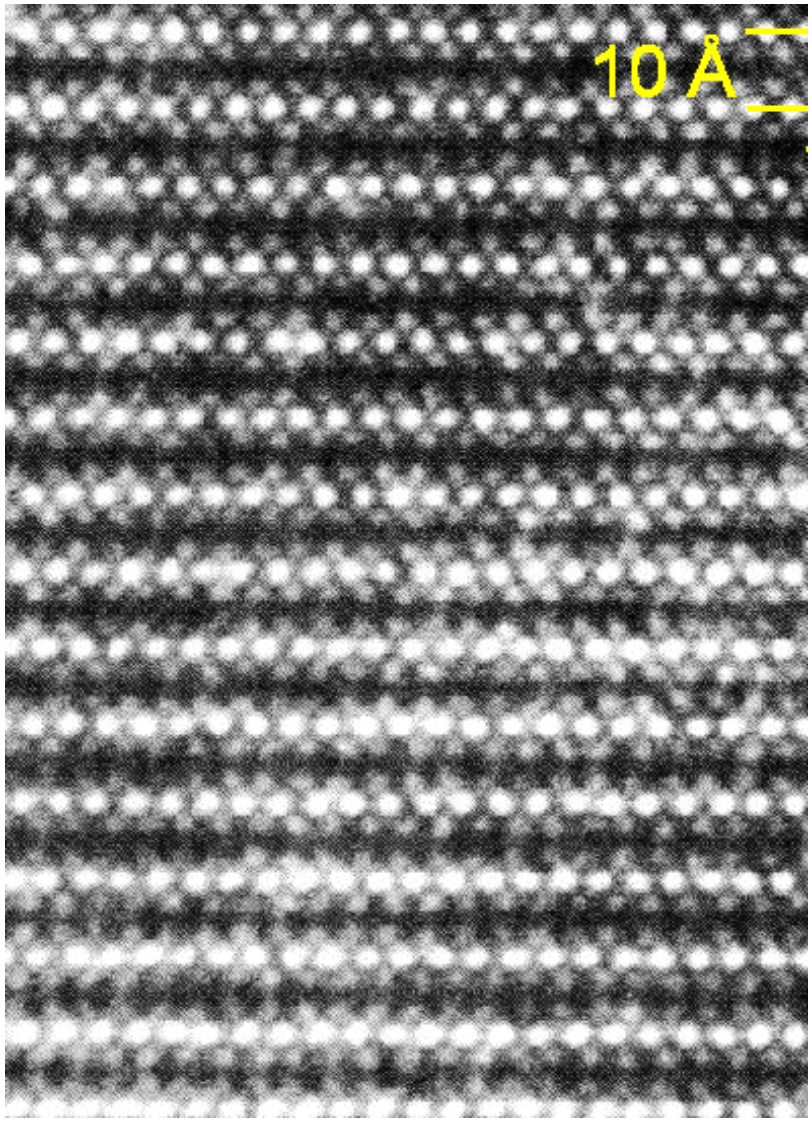

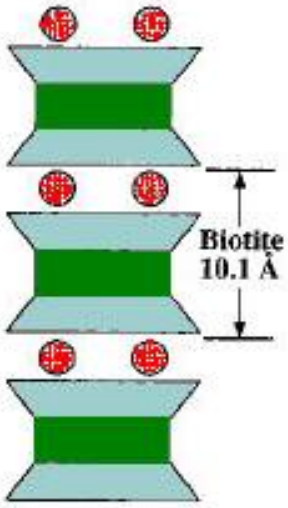

Ο ΠΟΛΥΤΥΠΙΣΜΟΣ ΤΟΥ ΒΙΟΤΙΤΗ ΣΥΣΧΕΤΙΖΕΤΑΙ ΣΥΧΝΑ ΜΕ ΤΗ "ΧΛΩΡΙΤΙΩΣΗ" (ΔΗΜΙΟΥΡΓΙΑ ΣΤΟΙΒΑΔΩΝ ΧΛΩΡΙΤΗ)

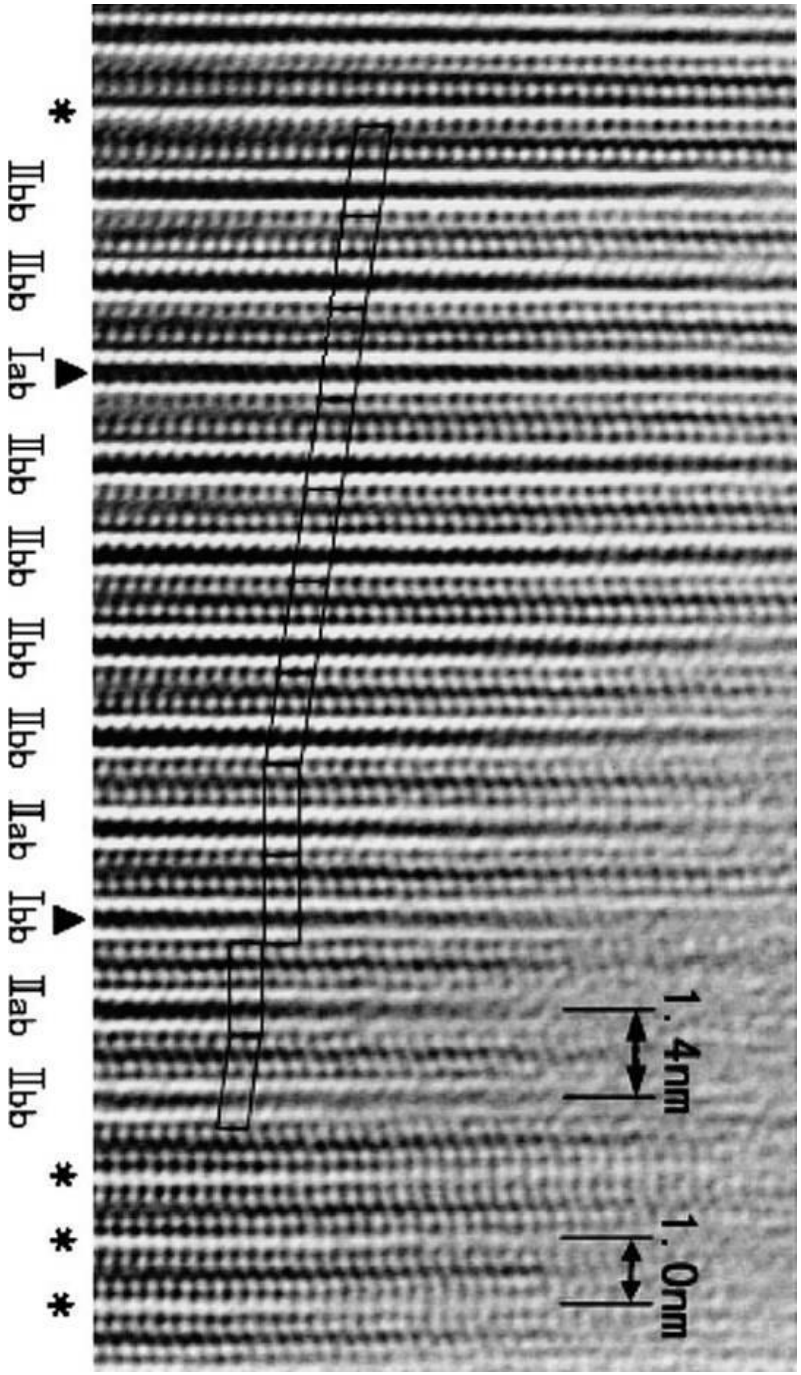

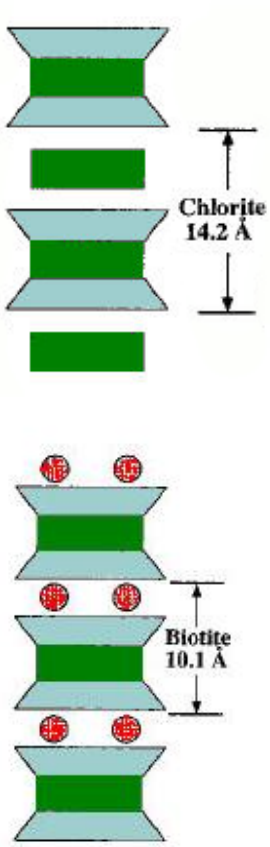

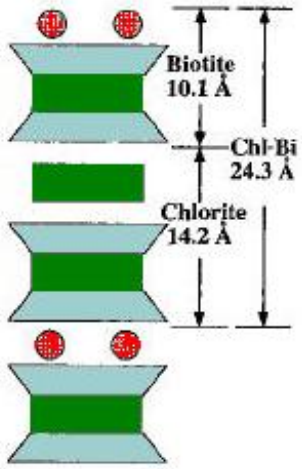

http://www.geo.auth.gr/courses/gmo/gmo212y/

Α. ΔΟΛΙΑΝΑ

ΜΕΤΑΜΟΡΦΩΜΕΝΑ ΠΕΤΡΩΜΑΤΑ
(Α. ΔΟΛΙΑΝΑ)

ΜΕΤΑΜΟΡΦΩΜΕΝΑ ΠΕΤΡΩΜΑΤΑ (Α. ΔΟΛΙΑΝΑ)

ΜΕΤΑΜΟΡΦΩΜΕΝΑ ΠΕΤΡΩΜΑΤΑ (Α. ΔΟΛΙΑΝΑ)

ΜΕΤΑΜΟΡΦΩΜΕΝΑ ΠΕΤΡΩΜΑΤΑ
(Α. ΔΟΛΙΑΝΑ)

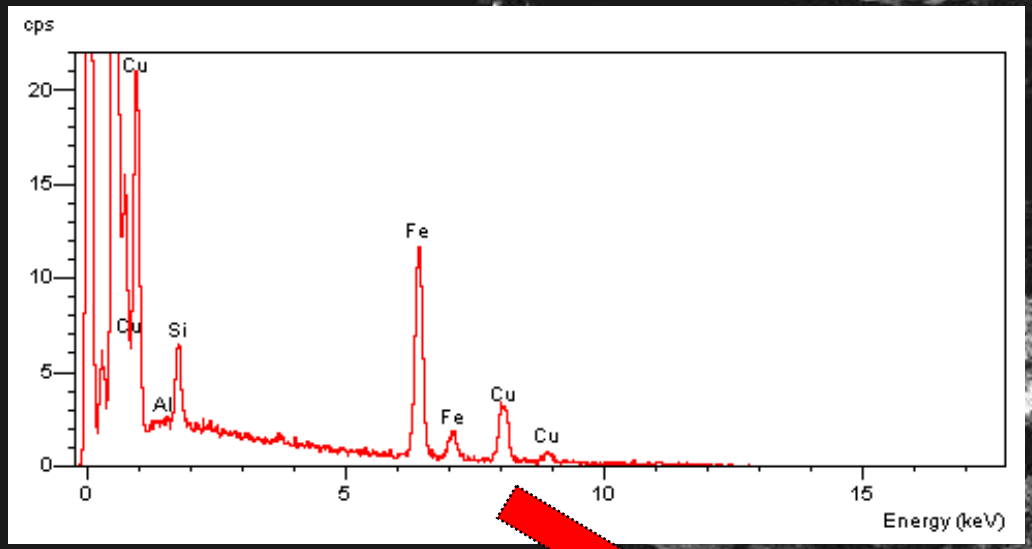

100 µm

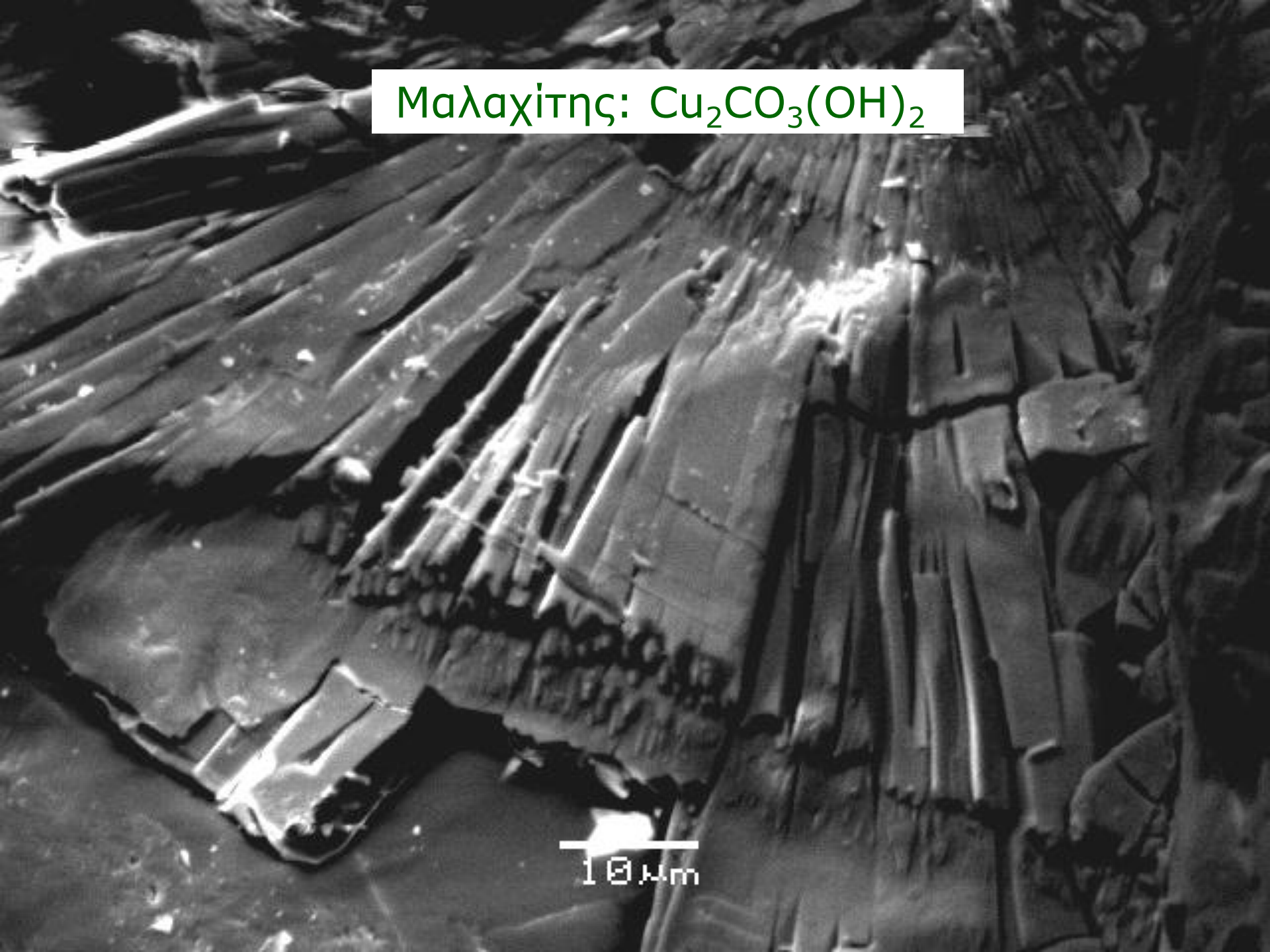
Μαλαχίτης: $Cu_2CO_3(OH)_2$
10 µm

ΦΥΛΛΟΠΥΡΙΤΙΚΑ ΟΡΥΚΤΑ

• ΟΡΥΚΤΑ ΤΗΣ ΑΡΓΙΛΟΥ

ΦΥΛΛΟΠΥΡΙΤΙΚΑ ΟΡΥΚΤΑ

• ΟΡΥΚΤΑ ΤΗΣ ΑΡΓΙΛΟΥ

Ορυκτά της αργίλου - Clay minerals

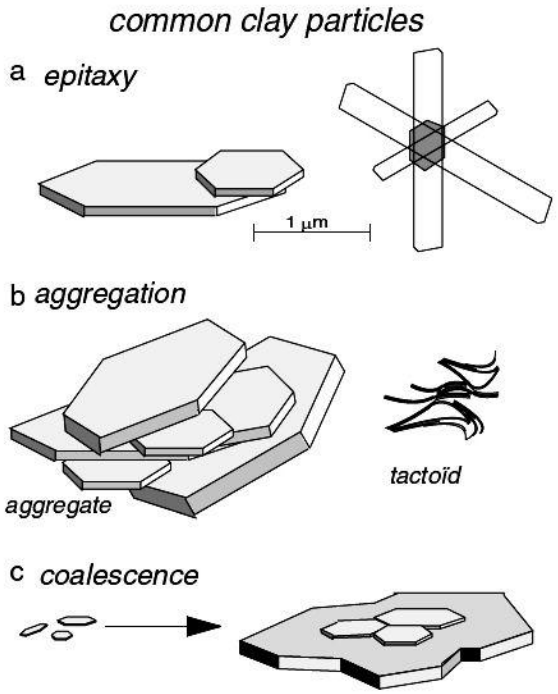

The main types of particles and aggregates of clay minerals. a) Epitaxy, i.e. growth on a crystalline support. b) Aggregation of rigid or flexible particles or crystallites (tactoid or quasi-crystal networks). c) Coalescence: neighbouring crystals are joined by the growth of common layers

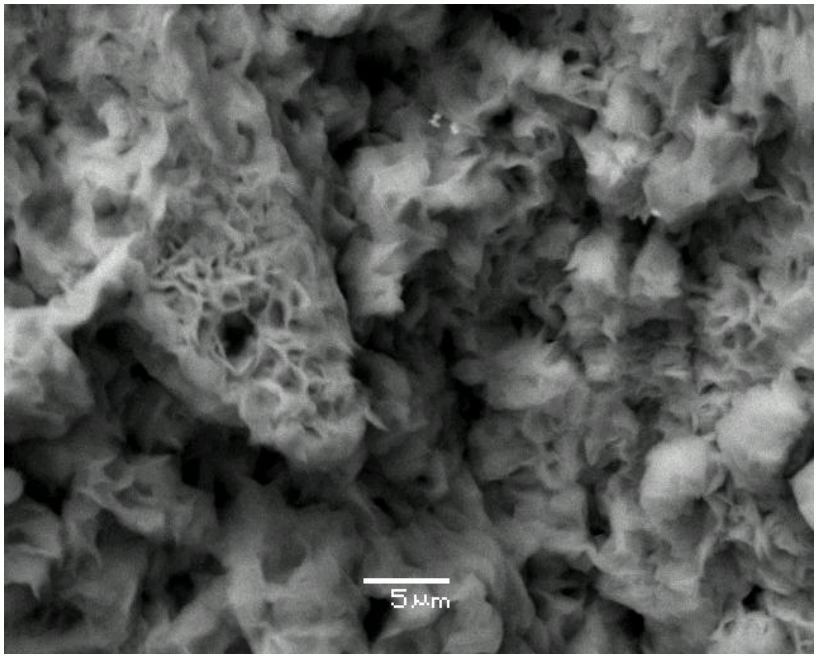

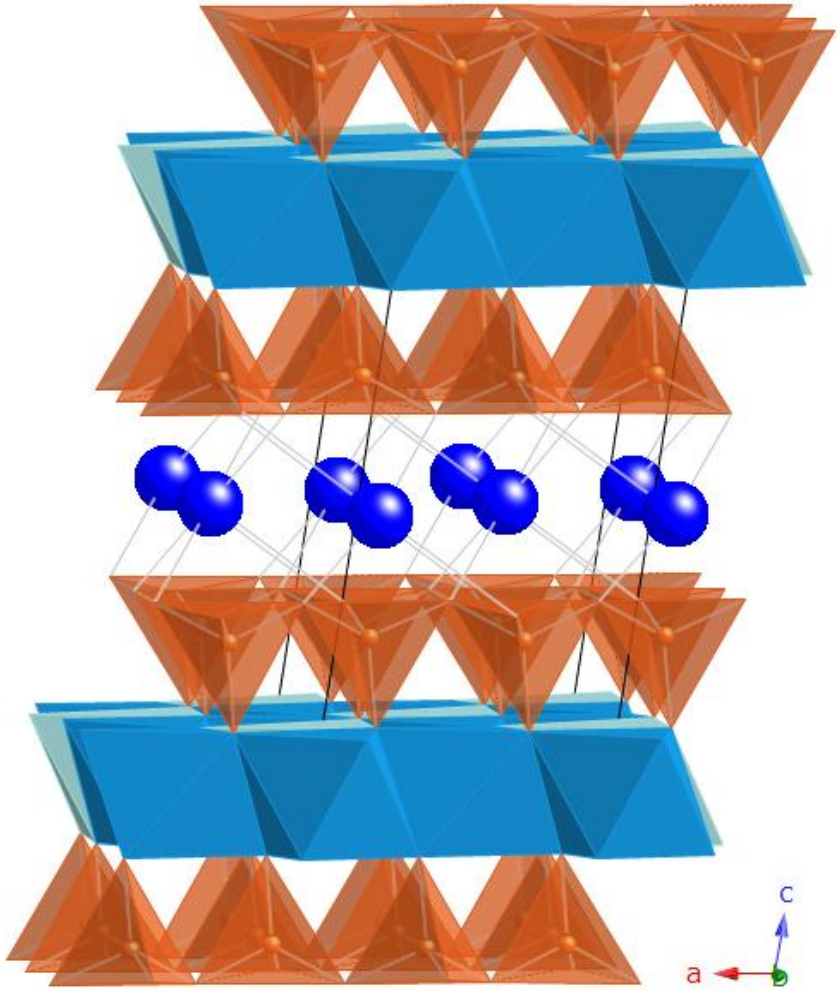

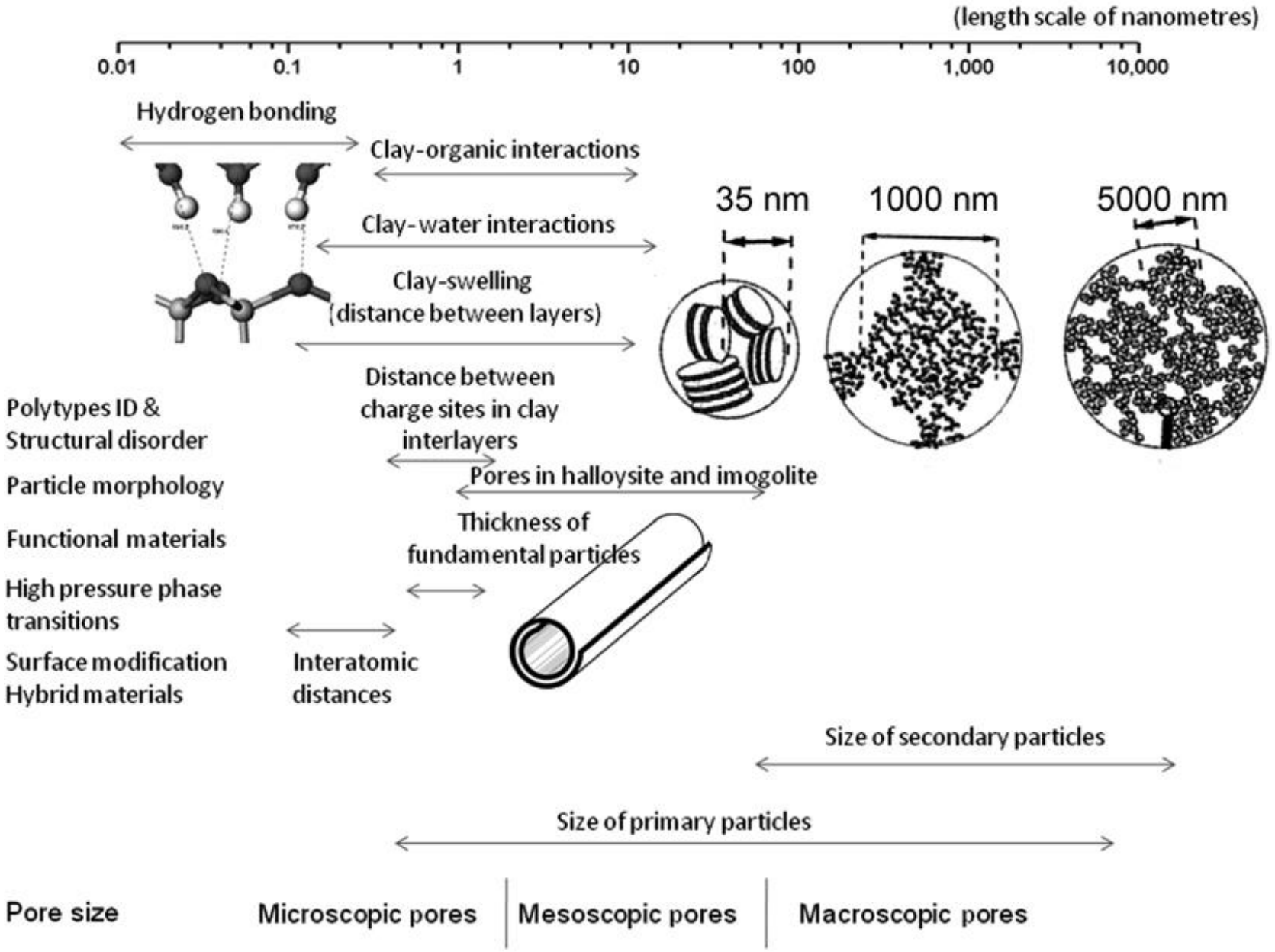

JOHNSTON, Clay Mineral. 2010

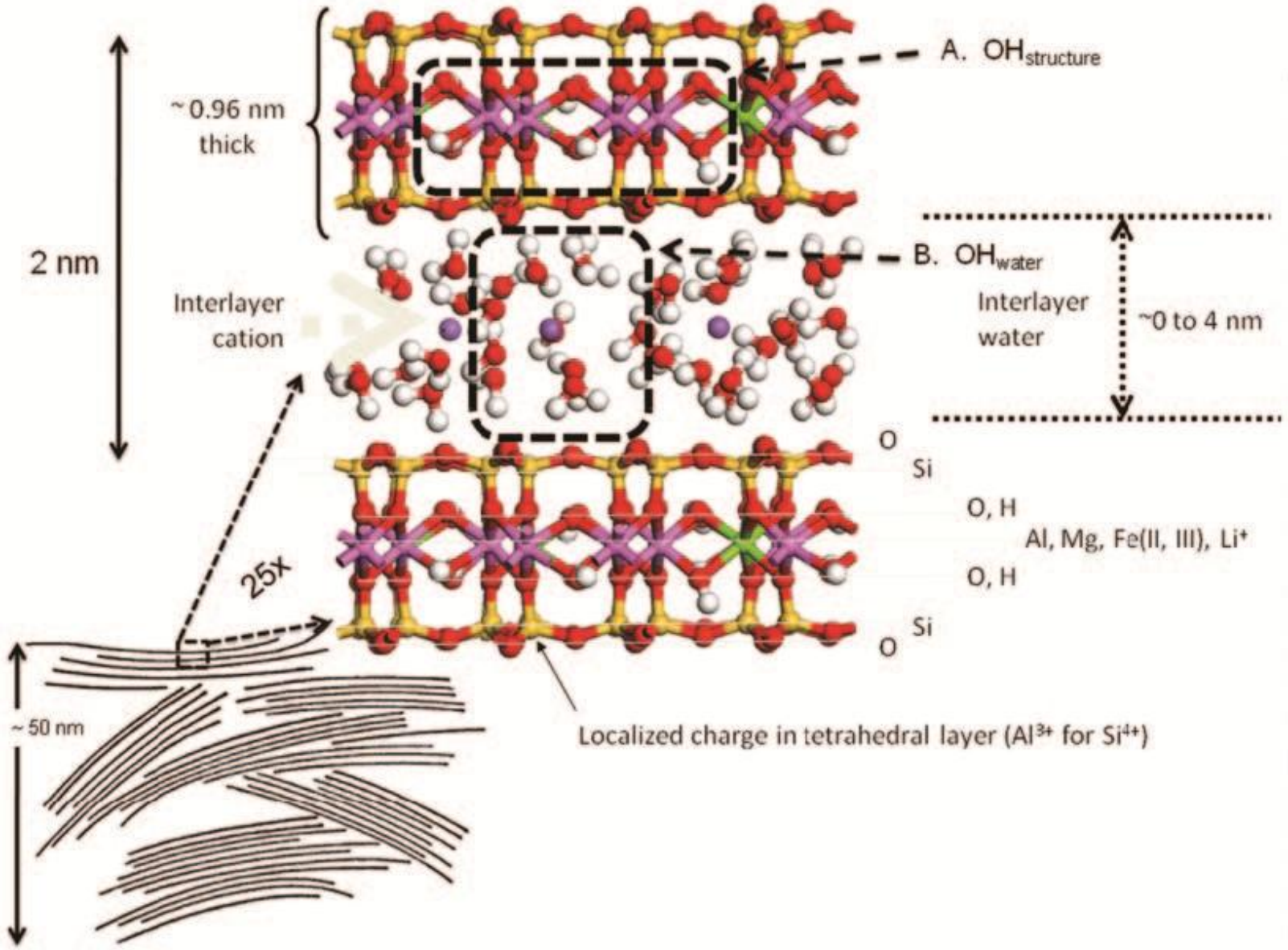

JOHNSTON, Clay Mineral. 2010

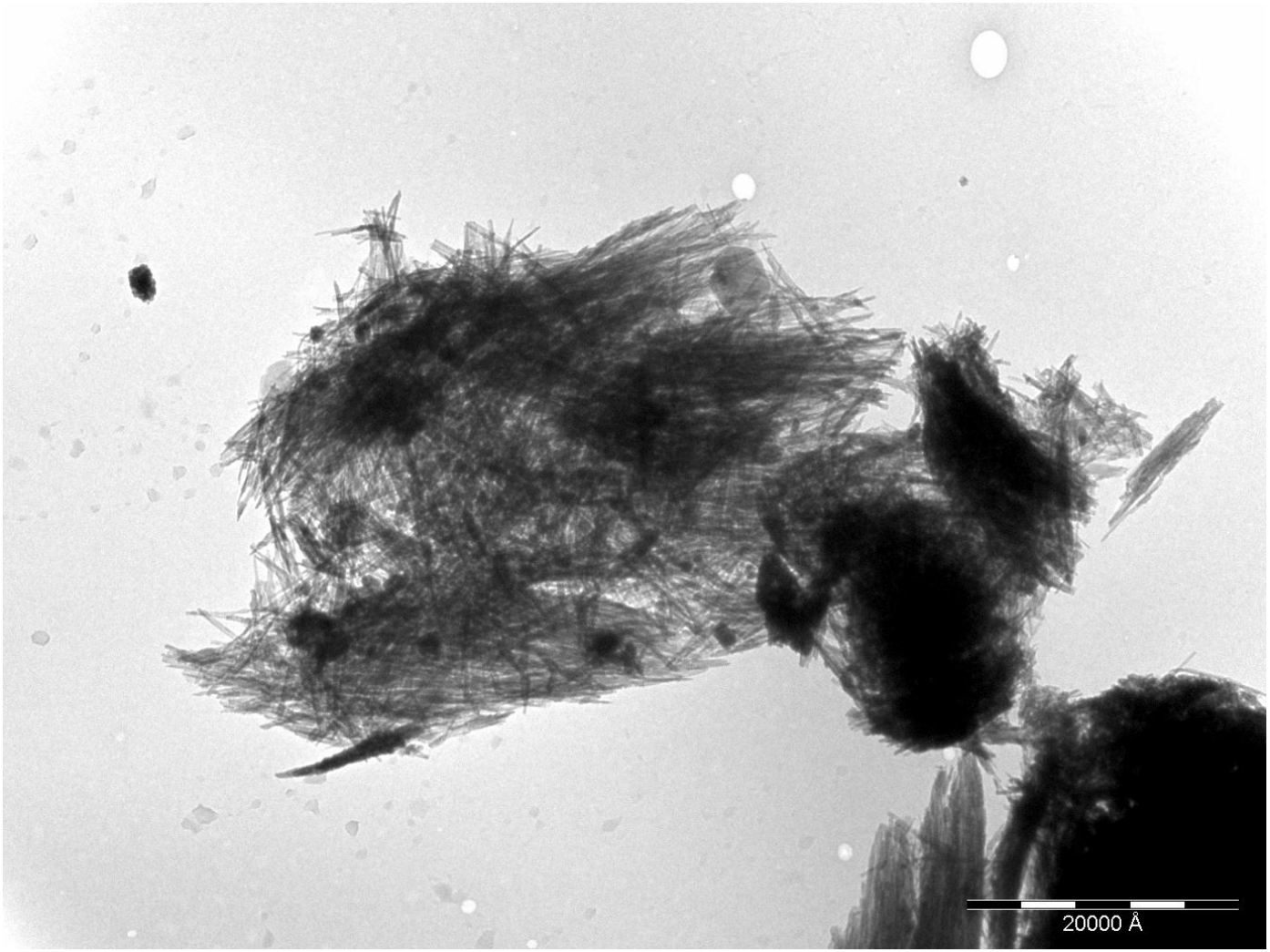

ugr Universidad de Granada

Centro de Instrumentación Científica
Universidad de Granada


ΦΛΥΣΧΗΣ
(ΗΠΕΙΡΟΣ)

Α. ΔΟΛΙΑΝΑ

Α. ΔΟΛΙΑΝΑ

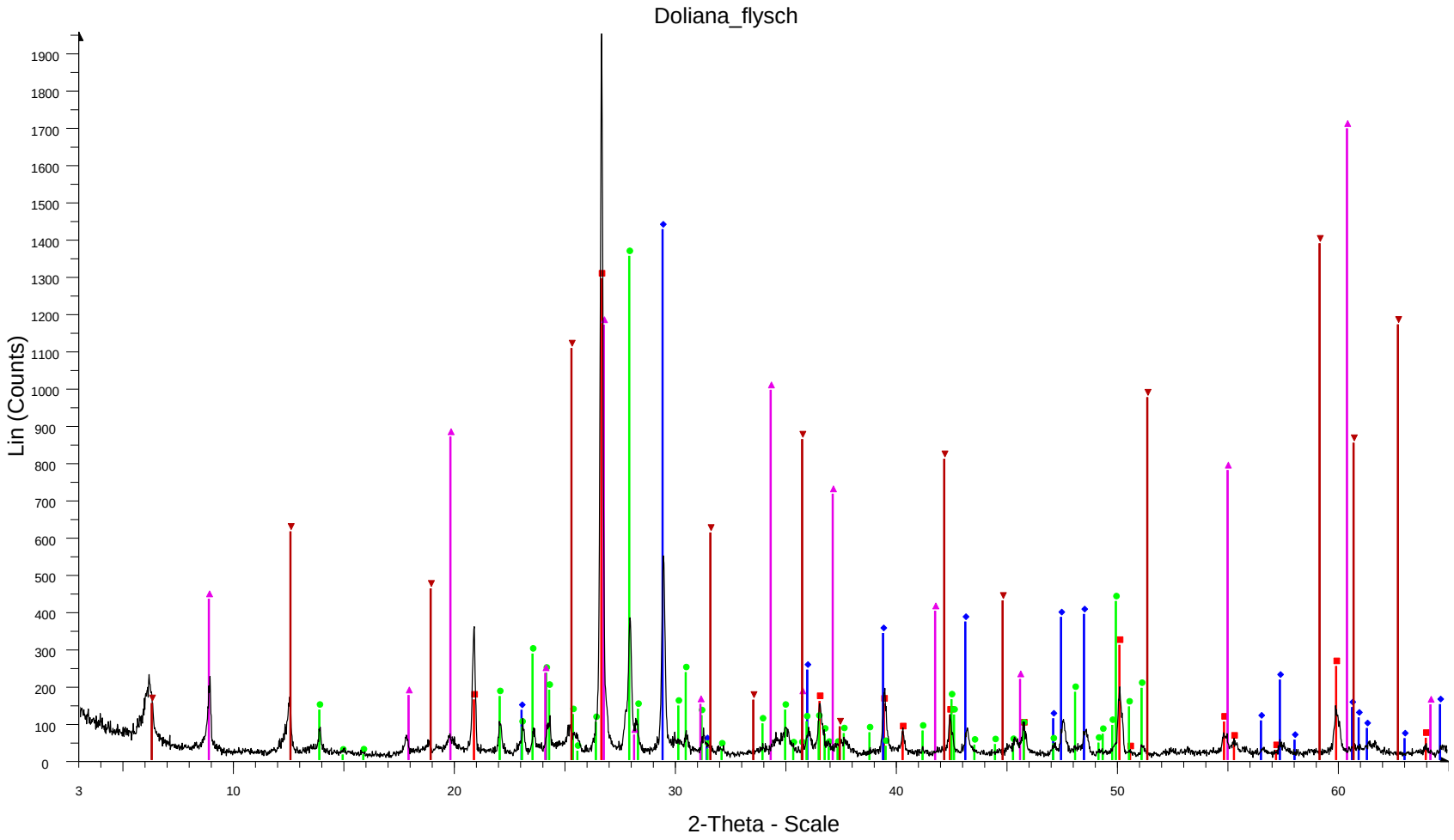

Doliana_flysch - File: Doliana_flysch.raw - Type: 2Th/Th locked - Start: 3.000 ° - End: 65.000 ° - Step: 0.020 ° - Step time: 1. s - Temp.: 25 °C (Room) - Time Started: 16 s - 2-Theta: 3.000 ° - Theta: 1.500 ° - Chi: 0.00 ° - Phi:
Operations: Import

00-046-1045 (*) - Quartz, syn - SiO2 - Y: 66.33 % - d x by: 1. - WL: 1.5406 - Hexagonal - I/Ic PDF 3.4 - S-Q 7.9 % -

00-005-0586 (*) - Calcite, syn - CaCO3 - Y: 73.10 % - d x by: 1. - WL: 1.5406 - Rhombo.R.axes - I/Ic PDF 2. - S-Q 14.8 % -

00-009-0466 (*) - Albite, ordered - NaAlSi3O8 - Y: 69.42 % - d x by: 1. - WL: 1.5406 - Triclinic - I/Ic PDF 2.1 - S-Q 13.4 % -

00-009-0343 (D) - Illite, trioctahedral - K0.5(Al,Fe,Mg)3(Si,Al)4O10(OH)2 - Y: 86.98 % - d x by: 1. - WL: 1.5406 - Orthorhombic - I/Ic PDF 1. - S-Q 35.2 % -

00-012-0243 (D) - Clinochlore - Mg-Fe-Fe-Al-Si-O-OH - Y: 71.13 % - d x by: 1. - WL: 1.5406 - Orthorhombic - I/Ic PDF 1. - S-Q 28.8 % -

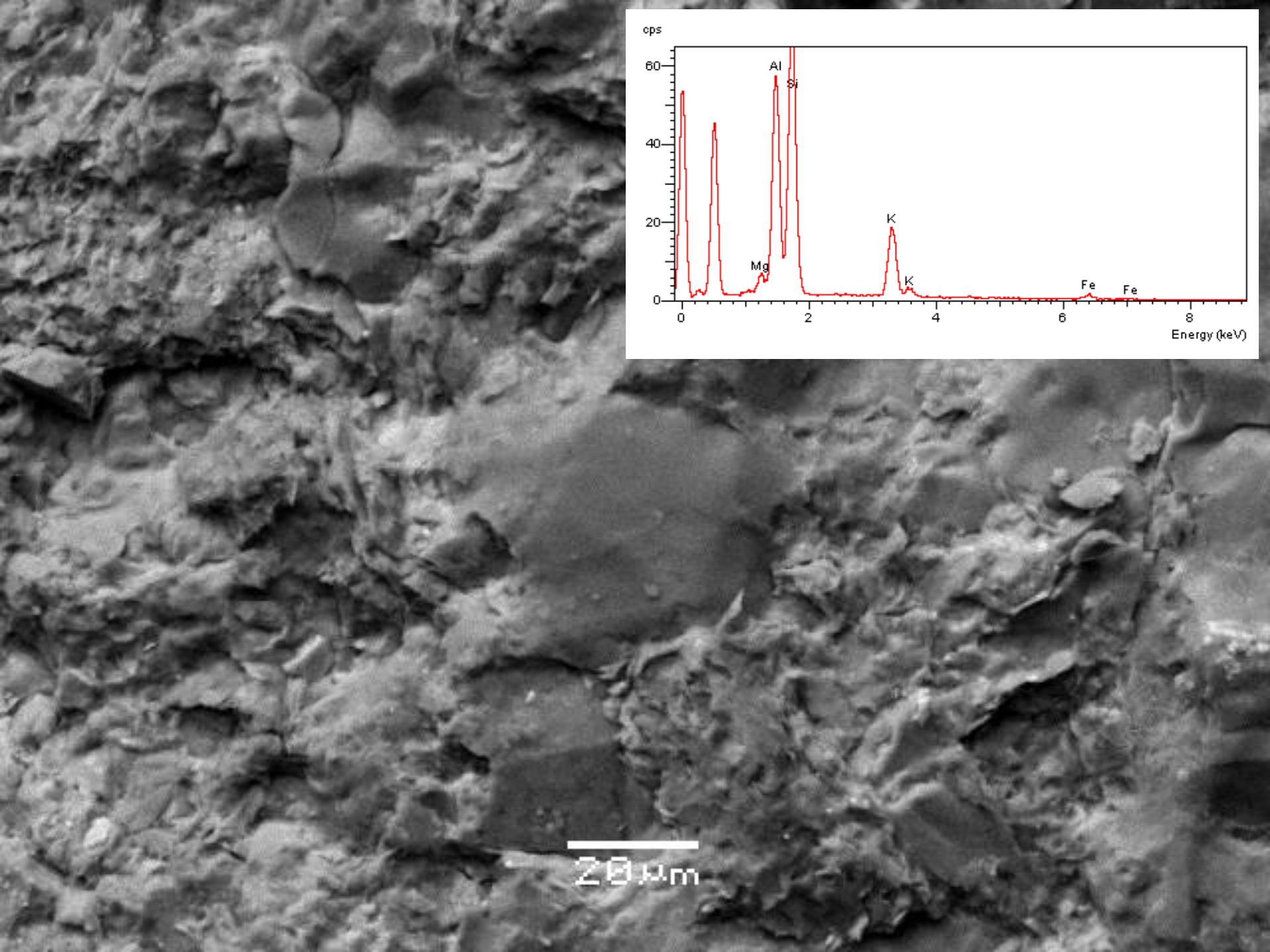
cps
60
40
20
0
Al
Si
Mg
K
K
Fe
Fe
0
2
4
6
8
Energy (keV)
20µm

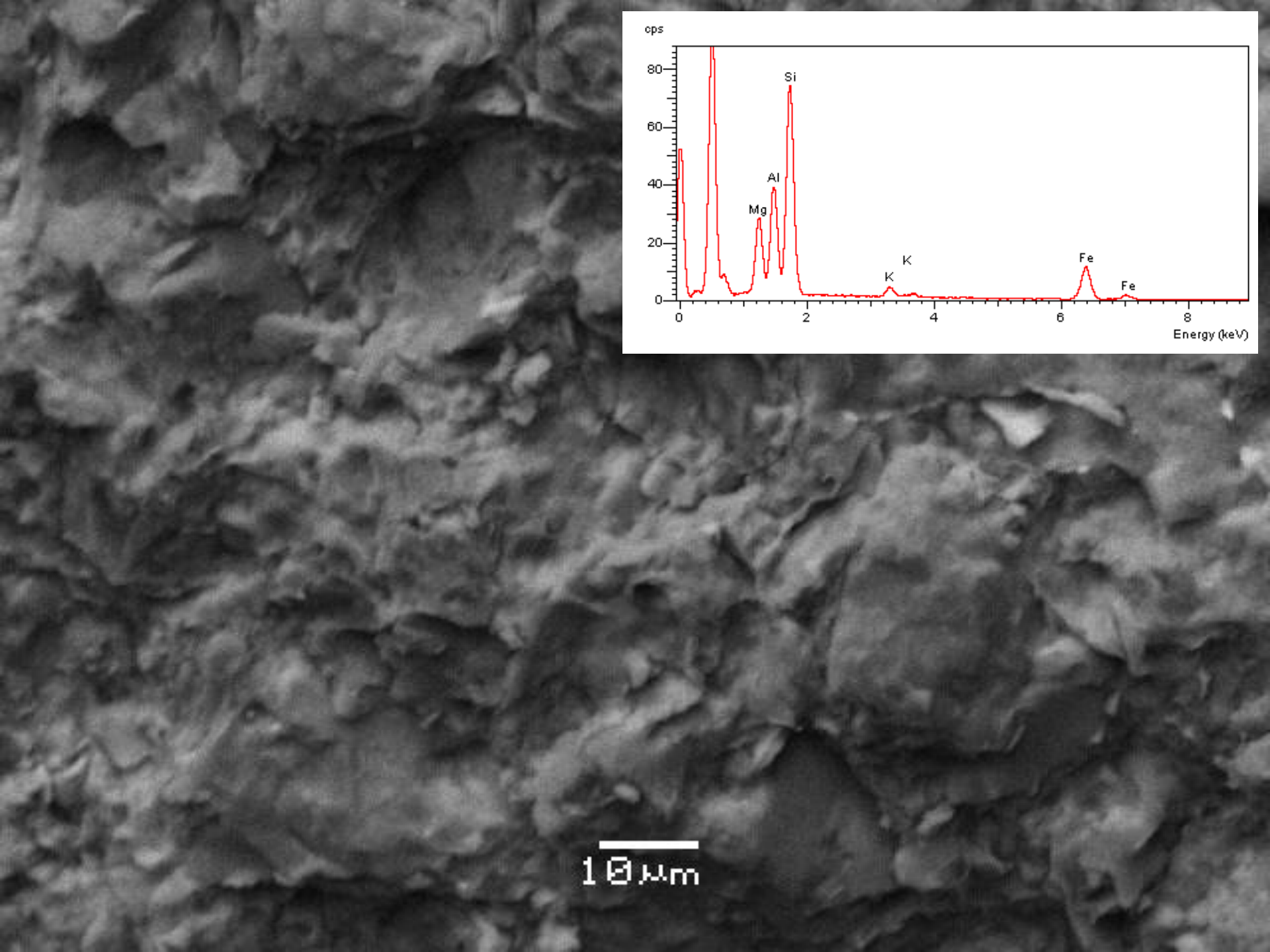
cps
80
60
40
20
0
Si
Al
Mg
K
K
Fe
Fe
0
2
4
6
8
Energy (keV)
10 µm


ΚΡΥΣΤΑΛΛΟΙ (ΚΛΑΣΤΙΚΟΙ)
ΖΙΡΚΟΝΙΟΥ – $ZrSiO_4$
10 μm


ΑΣΒΕΣΤΟΛΙΘΟΙ
(ΗΠΕΙΡΟΣ)

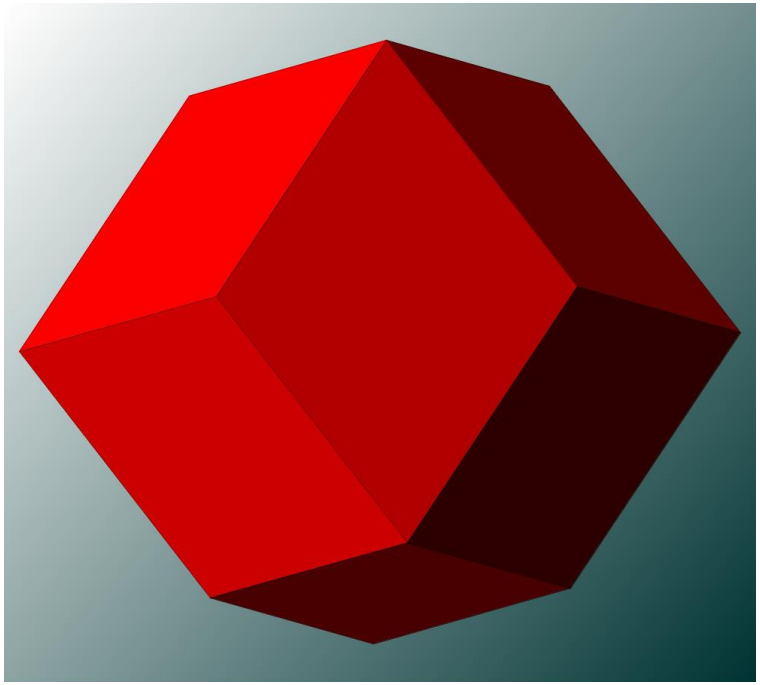

ΚΡΥΣΤΑΛΛΟΣ

ΓΡΑΝΑΤΗ

Αλμανδίνης σε σχιστόλιθο (http://www.geo.auth.gr/106/8_silicates/neso/almandine_04.jpg)

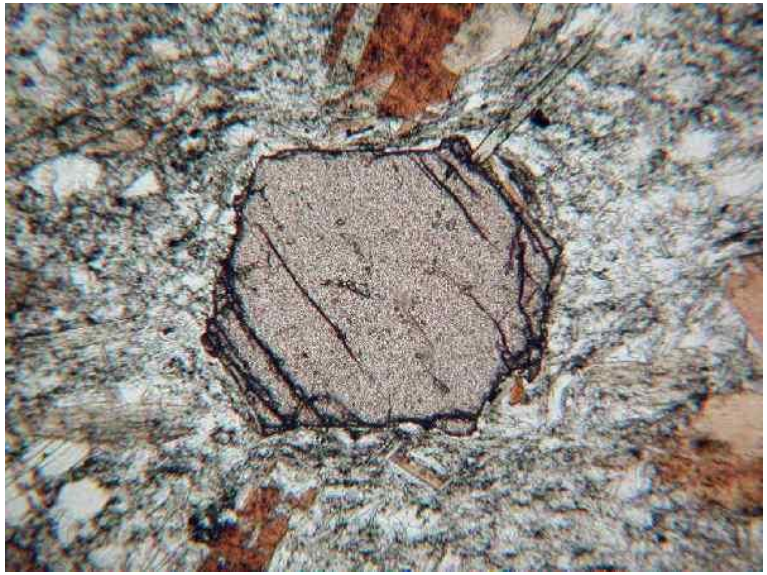

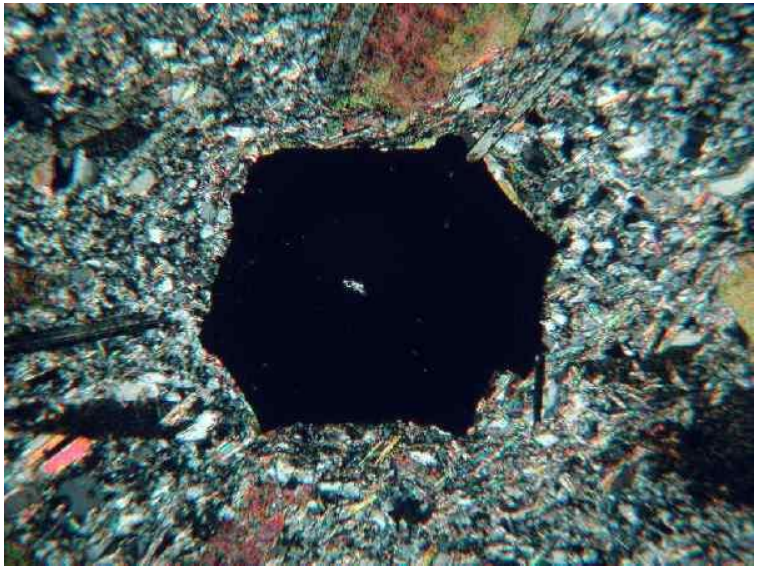

http://www.geo.auth.gr/courses/gmo/gmo212y/

American Mineralogist, Volume 98, pages 785–811, 2013

IMA REPORT

Nomenclature of the garnet supergroup

EDWARD S. GREW,[1,*] ANDREW J. LOCOCK,[2] STUART J. MILLS,[3,†] IRINA O. GALUSKINA,[4] EVGENY V. GALUSKIN,[4] AND ULF HÅLENIUS[5]

[1]School of Earth and Climate Sciences, University of Maine, Orono, Maine 04469, U.S.A.
[2]Department of Earth and Atmospheric Sciences, University of Alberta, Edmonton, Alberta T6G 2E3, Canada
[3]Geosciences, Museum Victoria, GPO Box 666, Melbourne 3001, Victoria, Australia
[4]Faculty of Earth Sciences, Department of Geochemistry, Mineralogy and Petrography, University of Silesia, Będzińska 60, 41-200 Sosnowiec, Poland
[5]Swedish Museum of Natural History, Department of Mineralogy, P.O. Box 50 007, 104 05 Stockholm, Sweden

ABSTRACT

The garnet supergroup includes all minerals isostructural with garnet regardless of what elements occupy the four atomic sites, i.e., the supergroup includes several chemical classes. There are presently 32 approved species, with an additional 5 possible species needing further study to be approved. The general formula for the garnet supergroup minerals is $\{X_3\}[Y_2](Z_3)\varphi_{12}$, where X, Y, and Z refer to dodecahedral, octahedral, and tetrahedral sites, respectively, and φ is O, OH, or F. Most garnets are cubic, space group $Ia\bar{3}d$ (no. 230), but two OH-bearing species (henritermierite and holtstamite) have tetragonal symmetry, space group, $I4_1/acd$ (no. 142), and their X, Z, and φ sites are split into more symmetrically unique atomic positions. Total charge at the Z site and symmetry are criteria for distinguishing groups, whereas the dominant-constituent and dominant-valency rules are critical in identifying species. Twenty-nine species belong to one of five groups: the tetragonal henritermierite group and the isometric bitikleite, schorlomite, garnet, and berzeliite groups with a total charge at Z of 8 (silicate), 9 (oxide), 10 (silicate), 12 (silicate), and 15 (vanadate, arsenate), respectively. Three species are single representatives of potential groups in which Z is vacant or occupied by monovalent (halide, hydroxide) or divalent cations (oxide). We recommend that suffixes (other than Levinson modifiers) not be used in naming minerals in the garnet supergroup. Existing names with suffixes have been replaced with new root names where necessary: bitikleite-(SnAl) to bitikleite, bitikleite-(SnFe) to dzhuluite, bitikleite-(ZrFe) to usturite, and elbrusite-(Zr) to elbrusite. The name hibschite has been discredited in favor of grossular as Si is the dominant cation at the Z site. Twenty-one end-members have been reported as subordinate components in minerals of the garnet supergroup of which six have been reported in amounts up to 20 mol% or more, and, thus, there is potential for more species to be discovered in the garnet supergroup. The nomenclature outlined in this report has been approved by the Commission on New Minerals, Nomenclature and Classification of the International Mineralogical Association (Voting Proposal 11-D).

FIGURE 2 Dark, fine-grained sedimentary shale, such as (**A**), is transformed at intermediate pressure and temperature into bright, shiny, mica schist with large garnet crystals (**B**). During this transition, the rock loses several weight percent H_2O. Such a transition is an important source of metamorphic fluid. Scale for these samples is similar to that of Figure 1.

B. Jamtveit; Elements (2010)

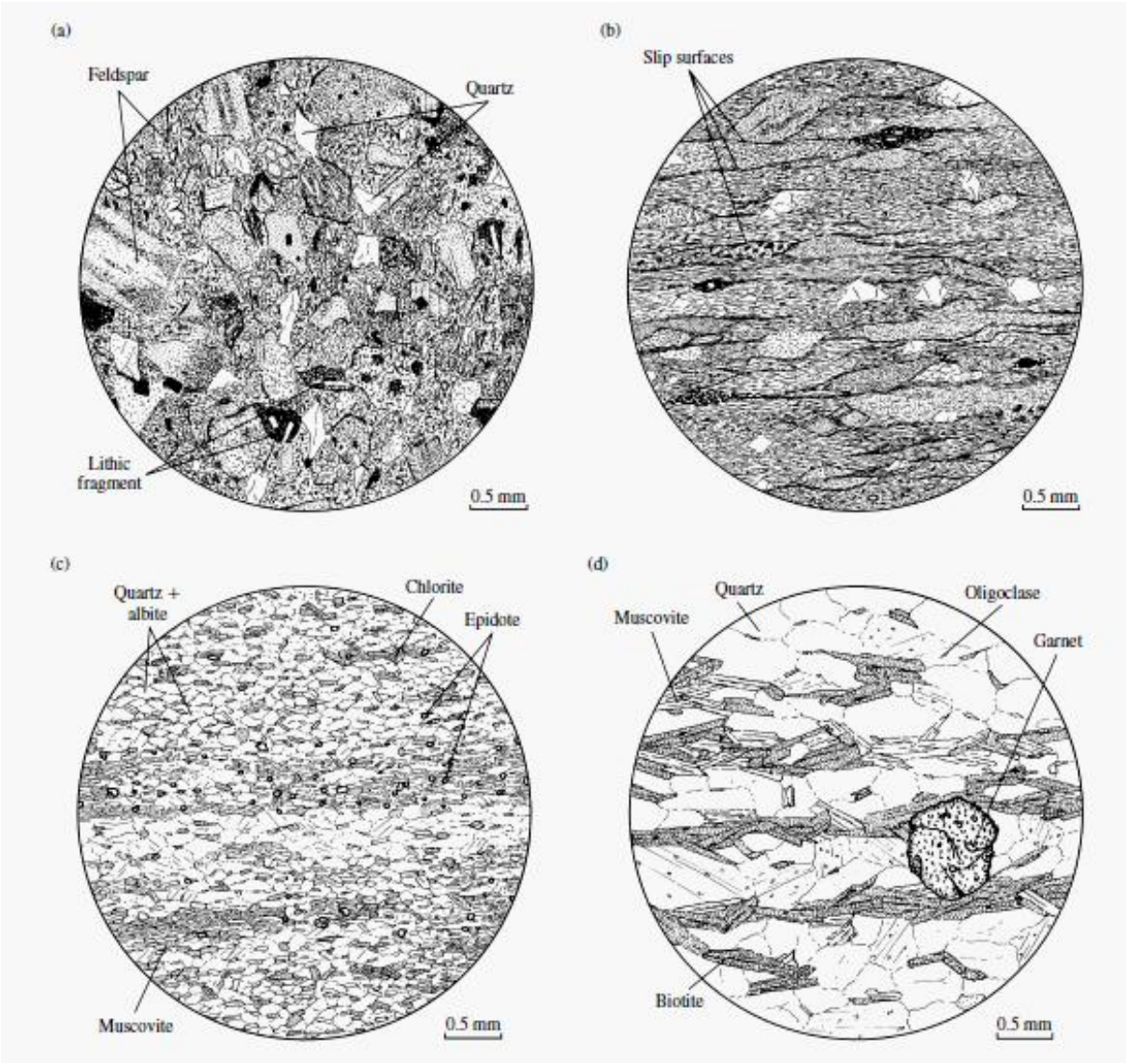

Progressive metamorphism and development of tectonite fabric in lithic wacke (graywacke); © Myron G. Best (2003)

Πορφυροβλαστικός ιστός

γρανατούχος αμφιβολίτης

γρανατούχος μεταπηλίτης

ανάδρομος εκλογίτης

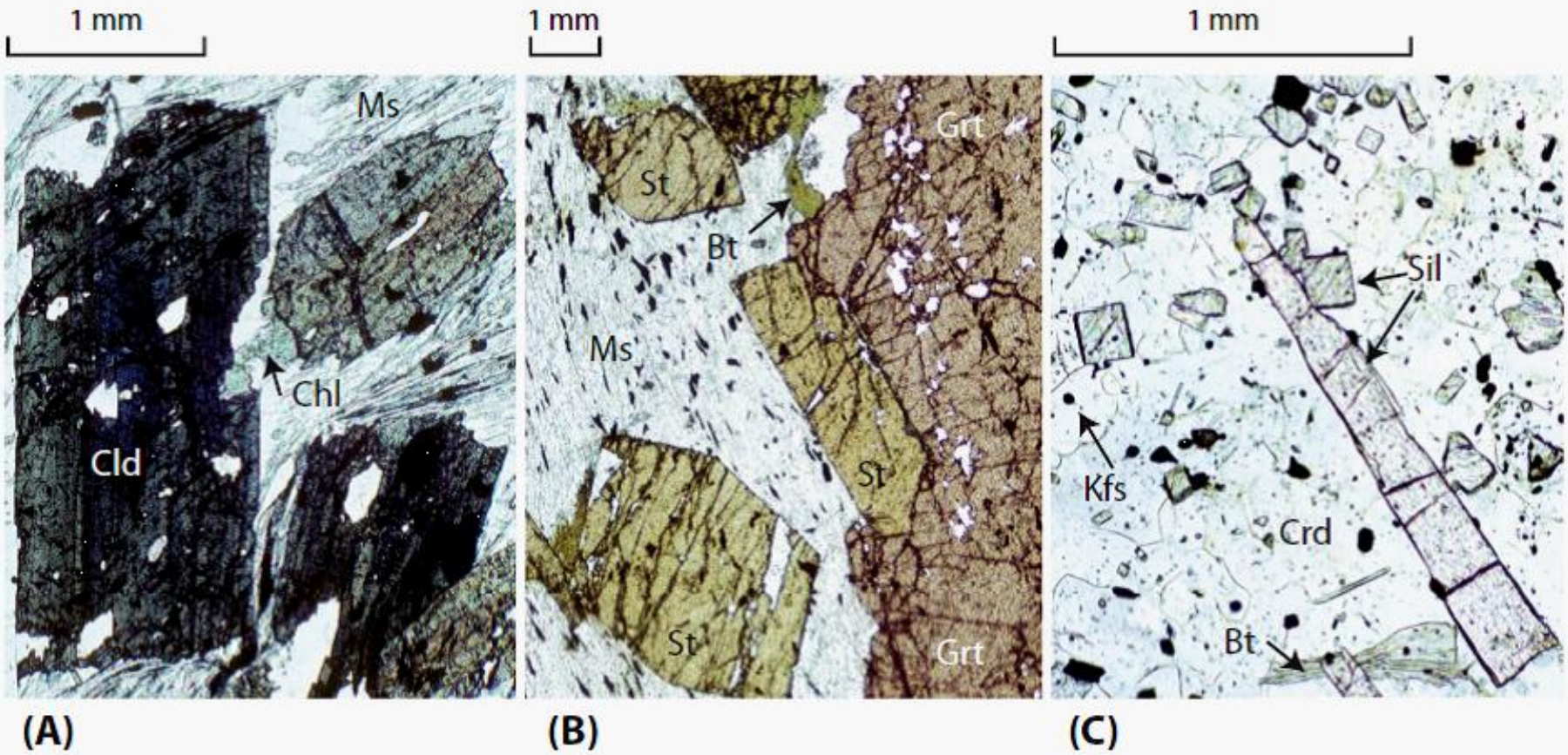

Figure 14.24 Photomicrographs of thin sections under plane light of metapelite from three different grades of metamorphism. **(A)** Chloritoid-muscovite-chlorite-quartz schist. **(B)** Staurolite-garnet-muscovite-biotite-quartz schist. **(C)** Sillimanite-cordierite-K-feldspar-biotite-quartz hornfels.

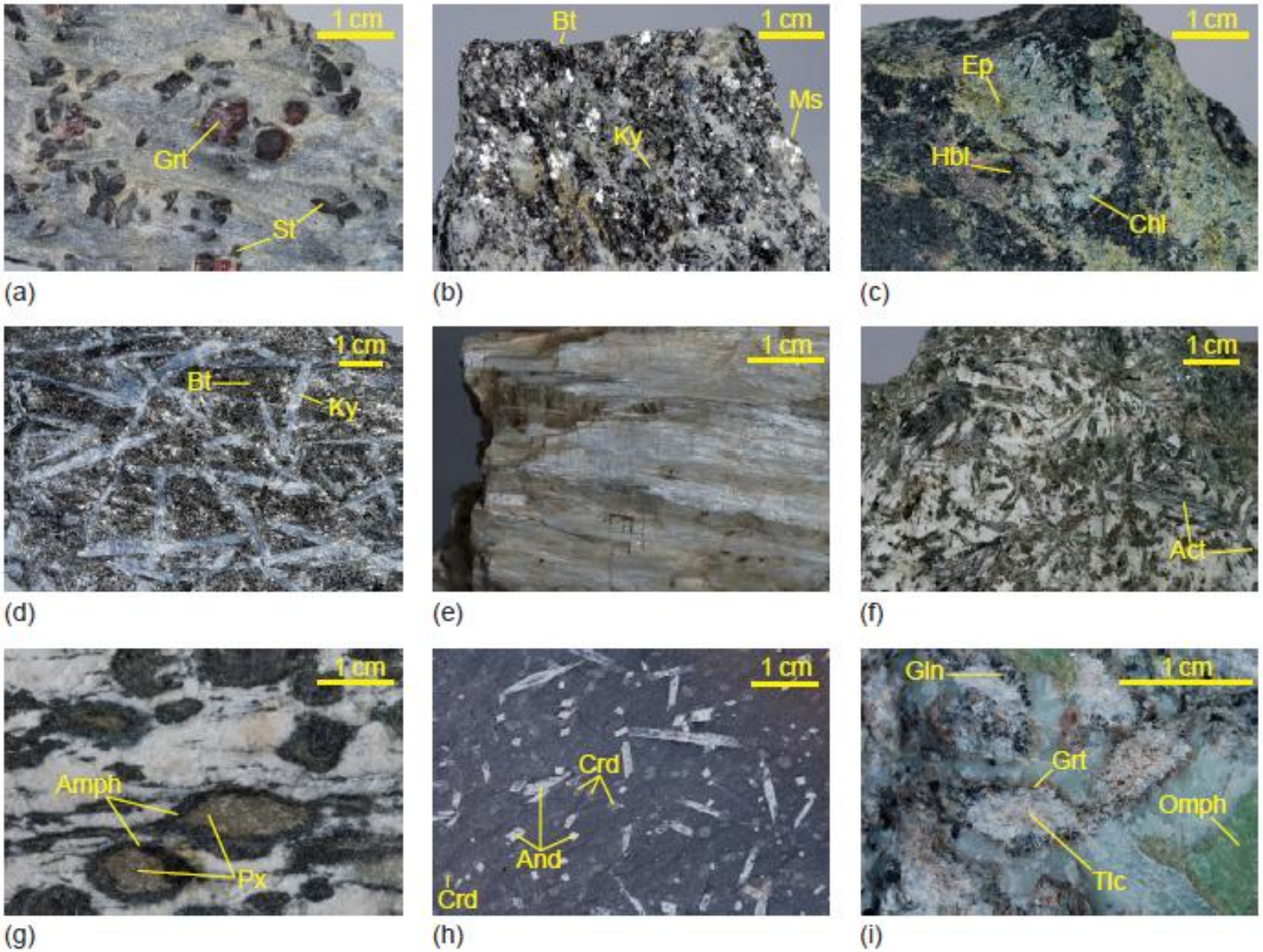

Examples of common metamorphic minerals;

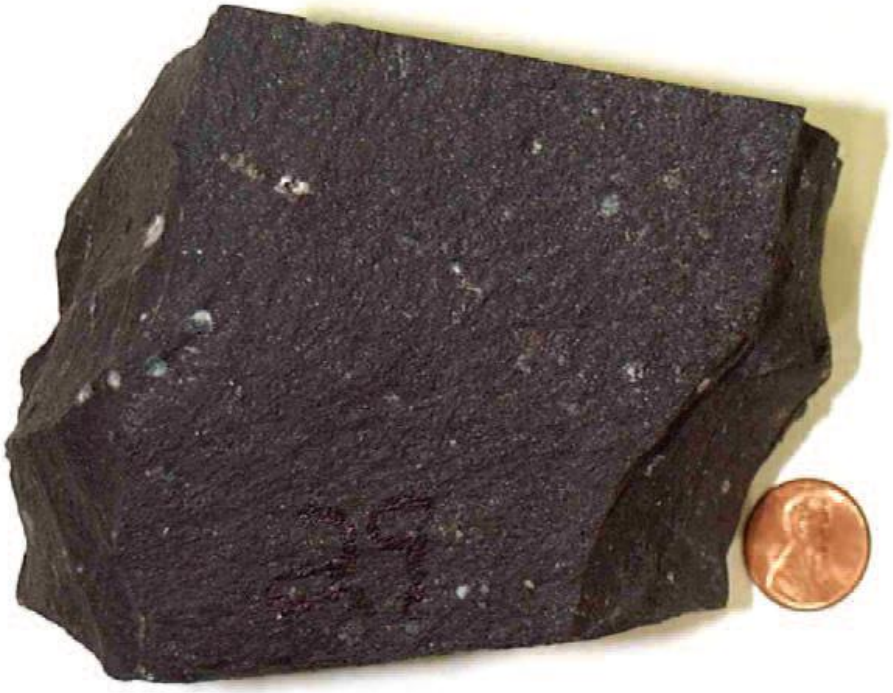

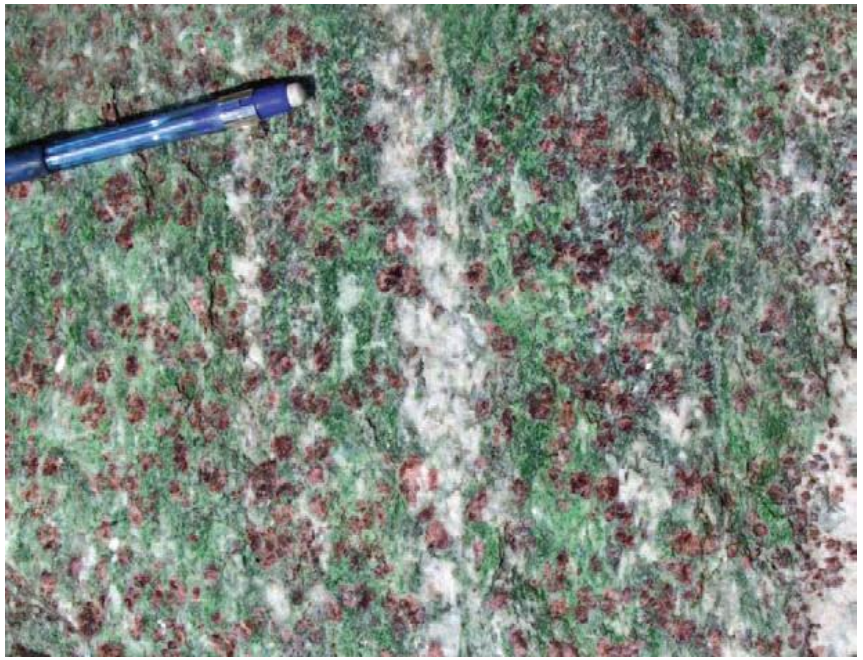

FIGURE 1 Dark, fine-grained basalt, such as (**A**), is transformed into a spectacular, coarse-grained, green and red eclogite (**B**) during metamorphism at high pressure and temperature. During the metamorphic transition, augite (pyroxene), plagioclase, and olivine in the basalt are transformed into garnet (red), omphacite (green), and clinozoisite (white). Density increases from about 2.9 g/cm^3 to about 3.5 g/cm^3, making the rock's transition important for large-scale geodynamic processes, including basin subsidence and subduction.

B. Jamtveit; Elements (2010)

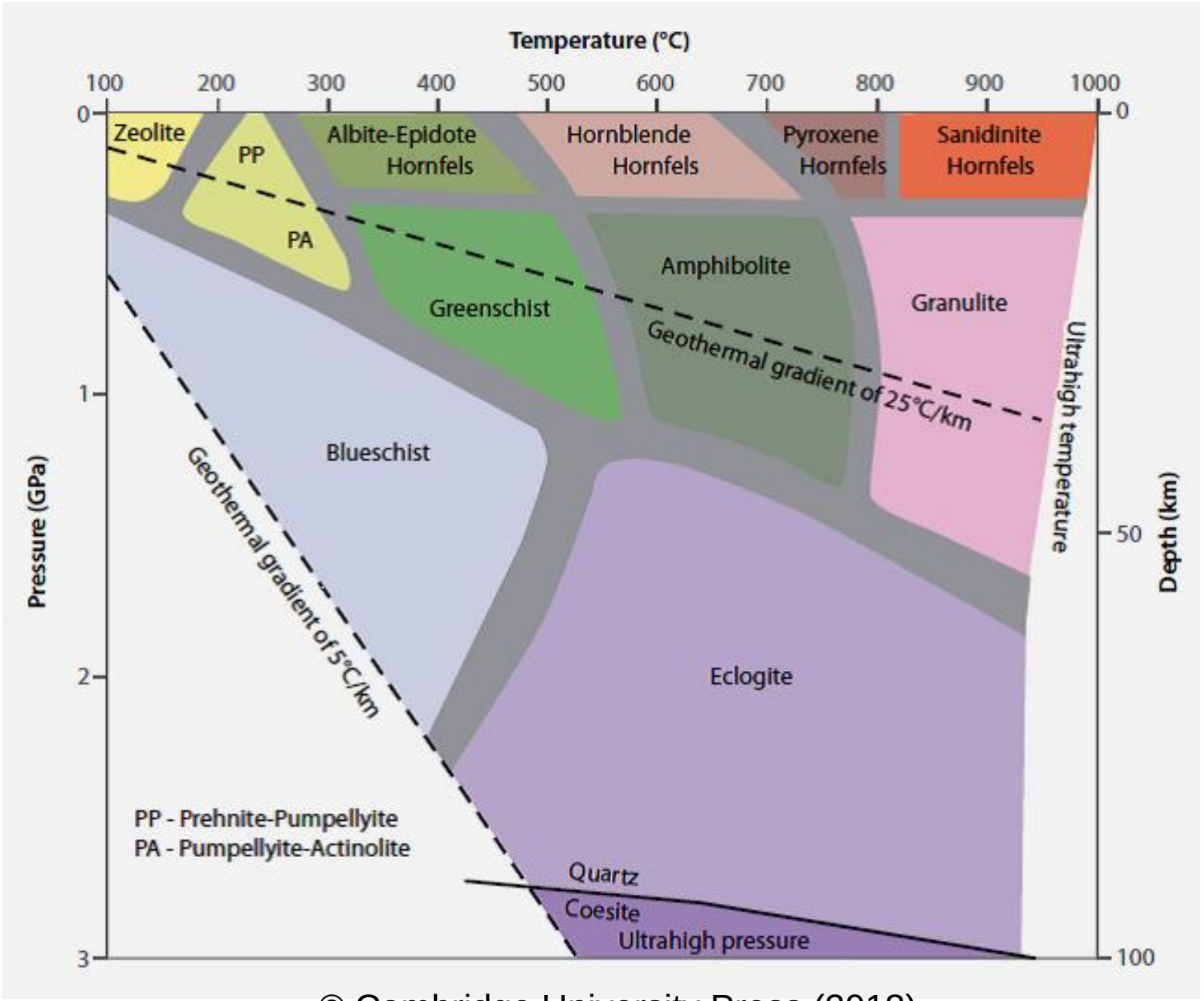

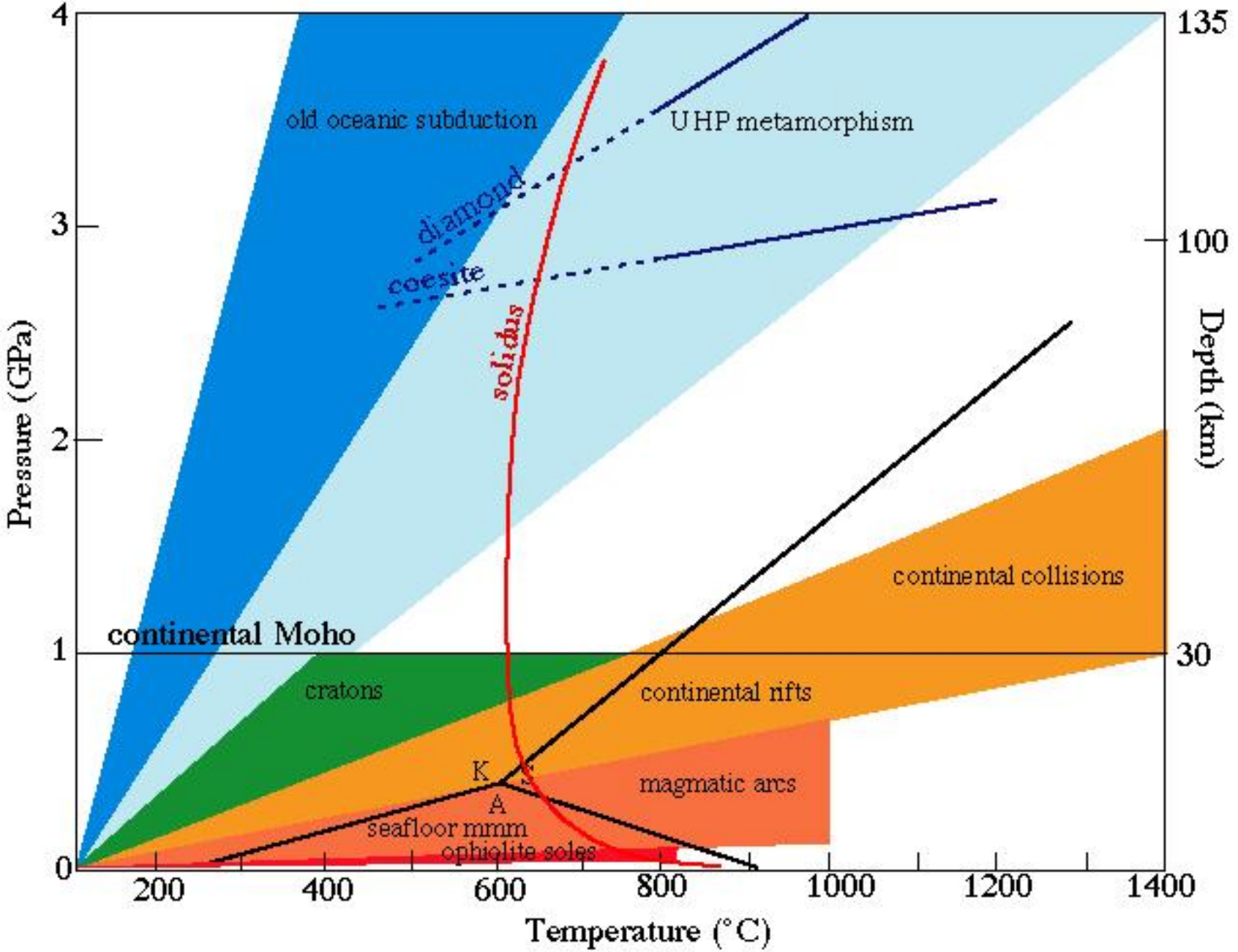
old oceanic subduction
UHP metamorphism
diamond
coesite
solidus
continental Moho
cratons
continental rifts
continental collisions
magmatic arcs
K
A
seafloor mmm
ophiolite soles
Pressure (GPa)
Depth (km)
Temperature (°C)
0
1
2
3
4
30
100
135
200
400
600
800
1000
1200
1400

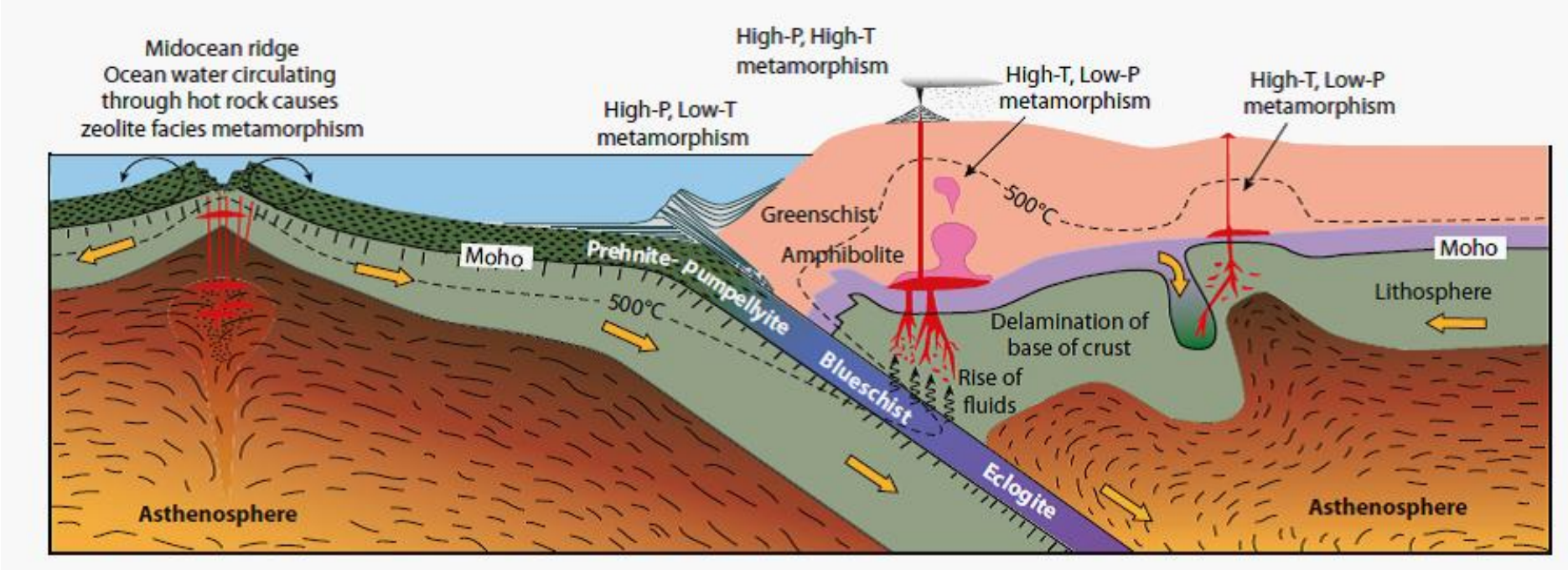

Eur. J. Mineral.
1992, **4**, 487-507

Carpholite, sudoite, and chloritoid in low-grade high-pressure metapelites from Crete and the Peloponnese, Greece

THOMAS THEYE[1], EBERHARD SEIDEL[2], OLIVIER VIDAL[3]

[1] Institut für Mineralogie, Ruhr-Universität Bochum, Universitätsstraße 150, 4630 Bochum, F.R. Germany

[2] Mineralogisch-Petrographisches Institut, Universität zu Köln, Zülpicher Straße 49, 5000 Köln, F.R. Germany

[3] Laboratoire de Géologie, Ecole Normale Supérieure, 24 rue Lhomond, 75005 Paris, France

The same parageneses as in Central Crete have been observed in *Western Crete* (400°C, 10 kbar) and in the *Peloponnese* (≈ 450°C, 17 kbar), but with carpholites richer in Mg. For these rocks, AFM three-phase parageneses show fixed mineral compositions, suggesting equilibrium with a hydrous fluid phase of constant composition. The highest grade of metamorphic evolution of metapelites from the Phyllite-Quartzite Unit is reflected by the appearance of almandine-rich garnet in the Peloponnese.

Considering metapelite assemblages involving quartz, carpholite, chloritoid, sudoite, chlorite and pyrophyllite, both the observed succession of AFM topologies and the calculated equilibrium curves offer possibilities for evaluating P, T and a_{H_2O} of very low to low-grade high-pressure metamorphism.

Key-words : Fe-Mg-carpholite, sudoite, chloritoid, high-pressure metamorphism, activity of H_2O, Phyllite-Quartzite Unit (Greece)

$$Mn^{2+}Al_2Si_2O_6(OH)_4$$

$$(Fe^{2+}, Mg, Mn)_2Al_4Si_2O_{10}(OH)_4$$

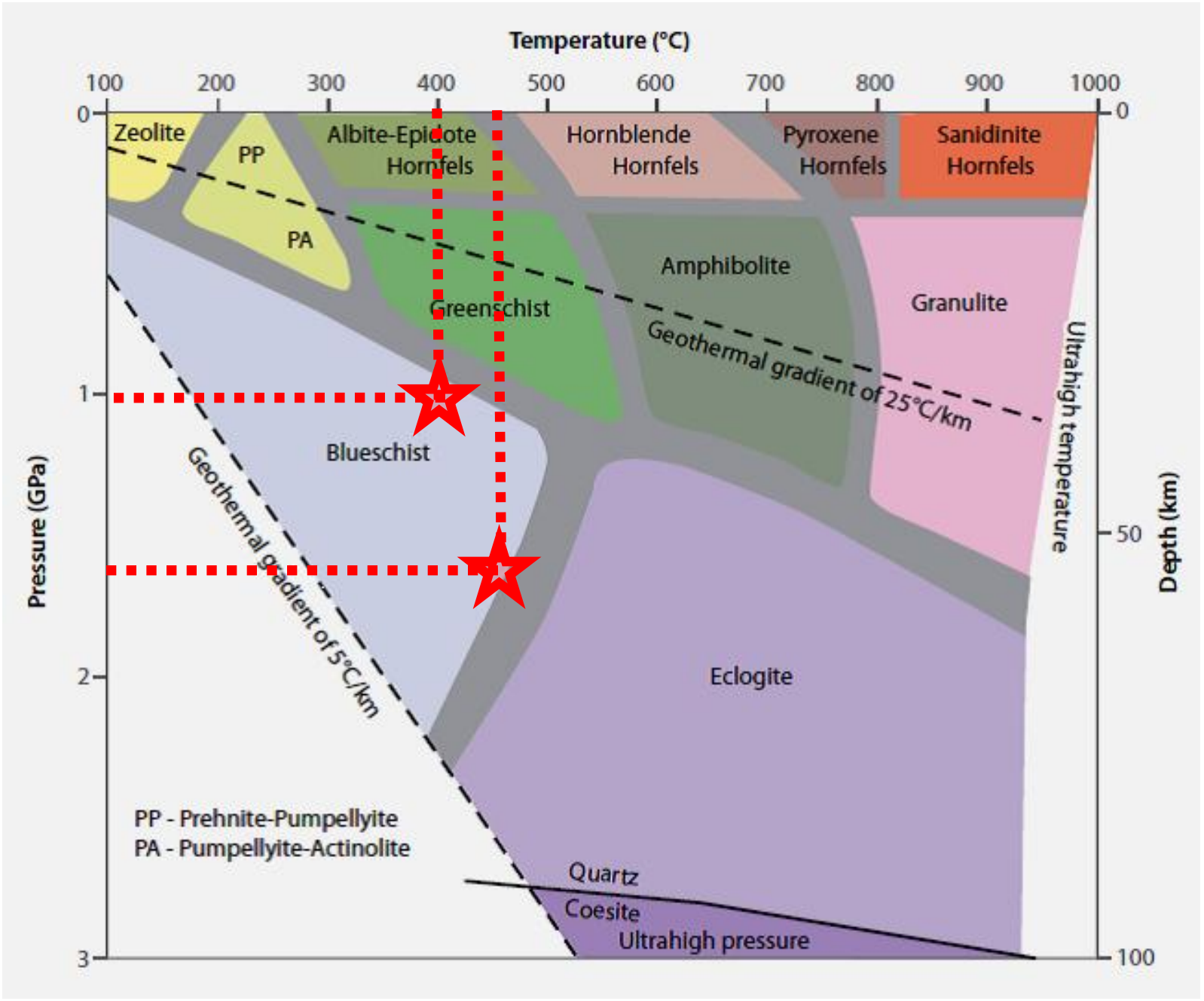
Temperature (°C)
100
200
300
400
500
600
700
800
900
1000
0
1
2
3
Pressure (GPa)
Zeolite
PP
PA
Albite-Epidote Hornfels
Hornblende Hornfels
Pyroxene Hornfels
Sanidinite Hornfels
Greenschist
Amphibolite
Granulite
Blueschist
Eclogite
Geothermal gradient of 25°C/km
Geothermal gradient of 5°C/km
Ultrahigh temperature
Depth (km)
0
50
100
PP - Prehnite-Pumpellyite
PA - Pumpellyite-Actinolite
Quartz
Coesite
Ultrahigh pressure

N.L. Bowen

(1922)

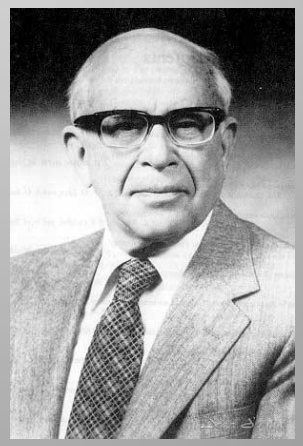

S. Goldich

(1938)

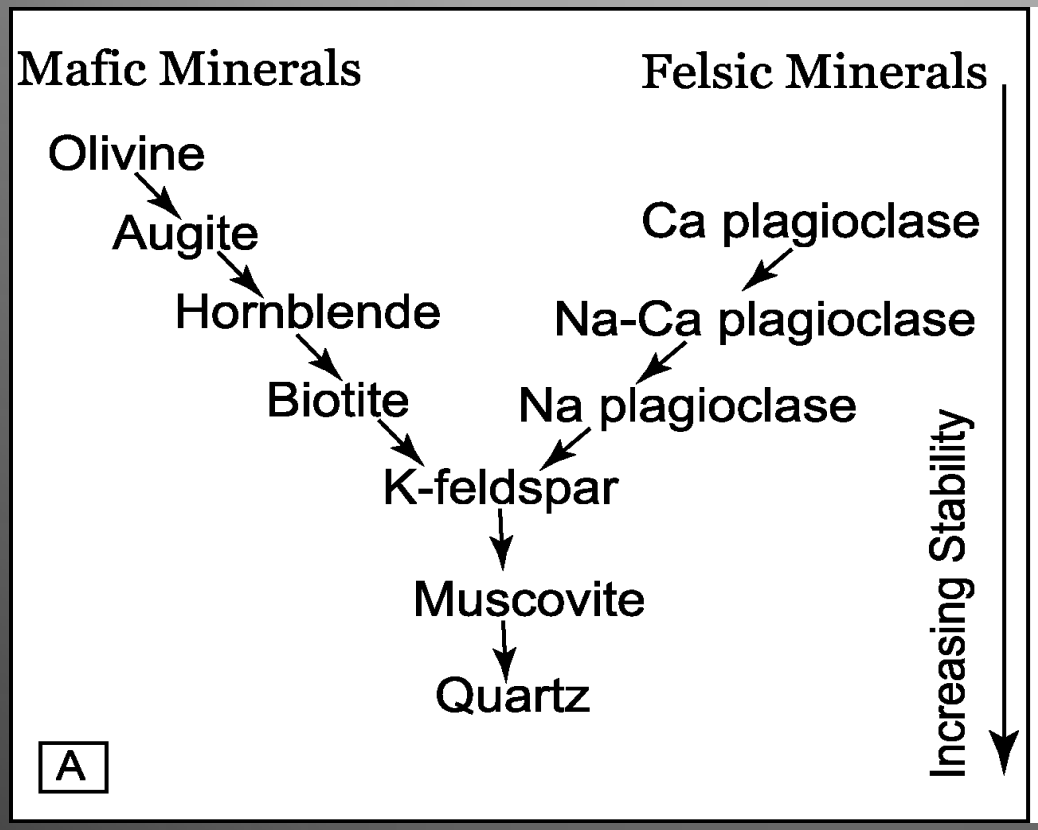

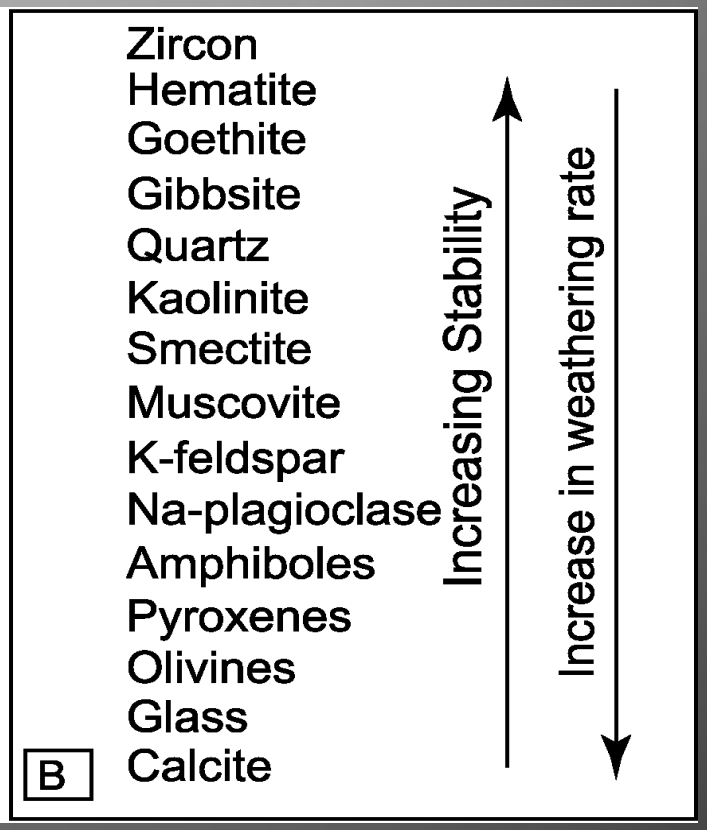

• DISSOLUTION RATE (*R*)

ΡΥΘΜΟΣ ΔΙΑΛΥΤΟΠΟΙΗΣΗΣ

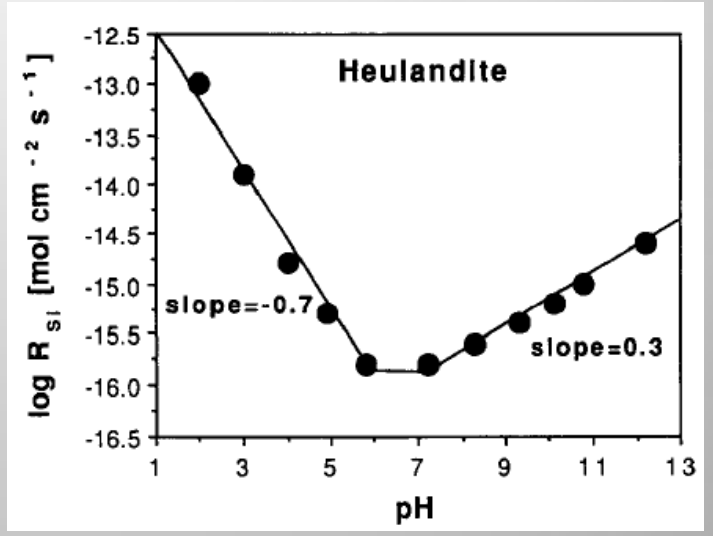

ΖΕΟΛΙΘΟΣ

-Log *R* (pH ~ 7)

11.8 mol/m^2/s

1 mm

300 000 yrs

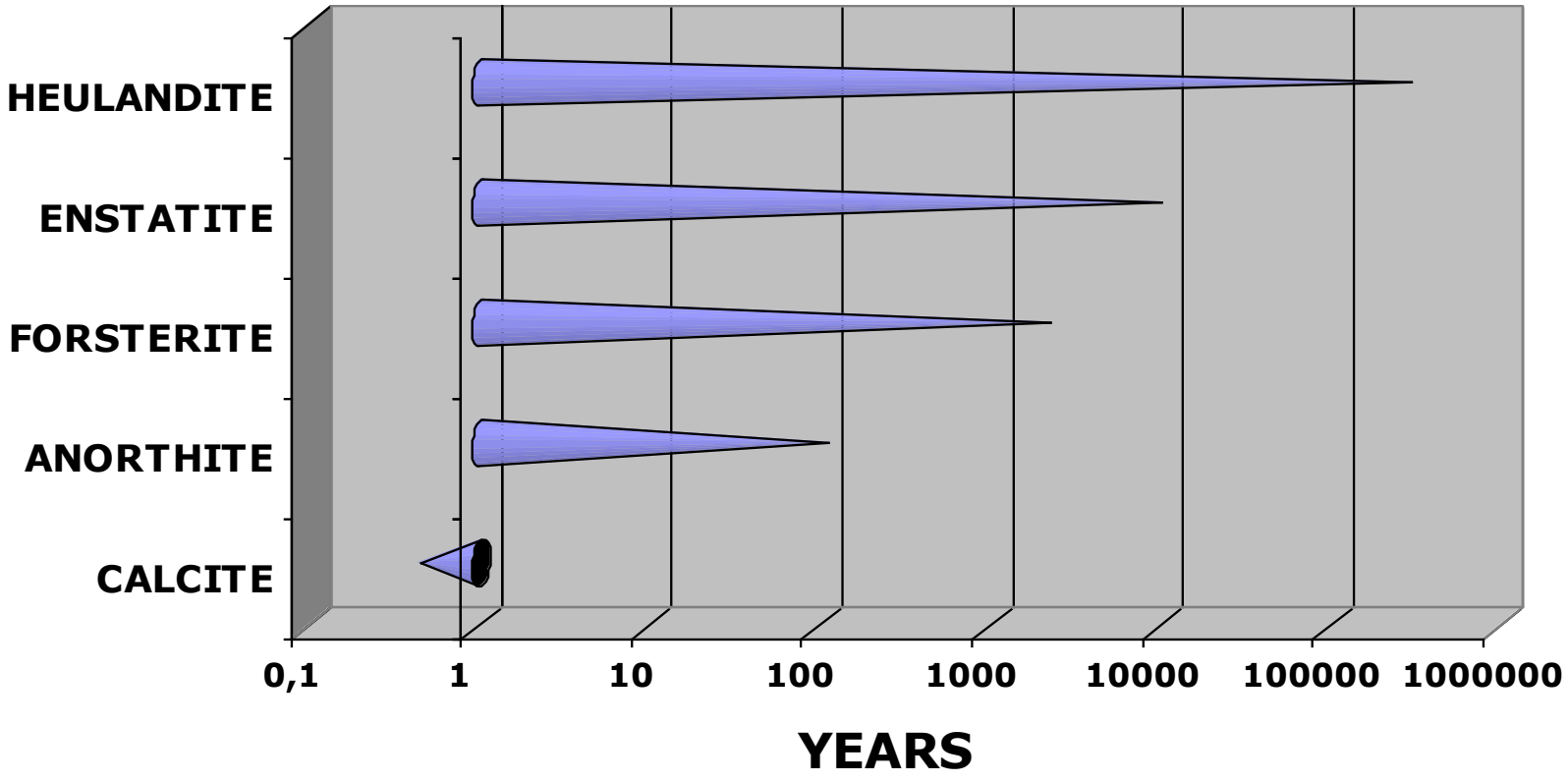

….. ΑΣΒΕΣΤΙΤΗΣ: 150 ημέρες

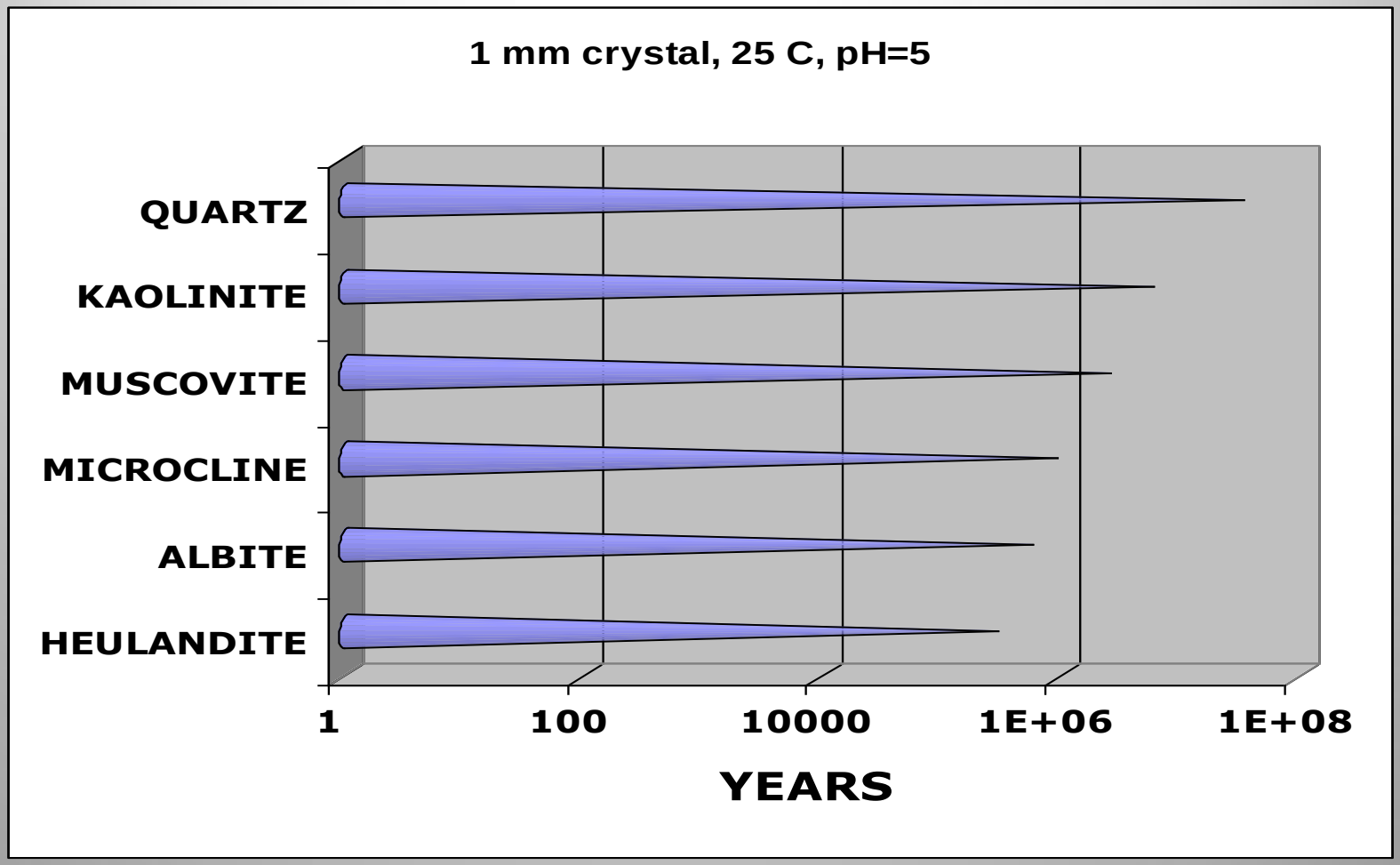

ΧΑΛΑΖΙΑΣ: 34 000 000 έτη.....

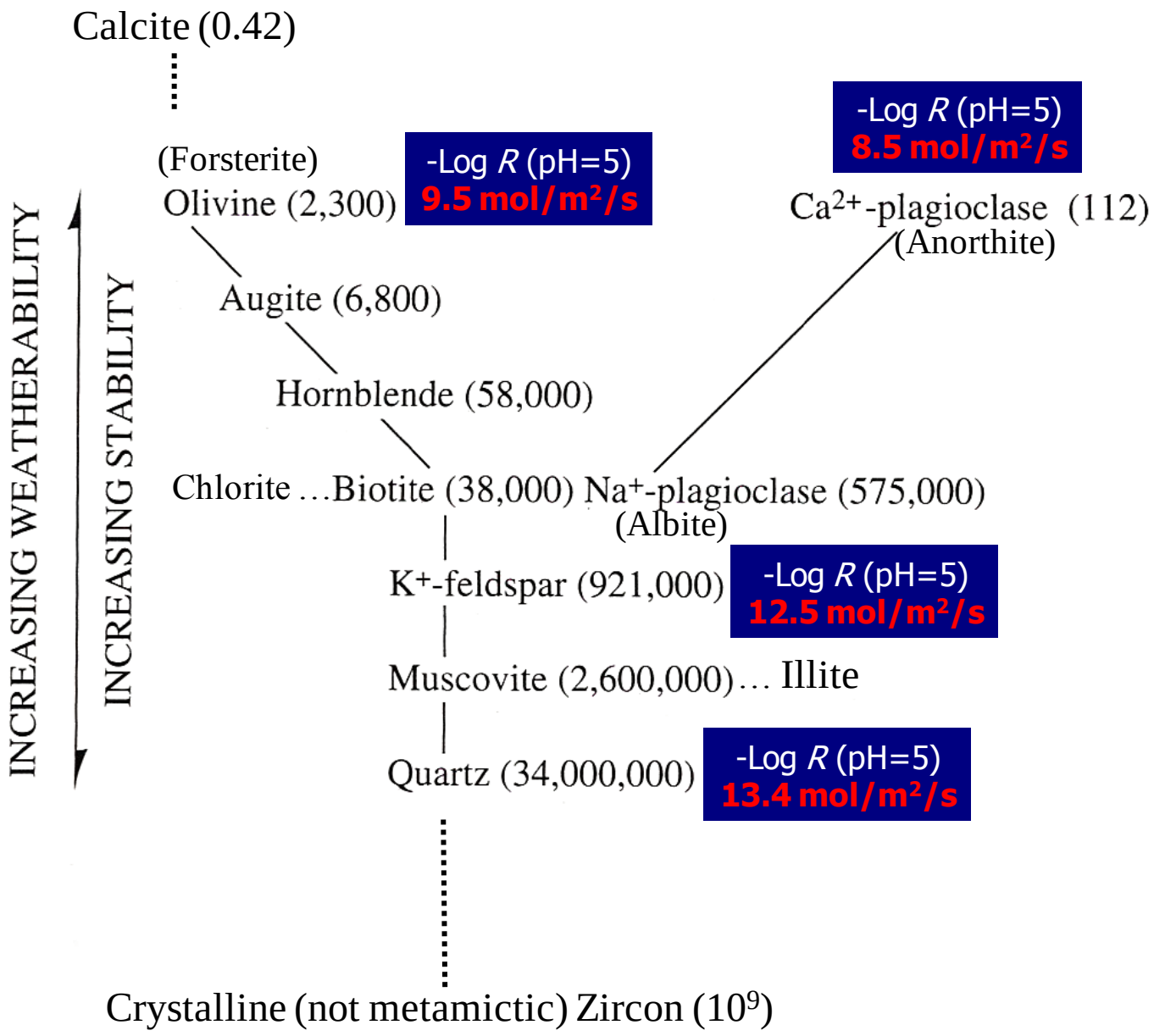
Calcite (0.42)
(Forsterite)
Olivine (2,300)
-Log R (pH=5)
9.5 mol/m²/s
-Log R (pH=5)
8.5 mol/m²/s
Ca2+-plagioclase (112)
(Anorthite)
Augite (6,800)
Hornblende (58,000)
Chlorite …Biotite (38,000)
Na+-plagioclase (575,000)
(Albite)
K+-feldspar (921,000)
-Log R (pH=5)
12.5 mol/m²/s
Muscovite (2,600,000)… Illite
Quartz (34,000,000)
-Log R (pH=5)
13.4 mol/m²/s
Crystalline (not metamictic) Zircon (10^9)
INCREASING WEATHERABILITY
INCREASING STABILITY

Α. ΔΟΛΙΑΝΑ


ΕΔΑΦΟΣ
Α. ΔΟΛΙΑΝΑ


ΚΑΡΣΤ


ΗΠΕΙΡΟΣ


ΗΠΕΙΡΟΣ

Α. ΔΟΛΙΑΝΑ


ΗΠΕΙΡΟΣ


22/06/2006
ΚΙΘΑΙΡΩΝ

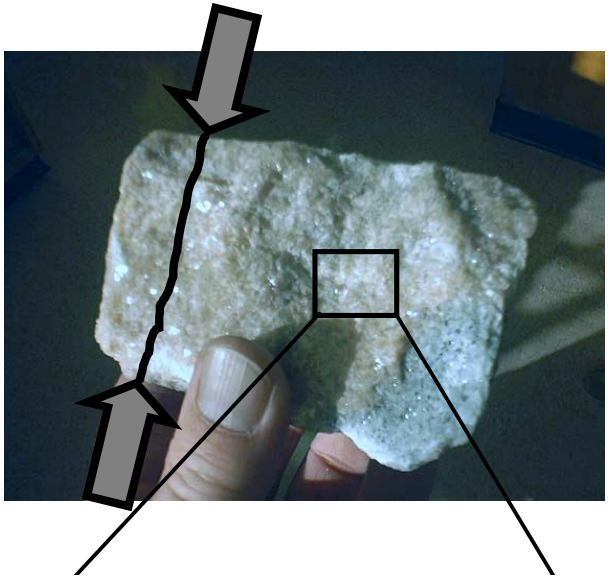

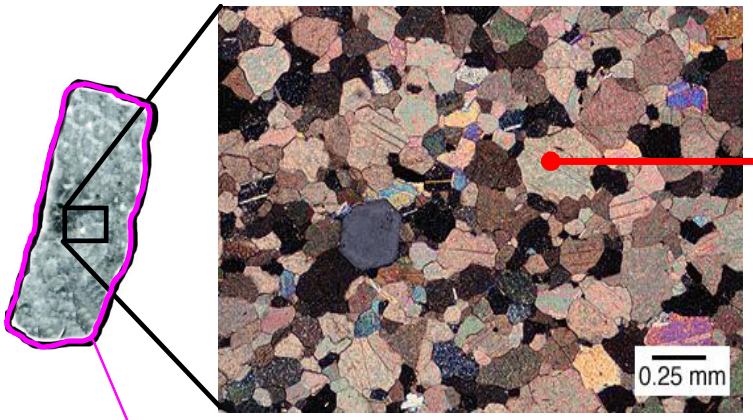

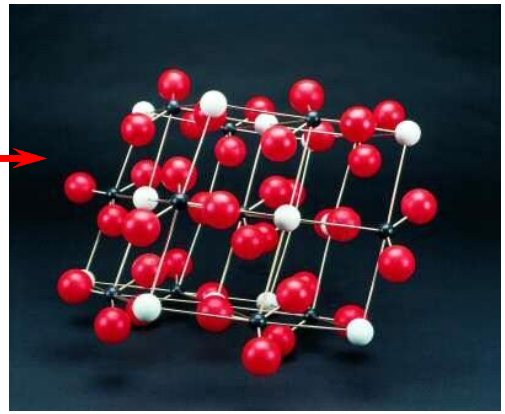

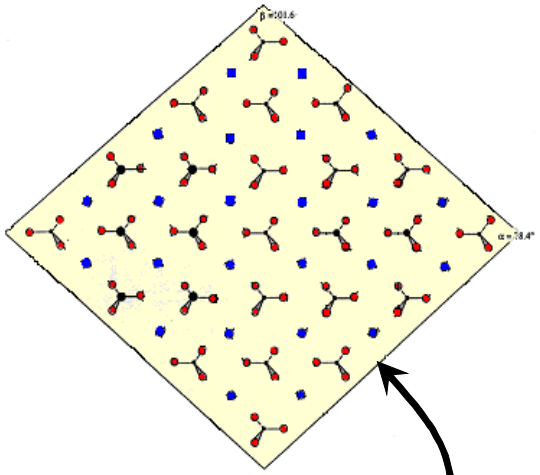

ΔΙΕΠΙΦΑΝΕΙΑ

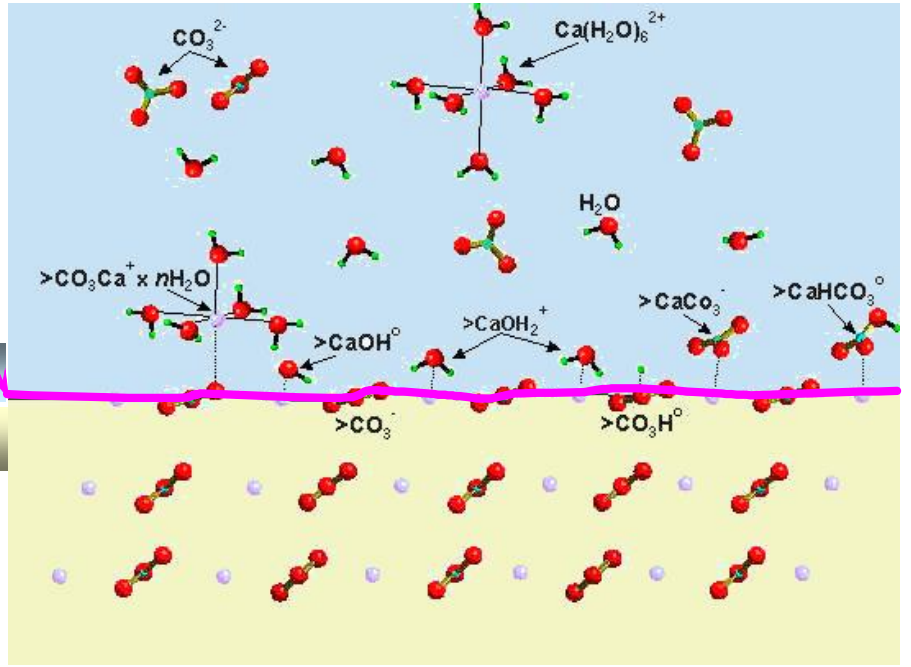

ΜΑΚΡΟΣΚΟΠΙΚΗ ΠΑΡΑΤΗΡΗΣΗ (Km/m/cm/mm-κλίμακα)

ΜΑΚΡΟΣΚΟΠΙΚΗ ΠΑΡΑΤΗΡΗΣΗ (Km/m/cm/mm-κλίμακα)

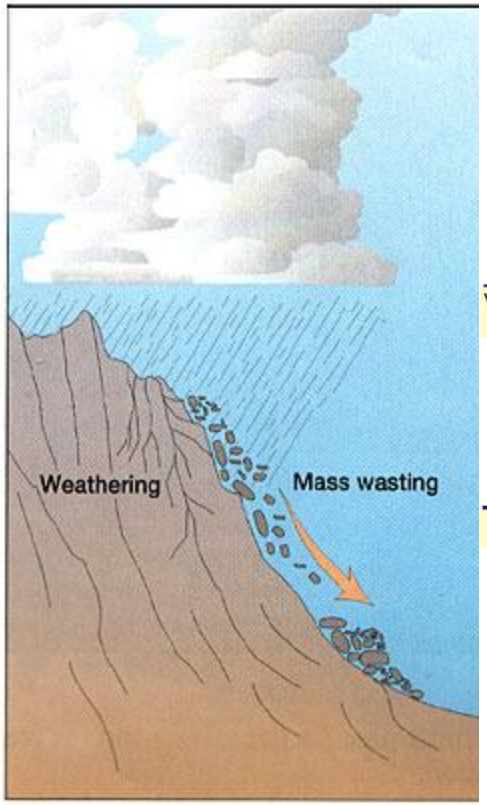

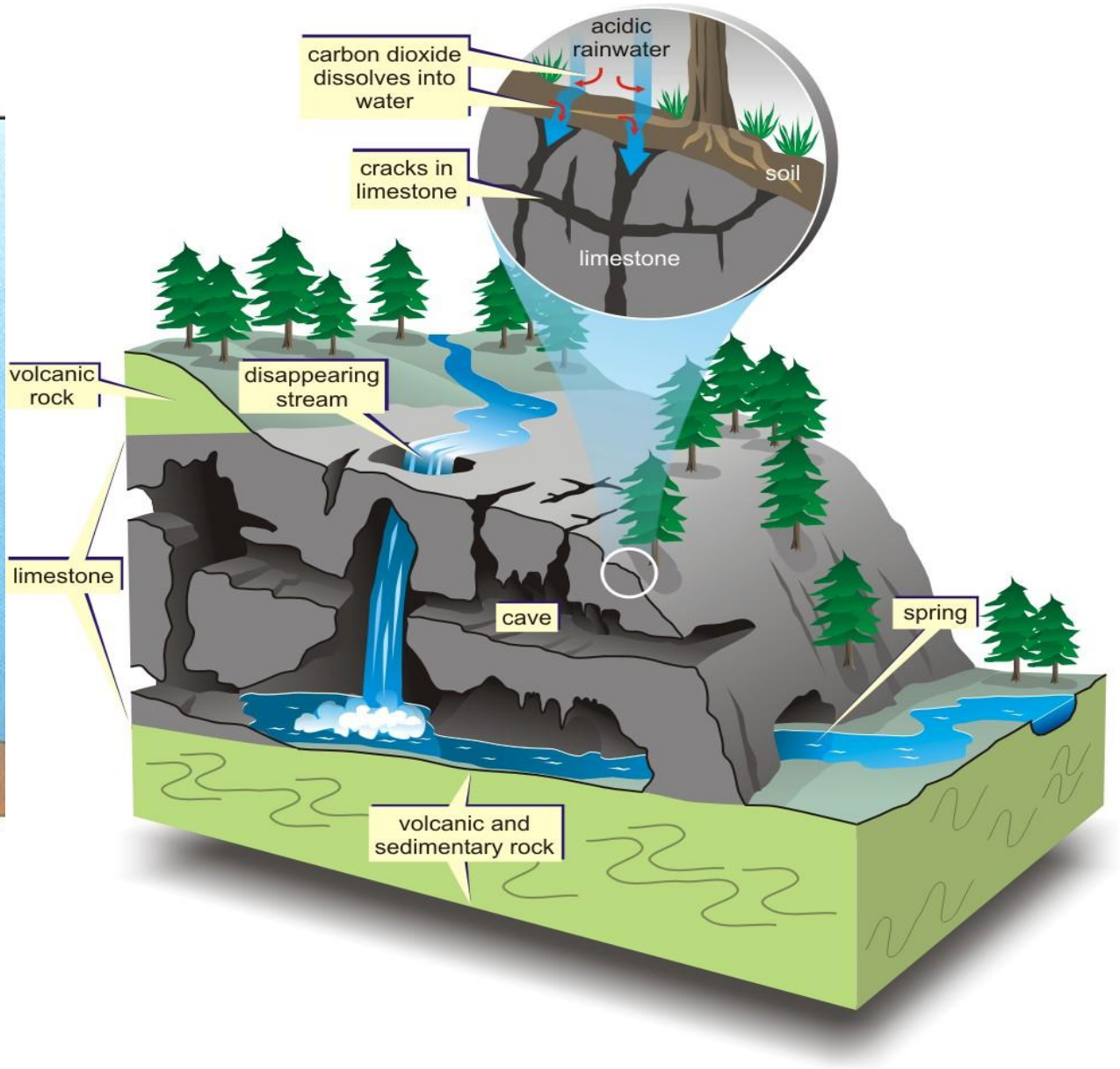


ΚΙΘΑΙΡΩΝ

ΜΑΚΡΟΣΚΟΠΙΚΗ - ΜΙΚΡΟΣΚΟΠΙΚΗ ΠΑΡΑΤΗΡΗΣΗ (Km/m/cm/mm/μm-κλίμακα)

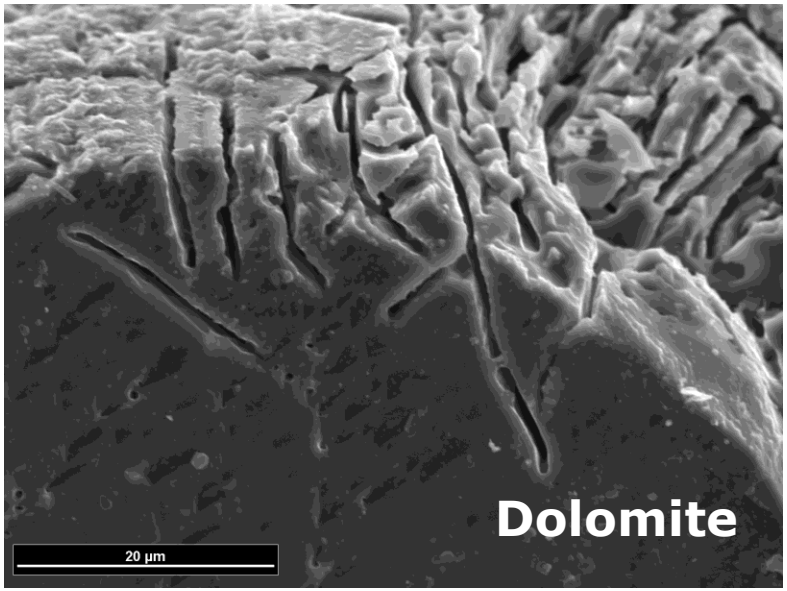

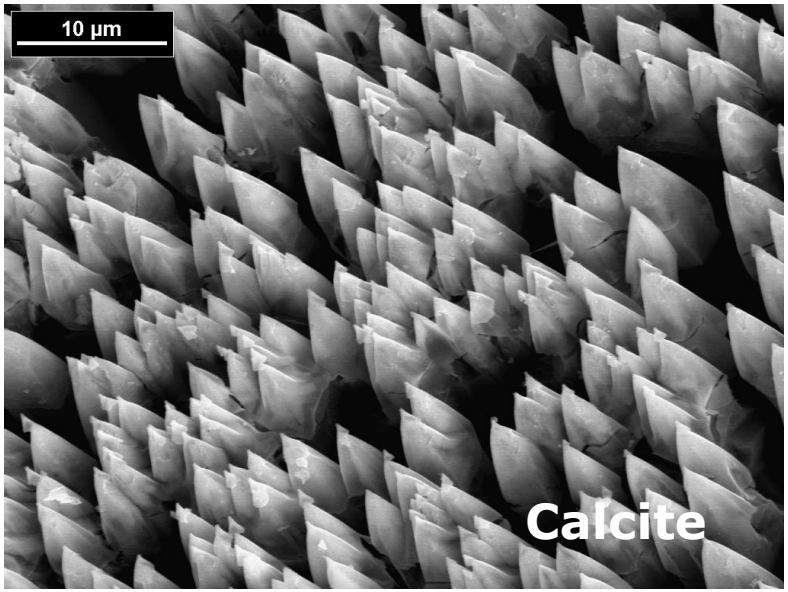

ex-situ & *in-situ* ΜΙΚΡΟΣΚΟΠΙΚΗ ΠΑΡΑΤΗΡΗΣΗ (nm/Å-κλίμακα)

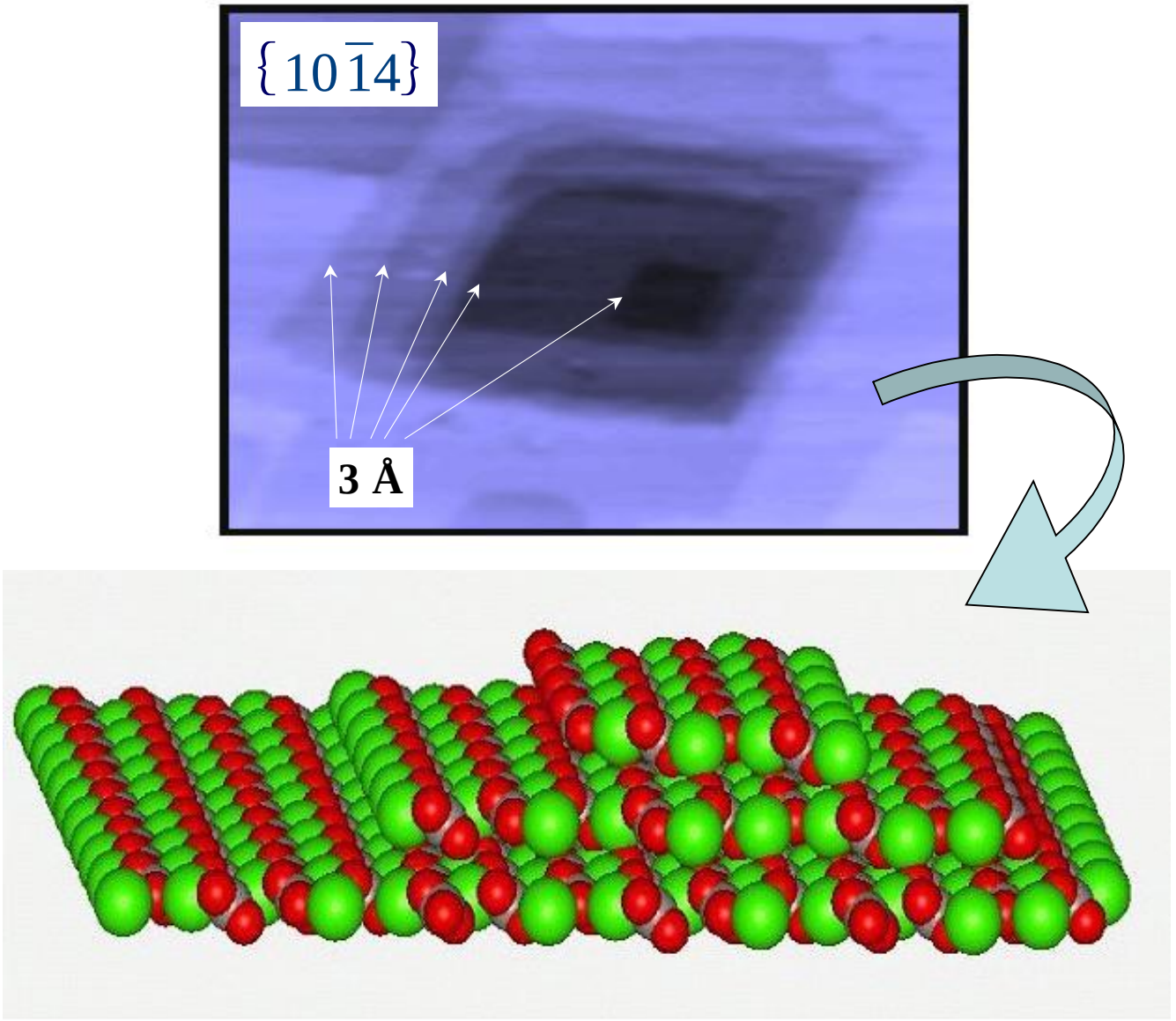


☺ ΚΑΡΣΤΙΚΕΣ ΣΤΙΓΜΕΣ 2014 ☺